8-2022

Effects of monovalent and divalent ions in factor xiii activation and crosslinking.

Richard Laporca Lumata
University of Louisville

EFFECTS OF MONOVALENT AND DIVALENT IONS ON FACTOR XIII ACTIVATION AND CROSSLINKING

By Richard L. Lumata
M.S., University of Louisville, 2022
B.S., Western Mindanao State University, 2006

A Thesis Submitted to the Faculty of the
College of Arts and Sciences of the University of Louisville
in Partial Fulfillment of the Requirements
for the Degree of

Master of Science in Chemistry

Department of Chemistry
University of Louisville
Louisville, Kentucky

August 2022

EFFECTS OF MONOVALENT AND DIVALENT IONS IN FACTOR XIII

ACTIVATION AND CROSSLINKING

By Richard Laporca Lumata
B.S., Western Mindanao State University, 2006
M.S., University of Louisville, 2022

A Thesis Approved on
June 22, 2022

by the following Thesis Committee:

Professor Muriel C. Maurer
Thesis Director

Professor Ying Li

Professor Andrew J. Wilson

Professor Michael A. Menze

DEDICATION

This thesis is sincerely dedicated to my parents:

To my dearest Mother Mrs. Evelyn Laporca Lumata

and to my departed Father Mr. Jose delas Peñas Lumata

ACKNOWLEDGEMENTS

It is with sincerest gratitude that I highly thank Dr. Muriel C. Maurer, my Advisor, for guiding me persistently throughout my graduate studies here in University of Louisville for the past 3 years. I have learned so much not only in Protein Chemistry but also my overall skills as a Chemist. Thank you so much for the patience and understanding, Dr. Maurer. To my thesis committee members, Dr. Ying Li, Dr. Michael Menze, and Dr. Andrew Wilson, I thank you for your very helpful insights on how I can improve my thesis manuscript. To my laboratory mates, I acknowledge Rameesa Darul Anne Syed Mohammed for training me with all the assays I had performed, and other Laboratory mates Francis Dean Ablan and Anoushka Bhat for their encouragement.

I also would like to thank my roommates Peter Armstrong, Faye Carvajal and Caleb Calvary for also guiding me here in the graduate study life in UofL. To my Family, my Mother Evelyn L. Lumata for the love and care. My siblings Lloyd Lumata, Analyn Lumata, Edwin Lumata and Jenica Lumata for giving me inspiration. And to my friends, relatives and classmates (Ryan Amilhussin, Clifford Tagactac, Meriam Lumio, Valerie Napalcruz, Nadine Ardiente, Joyce Delima, Deborah Ogulu, Bernard Adjei, Mohan Paudel, Sashil Chapagain, Harry Nambiar, Oskar Kharki, Touhid Islam, Dilmi Waidyaratne, and Tonia Schansberg, Eric Schansberg, and Jenny Jokinen), thank you so much for giving me the strength to finish this goal.

ABSTRACT

EFFECTS OF MONOVALENT AND DIVALENT IONS IN FXIII ACTIVATION AND CROSSLINKING

Richard L. Lumata

June 22, 2022

Factor XIII (FXIII) is an emerging target for treating blood clotting and cardiovascular related diseases. FXIII can be activated non-proteolytically by the presence of elevated Ca^{2+} levels (2-100 mM) or proteolytically by thrombin-cleavage of the Activation Peptide along with low mM Ca^{2+}. The studies herein utilized fluorescence to examine how monovalent and divalent ions influence the transglutaminase activity and conformation of FXIII. Monodansylcadaverine assays revealed that increasing ionic radius ($Cs^+ > K^+ > Na^+ > Li^+$) and increasing ionic strength (XCl^- levels and $SO_4^{2-} > Cl^-$) elevated FXIII-A transglutaminase activity. Intrinsic fluorescence studies revealed that only cations influenced FXIII conformation. For divalent salts, transglutaminase activity for $MgSO_4$ is ~3-fold higher than $MgCl_2$. Unlike transglutaminase 2, FXIII containing a mutation in the Cab3 calcium binding site (G262V) could not exhibit an improvement in activity. A FXIII Cab3 helix is proposed to be hindered which impacts non-proteolytically activated FXIII more than proteolytically activated FXIII. Both cations and anions influence FXIII's ability to interact with substrates.

TABLE OF CONTENTS

LIST OF TABLES

LIST OF FIGURES

CHAPTER I

FACTOR XIII (FXIII) IN BLOOD COAGULATION

Hemostasis: Introduction to blood coagulation

When a trauma injury occurs that affects a blood vessel (Fig. 1A), our normal body's response is to promote hemostasis. Upon vascular endothelium damage, collagen fibrils along with von Willbrand factor (vWF) are exposed at the vessel wall (1). The vWF links platelets to collagen via specific receptors in the platelet membrane known as Integrin $\alpha_2\beta_1$ and GPVI (2,3). At this stage, the platelets are activated from their resting state by changing their shape into dendridic or pseudopodia forms (4). The activated platelets subsequently release prothrombotic molecules such as Adenosine diphosphate (ADP). These ADP biomolecules bind to specific receptor in platelets promoting recruitment of more activated platelets (5). Platelets become crosslinked with each other in the presence of a mediator known as thromboxane. This platelet aggregate now forms the so-called platelet plug and triggers vasoconstriction that seals off the injury (Fig. 1B) (6). Platelet activation also simultaneously promotes the activation of the extrinsic and intrinsic pathways in the blood coagulation cascade (7) (Fig. 2) that will promote the last stage of the cascade which is the clot formation. Other clot components include platelets that initiate the vasoconstriction, red blood cells entrapped in a clot that regulate clot size (8), α_2-antiplasmin that acts as an inhibitor of plasmin (9), and fibronectin which is involved in tissue repair (10), etc. (Fig. 1C).

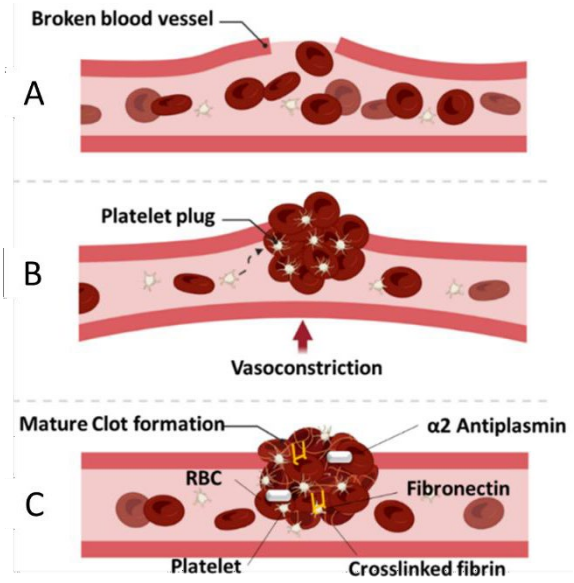

Figure 1. Blood coagulation. A) shows how clot formation occurs at the broken blood vessel B) red blood cell retention and platelets plug formation cause vasoconstriction C) clot formation. (Created with BioRender)

The extrinsic and intrinsic pathways are interconnected to initiate the activation of clotting factors. In the classical model of blood coagulation (Fig. 2A) (11), TF initiates in the extrinsic pathway activates coagulation FVII, FIX and eventually generation of FX to activate FII (thrombin) (12,13). Meanwhile, in the intrinsic pathway, several players are involved (Prekallikerin, Kallikerin, FIX, FXII, FXI). Both the intrinsic and extrinsic pathways merge in a common pathway known as the tenase complex. This complex then generates thrombin to promote soft and hard clot formation where fibrinogen and FXIII come in. The mechanism of this classical concept can be well-understood in the cell-based model of blood coagulation (14,15).

In the cell-based model (Fig. 2B), upon tissue damage, tissue factor (TF), a cell-bound transmembrane glycoprotein, triggers the activation of the extrinsic pathway and subsequently the intrinsic pathway (Fig. 2B). There are three basic steps in the cell-based model in a step-by-step fashion: (1) Initiation, (2) Amplification, and (3) Propagation (14,16).

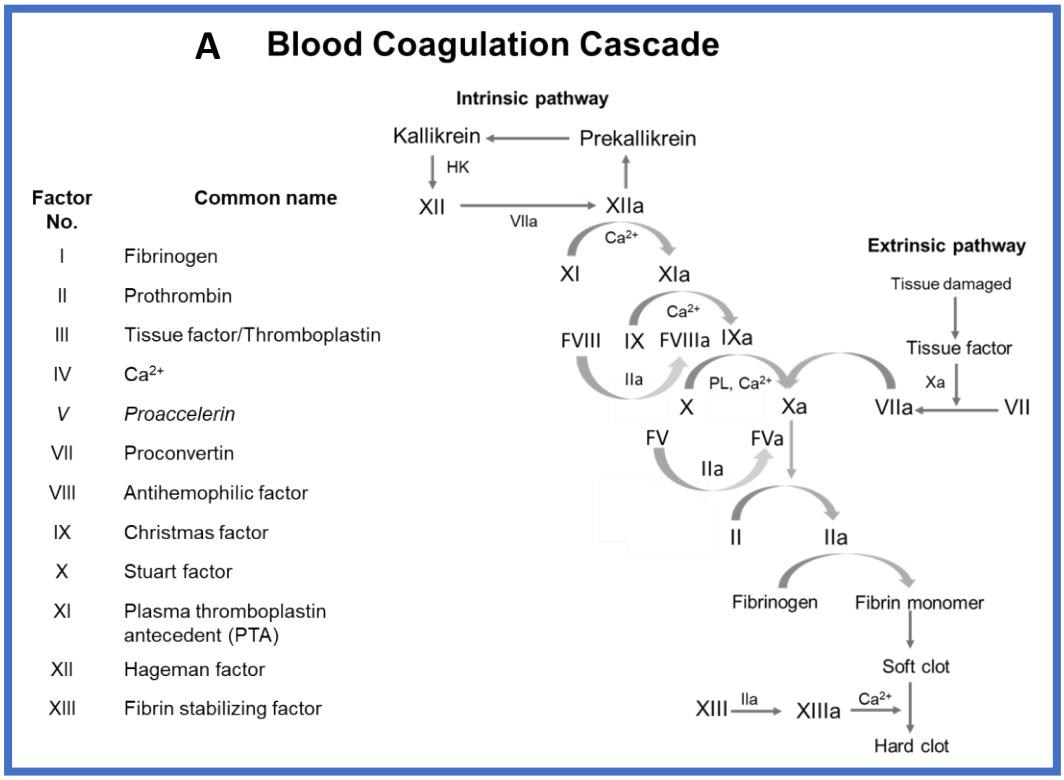

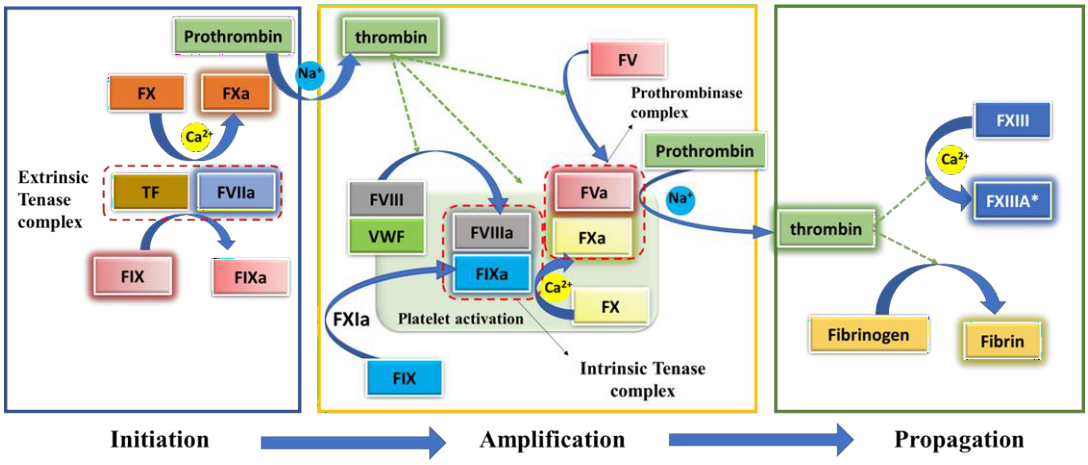

Figure 2. A) Blood coagulation cascade: The extrinsic and intrinsic pathway. FXIII plays role at the end stage of the cascade activated by thrombin and calcium which eventually facilitates isopeptide bond formation of fibrin to form a stable clot (hard clot). Modified cascade based on Adams et al 2009 coagulation cascade. B) Modified Initiation, Amplification and Propagation phases of the cascade from Bittar et al 2015.

In the "Initiation Phase" (Step 1), TF forms a complex with FVIIa (TF:FVIIa) that functions to activate zymogen FIX and FX to its active forms abbreviated as FIXa and FXa,

respectively (13,17). The generated FXa activates prothrombin (II) to thrombin (IIa). In this step, only a small amount of IIa is produced (Fig. 2A) (18). This thrombin generation from the initiation phase now plays a crucial role in the "amplification phase" (Step 2). Platelet activation primarily occurs in the amplification phase that triggers activation of several other coagulation factors not involved in the initiation phase (19). Thrombin, in the presence of Na^+, then facilitates the dissociation of FVIII from its cofactor, von Willebrand factor to become FVIIIa and it also further activates FIX to FIXa. In this event, FIXa forms a complex with FVIIIa (FIXa:FVIIIa), known as the intrinsic tenase complex (13). At the same time, the FIXa forms a complex with FVa known as prothrombinase complex (FIXa:FVa) that generates higher rate of thrombin formation. The presence of calcium ions generates a positive feedback loop which rapidly catalyzes the conversion of II to IIa. The amplification phase can activate thrombin 50 to 100-fold, much higher than the thrombin generated in the initiation phase. At this phase, thrombin also binds with the platelet Gplbα receptor that further increases interactions with other components of the plasma membrane such as the protease-activated receptor 1 (PAR-1) (20,21).

Colocalization of the tenase and prothrombinase complexes in the presence of calcium further enhances their efficiencies to generate more thrombin (22). This formation of huge amounts of thrombin is also known as "the thrombin burst" that allows formation of a much more stable clot. Finally, the third stage (Fig. 2C) emphasizes the "Propagation phase" (Step 3) which allows for continuous thrombin generation and clot formation (16). This final phase depends on the rate of platelet recruitment at the site of the injury which necessitates optimal thrombin generation for the activation of FXIII and fibrinogen (23).

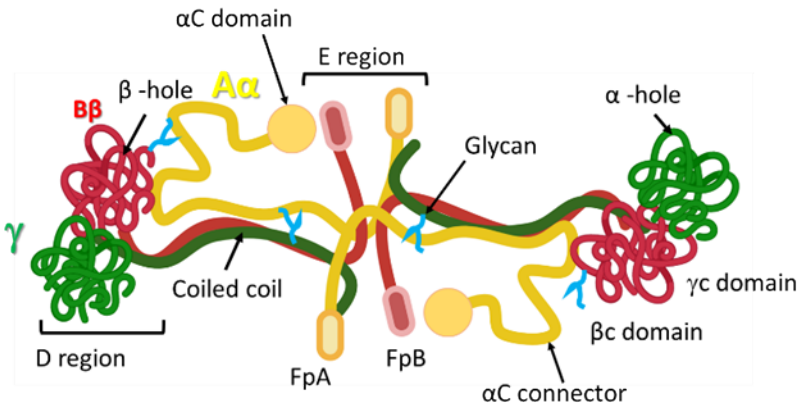

Figure 3. Full fibrinogen structure. Fibrinogen is a dimer of trimers containing α helical coiled coil (Aα, Bβ, γ), D, E, and αC regions.

Fibrinogen is a glycosylated protein (340kDa) containing nonidentical polypeptides namely, Aα, Bβ, and γ linked with disulfide bonds. It is also comprised of three regions, the central region (2 identical terminal D domains), the central E domain, and the αC region (Fig. 3)(24,25). The fibrinogen (Fbg) αC domain (221-610) is where most of the crosslinking takes place (26), and the Fbg (233-425) region contains three reactive glutamines (Q237, Q328, and Q366) (27).

Fibrinogen is converted to fibrin when the N-terminal fibrinopeptides A and B of the Aα and Bβ chains (Fig 4.) are cleaved off by thrombin (IIa) forming soluble fibrin. This cleavage leads to the exposure of α and β knobs that are subsequently inserted into γC and β holes of the D region to form protofibrils. Continuous aggregation of these protofibrils results in the formation of a fibrin mesh also known as a soft clot (28-30). Transglutaminase FXIII then comes in to make a more stable clot.

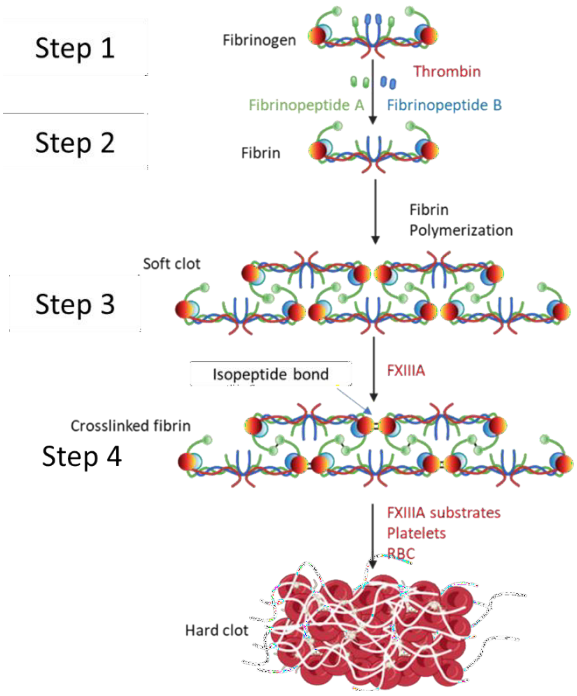

Figure 4. FXIII-A crosslinking via isopeptide bond formation using fibrinogen substrates. Step (1) Fibrinopeptide cleavage, Step (2) Formation of fibrin, Step (3) formation of soft clot ad, Step (4) hard clot (crosslinked fibrin). Created with BioRender.

Fibrin stabilizing factor (FXIII)

FXIII A_2 is distributed both extracellularly (31) and intracellularly (32). Coagulation FXIII A_2 is expressed mainly in the cytosol of megakaryocytes which are cells in the bone marrow that are also responsible for synthesizing platelets. The FXIII A_2 derived from platelets contains a concentration that ranges from 46-82 fg/platelet (33). Moreover, FXIII-A in platelet cytoplasm is 100-150x higher in concentration than FXIII found in plasma. Other origins of FXIII A_2 include the cytosol of monocytes, osteoblasts, osteoclasts, and macrophages as shown in Fig. 5 (34-36). There are three ways that FXIII A_2 can be activated: FXIII from plasma undergoes proteolytic activation by thrombin at low mM Ca^{2+}, FXIII A_2 to FXIII-A^o at low calcium in cells, and FXIIIA_2 to FXIII-A^o at high mM calcium in bones.

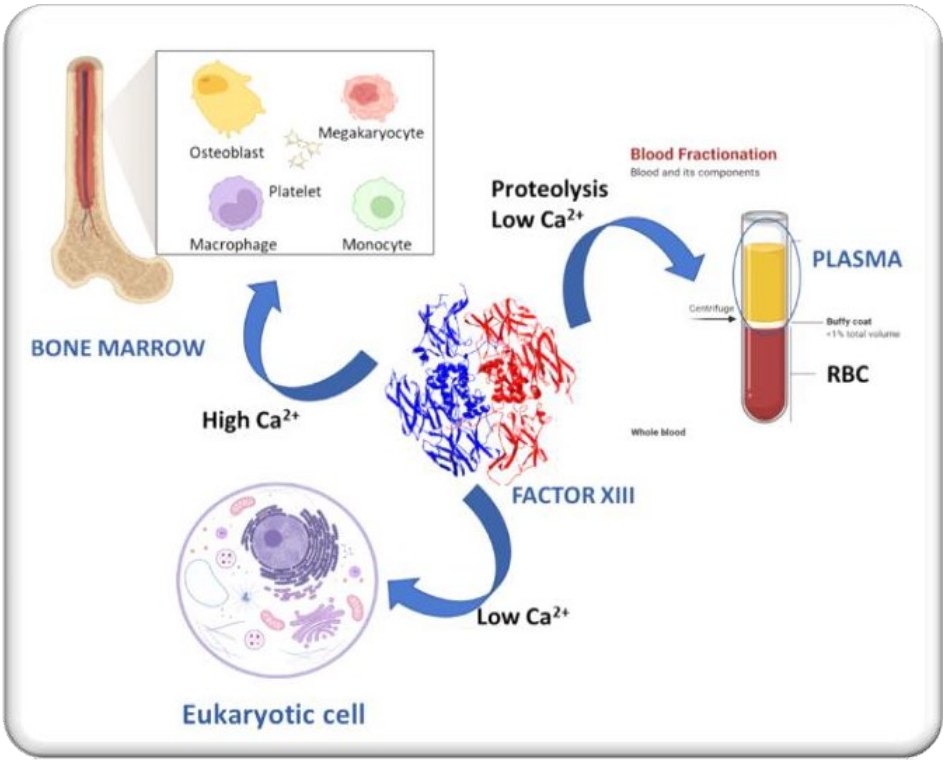

Figure 5. Sources of FXIII. Bone marrow specifically the megakaryotes synthesize the bulk of FXIII via platelet. and distributed intracellularly and extracellularly. Other sources come from monocytes, macrophages, osteoclast, and osteoblast. (Created with BioRender)

For over a century, FXIII has been a target for medical and pharmacological research due to its multifunctional roles in hemostasis, bone development (37), angiogenesis, wound healing (38), signaling processes (39), and several intracellular functions (36). Furthermore, congenital FXIII deficiency can lead to life-threatening conditions: intracranial hemorrhages, miscarriage, and umbilical cord bleeding (40). The main function of this type of transglutaminase (EC 2.3.2.13) is to catalyze the crosslinking of protein substrates via isopeptide bond formation between the side chains of glutamine and lysine residues (41).

Plasmatic FXIII circulates as a heterotetrameric (FXIII A_2B_2) protein complex whereas cellular FXIII exists as a homodimer FXIII A_2 (Fig. 7). The megakaryocytes are the major source of FXIII A_2. The liver synthesizes FXIII B_2 and this regulatory protein

circulates in excess in plasma and binds with FXIII A_2 to form FXIII A_2B_2 (42). The FXIII B_2 subunit serves as a protective group to prevent FXIII A_2 from undergoing premature activation. Furthermore, FXIII B_2 of FXIII A_2B_2 binds to fibrinogen specifically at the Fbg γ390-396 segment. Only 1% of the total FXIII A_2 circulates in plasma with the remainder proposed to bind to FXIII B_2 (33). FXIII A_2B_2 circulates in plasma with an average concentration of 22 mg/L and a half-life of 12 days (43). Besides crosslinking fibrin chains, plasma FXIII A_2B_2 is also responsible for red blood cell retention within the clot network (44,45).

Although FXIII and the rest of the transglutaminases are calcium-dependent, they lack the EF hand motif which is a type of helix-loop-helix structure with a high binding affinity for calcium (46,47). In plasma, FXIII A_2 associates noncovalently with the circulating FXIII B_2 forming the heterotetramer FXIII A_2B_2. Polgar et al 1990 introduced FXIII B_2 into FXIII A_2 activation with constant calcium concentration and found out that the resultant transglutaminase decreased as a function of increasing FXIII B_2 concentration. These results helped confirm that B_2 subunits interact with the FXIII A_2 subunits hindering premature FXIII activation (48). The two A subunits (83kDa) have the catalytic functions whereas the two beta subunits, FXIII B_2 (80kDa) serve as the carrier or regulatory group. Each B subunit consists of 10 sushi domains that are spatially folded (36,49).

Intracellular FXIII A_2 is activated to FXIII-A^o through nonproteolytic activation in the presence of higher mM calcium concentration. This activated form FXIII-A is a 731-residue polypeptide that contains five structural domains, namely: Activation Peptide (Ser1-Arg37) which is part of the N terminal domain, two β-barrel domains β-barrel 1 (Ser516-Thr628) and β-barrel 2 (Il629-Met731), β sandwich domain (Gly38-Phe184), and

one catalytic core domain (Asn185-Arg515) (36) as shown in Fig. 6. The catalytic core domain contains the catalytic triad Cys314, His373, and Asp396 (50) whereas the role of the Trp279 residue is to stabilize the oxyanion intermediate (36,51).

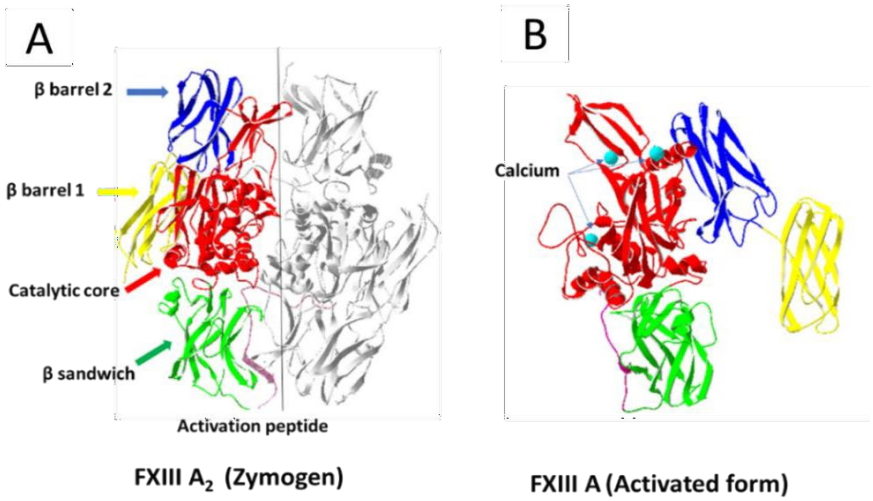

Figure 6) Activated vs inactivated forms of FXIII. A) FXIII A_2 zymogen (PDB ID IF13) and B) FXIII A Ca-Activated + 6-Diazo-5-oxonorleucinyl -inhibitor (PDB ID 4KYT). In the active state FXIII A, only the β barrel (blue and yellow) domains changed position drastically but the catalytic core (red) and β sandwich domain remain unchanged upon binding with calcium (sky blue). The activation peptide (pink) appears as a disordered polypeptide.

The research group of Stieler and collaborators published the first high resolution (1.98 Å) crystal structure of non-proteolytically activated FXIII-A^o (PDB 4KYT) in complex with an irreversible inhibitor ZED1301 (Ac-(D)-Asp-MA-Nle-Nle-Leu-Pro-Trp-Pro-OH) containing an electrophilic Michael acceptor (52). Their results revealed that binding of the inhibitor with monomeric FXIII-A (activated with 40 mM $CaCl_2$) creates a large conformational rearrangement to FXIII, and the β barrel domains swing aside upward at a 90^o angle to expose the catalytic core. Although there is large movement for the two FXIII β barrel domains, they still conserve their overall fold. Studies performed by the Philippou and Ariens groups demonstrated the significance of the two β barrel domains. Their results showed that removal of β-barrel 2 led to total loss of FXIII activity and that

truncations of both β barrels led to a 30% loss of activity. In addition, the β barrel 2 serves to protect the cysteine in its active site in the zymogen form of FXIII whereas β barrel 1 is needed to expose the active site during activation of FXIII (53). No conformational rearrangement and changes to the β sandwich domain occur during the activation. These results signify that the presence of β barrel domains plays a critical role in modulation of the FXIII catalytic activity.

Activated FXIII-A crosslinks fibrin(ogen)'s glutamine (Q) and lysine (K) substrates through isopeptide bond formation (γ-glutamyl-ε-lysyl amide bond) that increases clot stability which now can be called a hard clot (Fig 4a). This fibrin stabilizing factor plays essential roles in the crosslinking of protein substrates such as fibrin(ogen) to form a mesh-like structure (54,55).

Cellular vs Plasma FXIII

Intracellularly, FXIII exists as a proenzyme homodimer, FXIII A_2 (Fig. 7). The plasmatic FXIII A_2B_2 is proteolytically activated whereas the intracellular FXIII A_2 is

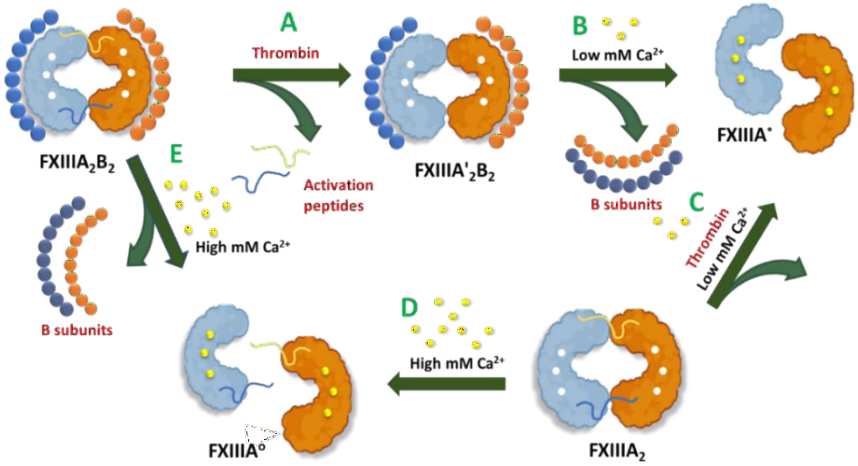

Figure 7.) Proteolytic and nonproteolytic activation of plasma FXIII $A_2B_2$and cellular FXIII A_2. The FXIII A_2B_2 undergoes cleavage of fibrinopeptide A and B via IIa (A) in the presence of low Ca^{2+} FXIII B_2 is released forming FXIII-A^* (B). C) Cellular FXIII A_2 forms FXIII-A^* at low Ca^{2+} and thrombin and FXIII A_2B_2 can also be nonproteolytically activated in the presence of high Ca^{2+} (D).

nonproteolytically activated (Fig 7). Proteolytic activation of FXIII A_2B_2 occurs as a multistage process. The first step involves the cleavage of the activation peptide (AP) located at the N-terminus of the A subunit of FXIII with thrombin hydrolyzing the Arg37-Gly38 peptide bond which leads to the formation of FXIII A'_2B_2 (56). The AP of FXIII blocks access to the FXIII active site (57) and stabilizes the FXIII A_2 dimer unit (58).

Calcium-assisted conformational rearrangement then occurs disrupting the noncovalent interactions of the A and B subunits forming two homodimers (FXIII A'_2 and FXIII B_2). With further calcium binding, the FXIII A_2 promotes conformational changes leading to the dissociation of the A subunits into FXIII-A monomers that exhibit transglutaminase activities (59-61). Both plasma and cellular FXIII become a monomer FXIII-A in its active state (60,62) as shown in Fig 7.

Anokhin et al. performed FXIII dissociation and activity assay with different calcium concentrations (4-100 mM $CaCl_2$). Results from the AUC studies demonstrated that the monomeric form of FXIII increases as calcium concentration also increases (60). A spectrophotometric assay with FXIII A_2 activated nonproteolytically, FXIII-A^o, revealed that transglutaminase activity also increases as a function of increasing calcium concentration (61). Other ions were also previously tested for FXIII activation, such as the monovalent ion sodium chloride (48,60,63).

Transamidation mechanism of FXIII

In the catalytic core domain of FXIII-A^o (PDB 4KYT), three calcium binding sites were observed. The calcium binding (Cab) sites contain the following residues: Cab1 (Glu 485, Glu 490, Ala 457, and Asp 436), Cab2 (Asp 349, Asp 351, Asp 343, Asn 347, and

Gln 459), and Cab3 (Asp 270 Asp 271, Ala 264, Lys269, and Asn 267) (52). Upon calcium binding to site 1, α helices at Cab2 shift slightly and promote rotational movement of the three stranded β sheet by the loop containing Asp 367 coordinating with Asp 351. These movements cause the formation of the catalytic diad involving residues His 342 and Glu 401 needed for FXIII activity. The Cab3 contains the residues involved for Lysine (K) - substrate binding region such as Lys 269. A loop in this region is also rearranged upon calcium binding (51).

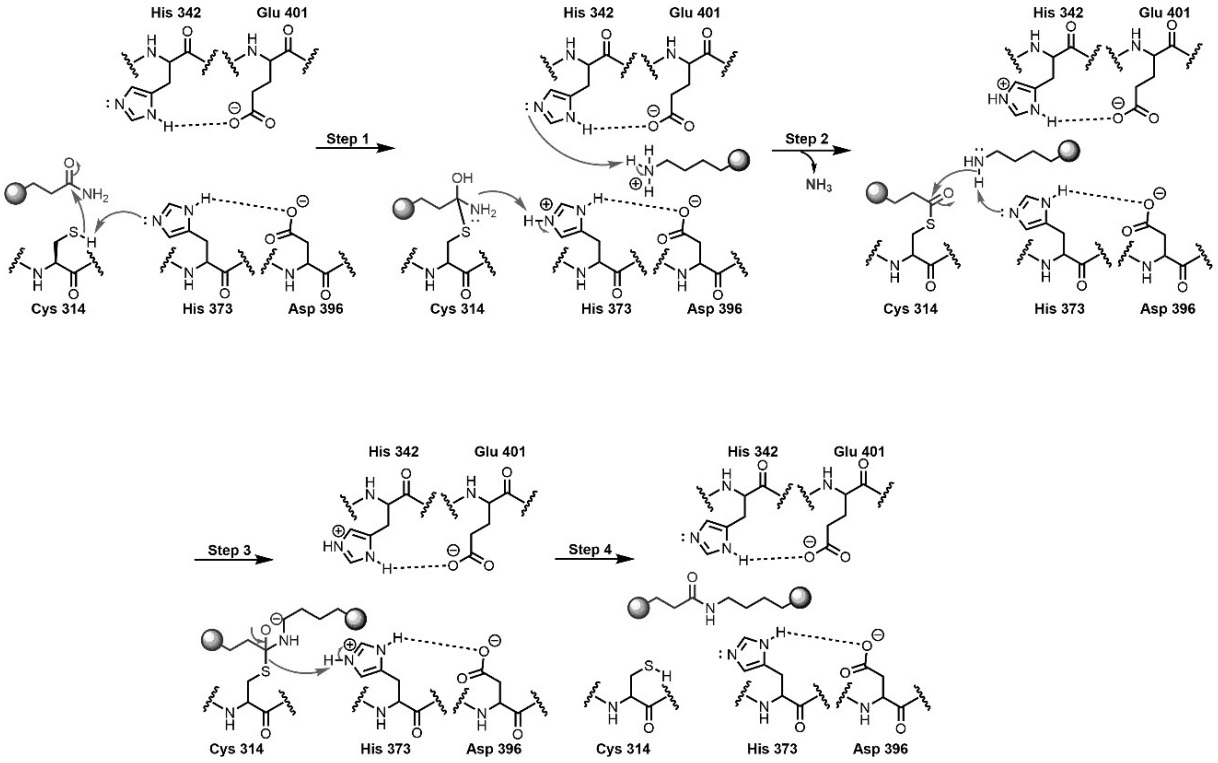

Figure 8. Transamidation mechanism of FXIII. Modified FXIII transamidation mechanism as proposed by Imhof et al 2020.

FXIII contains an active site that contains a cysteine-like proteinase (64). The active site consists of a catalytic triad (Cys314, His373, and Asp396) and a catalytic diad (His342 and Glu401) (52,57). In the general transamidation of fibrin substrates, one fibrin monomer

serves as a glutamine donor and another fibrin becomes a lysine donor to form an isopeptide bond (65). In the first step of the reaction, the cysteine residue Cys314 of FXIII-A must be deprotonated via a general base, His373, making Cys314 a stronger nucleophile (Fig. 8). The amide nitrogen of Cys314 is then protonated via proton transfer from the protonated His373 (Step 1 -2) which occurs only if there is a cysteine-thiolate protonated ion pair (51). Case and Stein proposed that there exists a neutral catalytic diad of Cys314-His373 ion pair and the thiolate of Cys makes a nucleophilic attack in the rate-limiting step (66). This was confirmed by their potential energies between Cys314 and His373 using QM/MD calculations where the protonated form of Cys314 (54.7 kj/mol) obtained a significantly much higher energy than the protonated His (36.1 kj/mol) (51). Hence, the protonated ion-pair form of His has a much higher stability than the protonated Cys ion-pair form. In step 2 of the mechanism, the imidazolium thiolate of Cys314 makes a nucleophilic attack to the carboxyamide of the acyl donor, Glutamine. This attack leads to the formation of a tetrahedral intermediate followed by release of the ammonia by a general acid (imidazolium) to form the acyl-enzyme. This acyl enzyme can undergo two different reactions depending on the type of the acyl, acceptor: H_2O or Lysine containing protein or peptide. In the presence of a Lysine-containing substrate, the imidazole group of Cys314 now functions as a general base making a nucleophilic attack to the thioester of Lysine leading to deprotonation of the neutral lysine substrate forming a tetrahedral intermediate (Step 3). Subsequently, decomposition of this intermediate releases the thiolate and forms the transamidation product via isopeptide bond formation and regenerates a free, catalytically active FXIII A (Step 4). However, in the absence of the Lysine substrate, H_2O

becomes a substrate of the acyl enzyme and promotes the hydrolysis of the glutamine residue into glutamic acid (51).

Transglutaminase 2

Another type of transglutaminase that is closely related to FXIII is Transglutaminase 2 (TG2) which is a multifunctional protein involved in post translational modification, crosslinking of protein substrates, neurodegenerative disease, GTP hydrolysis, scaffold activity, and a wide spectrum of other biological activities. Due to these various functions, it plays important roles in wound healing, angiogenesis, apoptosis, celiac disease, and several other cellular processes. Structurally, both TG2 and FXIII share common domains including a catalytic domain, two C-terminal β barrel domains, and the N terminal β sandwich domain. An exception is that activation peptides are absent in TG2. Unlike FXIII which is activated by thrombin and/or calcium, TG2 is allosterically regulated by calcium and GTP (Fig. 9) under fluctuating physiological conditions. In a recently published paper, Arek et al. 2021 demonstrated how extracellular TG2 forms a molecular redox reaction gate capable of activating or deactivating the protein (67). At high calcium concentration, initial binding of Ca^{2+} to a high affinity calcium binding site protects TG2 from oxidative deactivation and helps promote calcium binding to a weaker binding site developing an allosteric effect to activate TG2 (Fig. 9). Overall, Ca^{2+} positively regulates TG2 whereas nucleotides such as GTP, GDP or ATP negatively regulate TG2 (68). Similar to FXIII, TG2 also forms an open conformation upon activation (Fig. 8C).

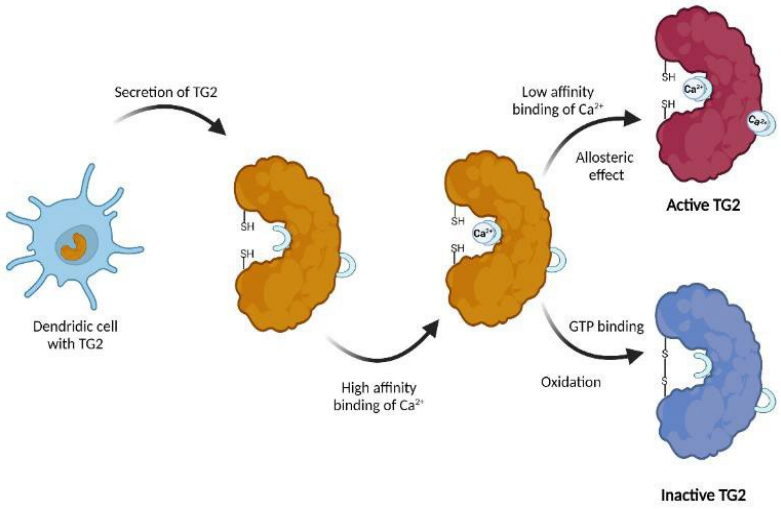

Figure 9. a) Transglutaminase 2 (TG2) activation mechanism. – Modified mechanism based on Khosla et al 2021 (*J. Am. Chem. Soc.* 2021, 143, 10537-10540). Created with BioRender.

Overall Goal of the Study

The primary goal of this MS Thesis study was to examine the transglutaminase activity of recombinant human wild type FXIII under different ionic concentrations and to probe the conformational rearrangements to FXIII that may be occurring in these environments. Besides the commonly used Ca^{2+} and Na^{+}, the ions Li^{+}, K^{+}, Cs^{+} and Mg^{2+} were studied. In an additional project, a TG2 mutation (G262V) located near Cab3 were introduced into comparable positions of FXIII-A_2. Impacts on FXIII-A_2 activation and subsequent crosslinking abilities were examined. Influences on Cab3 and the lysine binding surface could be used to tune the properties of FXIII.

CHAPTER II

EFFECTS OF IONS IN FXIII ACTIVATION VIA MONODANSYL CADAVERINE INCORPORATION TO FIBRINOGEN αC (233-425)

Introduction

Fibrin stabilizing factor or FXIII is a calcium-dependent transglutaminase where calcium serves as a cofactor regardless of the FXIII source, in plasma as FXIII A_2B_2 (heterotetramer) or in cells as FXIII A_2 (dimer). FXIII contains three calcium binding sites within the catalytic core domain (52). Cellular FXIII A_2 was selected as the target transglutaminase in the present study. Proteolytic activation of FXIII A_2 requires low mM Ca^{2+} and thrombin (IIa) cleaves the AP fragment to become FXIII-A* (69) whereas nonproteolytic activation is promoted in a high mM Ca^{2+} (70) environment to become FXIII-A^o (61). For this project, the focus was on cellular FXIII A_2 and how divalent and monovalent ions contribute to generating FXIII-A^o that exhibits transglutaminase activity.

Physiologically, both monovalent and divalent ions are present both extracellularly and intracellularly. Table 1 shows a summary of cations and anions present in human plasma and cells with their corresponding concentrations. In plasma, Na^+ (150 mM) is the chief cation (71), on the contrary, in the cytoplasm of cells, K^+ (150 mM) dominates with a concentration about ~30 fold higher than the Na^+ (72,73). These monovalent cations (Na^+ and K^+) were proposed to help activate FXIII in the presence of low Ca^{2+}, but no data were

available to compare whether K^+ exhibited similar or higher transglutaminase activity as compared to Na^+ (48). Previous studies suggested that increased Na^+ concentration helped increase platelet aggregation (74) whereas KCl supplementation decreased platelet reactivity (71).

Table 1. Physiological concentrations of selected ions (in mM) in human plasma and cells

Ionic sources	Monovalent cation		Divalent cation		Anion	
	Na^+	K^+	Mg^{2+}	Ca^{2+}	Cl^-	SO_4^{2-}
Intracellular (cytosolic)	10-35[75]	140-150[72,76]	17-20[73,77,78]	~ .0001[79]	5[80]	Not known
Extracellular (Plasma)	135-145[75]	3.5-5[72,76]	1.2-1.4[73,77,78]	2.-2.6[81,82]	120[80]	0.5[83], 1-2 [84]

Extracellular calcium in plasma is much higher in concentration than the intracellular Ca^{2+} in cells (82). Moreover, Mg^{2+} concentration in cells exceeds Mg^{2+} in plasma (73,77,78). Upon platelet activation, calcium levels in their cytosol are increased via calcium channels in the endoplasmic reticulum thereby elevating Ca^{2+} to supraphysiological levels. The Cl^- concentration in plasma is about ~20 fold higher than it is in the cytoplasm of cells. Other salts (LiCl, CsCl, ChCl and TMAC) were also investigated. Li^+ is a popular drug used for treatment in bipolar disorder whereas CsCl is a supplement for cancer treatment. In addition, LiCl supplementation has been found to increase platelet count and aggregation (85-87).

Two organic salts were also examined. Choline chloride (ChCl) was used previously as a cationic molecule to demonstrate that thrombin (88) and FXa (89) have distinct Na^+ binding sites. Tertramethylammonium chloride (TMAC) is a smaller organic cation that has been used as a molecular enhancer for isothermal exponential amplification reactions and other biochemical assays (90).

The current study focused on investigating the effect of selected monovalent and divalent ions on nonproteolytic activation of recombinant cellular FXIII A_2. Overall, the paramount goal of this study was to examine for changes in FXIII-catalyzed crosslinking of fluorescent monodansylcadaverine (MDC), a lysine mimic (91), into reactive glutamine of Fibrinogen αC (233-425). Fluorescent intensity (FLR) generated for crosslinking product as a function of ion concentration and reaction time provided a measure of FXIII transglutaminase activity.

Materials

Recombinant FXIII zymogen (FXIII A_2) was kindly provided by the late Dr. Paul Bishop (Zymogenetics, Seattle, WA, USA). Recombinant human thrombin (rhIIa) stocks were procured from Dr. E. Di Cera and Ms L. Pelc (St. Louis University, St. Louis, MO, USA). N,N-dimethylated β-Casein from bovine milk and the lysine mimic monodansylcadaverine (MDC) were both purchased from Millipore Sigma (St. Louis, MO, USA). The crosslinking agent for gel electrophoresis, 30% Acrylamide/Bis solution, and the dual-color molecular weight standards were purchased from Bio-Rad Laboratories, Inc. (Richmond, CA, USA). The catalyst TEMED (N,N,N,N-Tetramethylethylenediamine) (MP Biomedicals, Solon OH, USA) and the protein denaturant SDS (sodium dodecyl sulfate) were purchased from VWR Life Science, Ohio, USA. The monovalent ions NaCl and Li_2SO_4 were purchased from Fisher chemical (Fair Lawn, NJ, USA) whereas LiCl, KCl, CsCl, $MgCl_2$, and $MgSO_4$ were from Sigma (St. Louis, MO, USA).

Methods

Expression and Purification of Fibrinogen αC WT (233 – 425)

Fibrinogen αC (233 – 425) is part of the C terminal region of the Fbg αC. This αC region contains three reactive glutamines (Q237, Q328, and Q366) utilized by FXIII to form isopeptide bonds with lysine substrates (92-94). The Fbg αC region also has a FXIII binding site involving αC (389-403). Stocks of Fbg αC (233 – 425) fragment were expressed and purified using the steps described below:

Recombinant protein expression

The PGEX-6P-1 plasmid containing complementary DNA for Gluthatione S-transferase (GST)-tagged Fbg αC fragment (233-425) was generously provided by the Ariens and Philippou Labs of the University of Leeds, UK. This plasmid was transformed into *E. coli* BL21 cells. Sterilized ZYP.08G medium (non-inducing) was prepared containing the following reagents (5mL total volume): 4.7 mL ZY media, 5 µL of 1 M $MgSO_4$, 100 µL of 40% M glucose, 250 µL 20X NPS [Na_2HPO_4, KH_2PO_4, $(NH_4)_2SO_4$] mixed in 50 mL VWR tube. A BL-21 cell stock for Fbg αC (233-425) was added into the prechilled ZYP.08G media and subjected to incubation at 27-28^oC for 15 h at 180 rpm.

The cultured BL-21 cells were then transferred into filtered and sterilized ZYP-5052 autoinducing media containing the following reagents: 1% tryptone, 0.8% glucose, 0.5% yeast extract, 0.2% lactose, 50 mM KH_2PO_4, 1 mM $MgSO_4$, 50 mM Na_2HPO_4, 25 mM $(NH_4)_2SO_4$, and 100 µg/mL ampicillin. The culture was incubated at 37^oC at 225 rpm for 2 h. The ZYP 50x5052 media provides a very suitable growth for activation of the cultured *E. coli* BL 21 cells. Initially, the cells metabolize the limited amount of glucose

as a preferred carbon source to generate a high-density culture without inducing the expression of protein. After consuming glucose, the cells consume glycerol and lactose where lactose promotes the activation of *lac* promoters and thus induce the expression of RNA polymerase. This expression leads to transcription of the cloned DNA and translation into protein. Optical density (OD) was monitored after the 2h period and when the OD reached within 0.5 to 0.8, the heat was turned off, and the culture was subjected to continuous incubation at 170 rpm for a 22h period at RT. A small volume (1 mL) of the culture was also kept and stored in -20^{o}C for SDS PAGE analysis.

Cultures were then collected and subjected to centrifugation at 8000 rpm in a JA-10 rotor to obtain the biomass. The supernatant was then discarded, and *E. coli* wash buffer was added to the pellets. The mixture was stirred in the cold room for about 40 min until the pellets were fully homogenized. The bacterial suspension was then transferred evenly into four 50 mL conical tubes and centrifuged at 5000 rpm (4^{o}C for 30 min) using an Allegra centrifuge with a SLC-4000 rotor. The supernatant was properly discarded. The biomass pellets were stored at -20^{o}C for SDS PAGE analysis.

Recombinant protein extraction and purification

The frozen biomass pellets were added to cold 50 mL *E. coli* lysis buffer (TBS) containing 50 mM Tris acetate and 150 mM NaCl (pH 7.4). The resuspension was done by vortexing the pellets vigorously and transferring them into a small beaker with a stirrer. Protease inhibitors were then added: 40 mg Benzamidine chloride, Aprotinin (60 µL, 2 mg/ mL), pepstatin A (1 mM in isopropanol), and leupeptin (130µL, 40 mM). This step was subsequently followed by the addition of 60 mg lysozyme and after 2 min, 30 mg SDC

(Sodium deoxycholate) in 1 mL of the allotted buffer was added which made the lysate viscous. In addition, 3 mL of 20% Triton X-100 and 200 µL of $MgSO_4$ were added. DNase (10 mg/mL) and RNase (10 mg/mL) were the last reagents added. Finally, the lysate was transferred into the cold room for incubation and continuous stirring for 1.5-2h. The lysate was then subjected to centrifugation using a Beckman JA-20 rotor at 13,500 rpm (equilibrated at 4ºC) for 20-25 min and filtered by vacuum filtration using a 0.45 µM filter. The lysate was then filtered using a 0.2 µm membrane filter and the clarified lysate was loaded onto a 1 mL capacity GST-trap affinity column attached to a Fast protein liquid chromatography system (Akta Prime). Tris buffered saline (TBS) was used to wash the column until the absorbance reached the baseline at 280 nm. The fibrinogen αC was cleaved off from the GST-tag via in-column digestion using 100-200 µg HRV3C protease incubated with the resin GST-Fbg αC at 4ºC for 18 h. TBS was then employed to elute the Fbg αC. To release the GST from the column, TBS with 20 mM reduced glutathione was applied. Using a UV/VIS spectrophotometer, the absorbances of the eluted Fbg αC fractions were measured at 280 nm and the concentration was determined using an extinction coefficient of 12571 M^{-1} cm^{-1} for αC WT. Finally, the purity of the Fbg αC fractions were checked by SDS PAGE (4% stacking gel and 15% resolving gel). The said fractions were then stored at -80ºC.

Monodansylcadaverine (MDC) incorporation assay

Nonproteolytic activation - Monovalent and divalent ions

A. FXIII A_2 activation mixture using cations in the presence of 4 mM Ca

Nonproteolytic activation of FXIII A_2 to FXIII-A^o was performed using an activation mixture (20 µL) containing 2µM rFXIII A_2, 50 mM Tris acetate buffer pH 7.4, a

monovalent ion/divalent ion (LiCl, NaCl, KCl, CsCl, ChCl, TMAC, $MgCl_2$, Li_2SO_4, $MgSO_4$) and 4 mM $CaCl_2$. This 4 mM Ca^{2+} is expected to target the major Ca^{2+} binding site (Cab1) on FXIII-A. For NaCl, KCl, and $C_5H_{14}NO.Cl$ (Choline chloride or ChCl), the monovalent cation concentrations tested were 150 mM, 350 mM, 425 mM, and 500 mM. For TMAC (Tetramethylammonium chloride) and the rest of the ions (LiCl, KCl, CsCl, Li_2SO_4, $MgCl_2$ and $MgSO_4$), a single 350 mM final concentrations of monovalent/divalent cation was used in the activation reactions. The mixture was incubated for 1h at 37ºC.

A. FXIII A_2 activation mixture using 100 mM Ca

The concentration of calcium in Tris acetate buffer (pH 7.4) was raised to 100 mM and no other monovalent or divalent ion was added. The mixture was incubated for 1 h at 37ºC. The 100 mM Ca^{2+} should be able to fill all Ca^{2+} binding sites (Cab1, 2 and 3) on FXIII.

2. Reaction mixture

A. FXIII reaction mixture using cations in the presence of 4 mM Ca

A volume of 8 μL of the activation mixture was added to the FXIII reaction mixture giving a final volume of 160 μL and final concentrations of the reaction components: 100 nM FXIII, 4 mM Ca, 5 μM Fbg αC (233-425), 350 mM monovalent or divalent ions and 1 mM MDC all in Tris Acetate buffer. The reaction mixture had been equilibrated at 37ºC prior to the addition of the activation mixture.

B. FXIII A_2 Reaction mixture using 25 mM $CaCl_2$

A transglutaminase assay that monitors the ability of the different activated forms of FXIII-A^o to crosslink fluorescent MDC into the reactive Qs of Fbg αC (233-425) was employed. The transglutaminase dependent reaction catalyzes isopeptide bond (γ-glutamyl-ε-lysyl) formation. To assess the extent of crosslinking at varying time points (2, 5, 7, 10, 15, 30, 45 min), 20 μL of the reaction mixture were added to a tube containing 7 μL of 5X reducing buffer (10% SDS, 0.5 M Tris pH 6.8, 40% glycerol, 0.02% bromophenol blue, and 5% β-mercaptoethanol) for quenching. The time points were then further quenched and prepared for SDS analysis by boiling each sample for 1 minute.

The quenched MDC crosslinking samples were run on SDS PAGE gels under reducing condition (4% stacking gel and 15 % resolving gel). The sample volume was 20 μL per well. Prior to loading, the samples were vortexed and centrifuged shortly to get well homogenized sample mixtures. Molecular weight marker (Precision plus, Biorad) and the positive control, 5 μM of N, N-dimethylated β-Casein crosslinked to MDC with FXIII-A*, was also loaded in the gel. Using a BioRad Geldoc system XR^{TM}, UV light was used for viewing the fluorescent bands. The gel was then stained with Coomassie blue-G250 so that the protein amounts could be quantified and later normalized across different lanes. After destaining the gel, an image was recorded of the protein bands under white light using the same BioRad gel documentation system.

β-Casein and monodansyl cadaverine crosslinking as positive control

Activation mixture

N,N dimethylated β-Casein, is a historical FXIII substrate derived from bovine milk, and it was used to obtain a crosslinking positive control sample. In this study, β-Casein serves as the glutamine donor instead of the fibrinogen. The positive control sample (β-CaseinxMDC) was prepared by using proteolytically activated FXIII-A*. For the proteolytic activation of FXIII A_2 to FXIII-A*, the activation components with their final concentrations were: 4 mM $CaCl_2$, 58 nM recombinant human thrombin (rhIIa), and 2 μM FXIII A_2 all mixed in Tris acetate buffer (pH 7.4). This activation mixture was then incubated at 37^{o}C for 30 min. Phe-Pro-Arg Chloromethyl ketone (PPACK) uses a D-Phe instead of a typical L-Phe. A 1 μL of PPACK (190 nm) was added to inhibit thrombin.

Reaction mixture

A volume of 24 μL FXIII-A* activation mixture was added to the reaction mixture (4 mM $CaCl_2$, 5 μM β-casein, and 1 mM MDC) making its total volume be 500 μL. This mixture was then incubated for 6 min and subsequently added with 175 μL of 5x reducing buffer for quenching and boiled for 5 minutes before being aliquoted in 600 μL microfuge tube and stored at -80^{o}C. For SDS PAGE runs, 20 μL of this positive control were loaded into the gel (4% stacking gel and 15% resolving gel) and run under reducing conditions.

Quantification and Statistics of MDC results

ImageJ 1.53e (NIH) was used to quantify the fluorescent and white light protein bands generated from crosslinking of MDC-Fbg and the MDC-β-Casein. The exposure time was taken at 64s under UV light. Three replicates were performed per each sample tested. BioRad Molecular weight marker (Precision Plus Protein^{TM}) was used to monitor the MW of the crosslinked MDC-Fbg and the β-Casein-MDC products. Each MDC-Fbg band generated per time point was quantified against % fluorescent intensity of the control (MDC-β-Casein) and normalized with the total protein signal from the Coomassie-stained bands. Using the normalized fluorescence intensity data from three replicates, a graph was plotted versus time (min).

Finally, using GraphPad Prism 9.0, a pseudo first-order kinetic fit was generated using the equation model [$Y=Y_o + (Plateau - Y_o) *(1- exp(-Kx)$]. The Y represents the fluorescence intensity (with FXIII), Y_o the initial zero time point (no FXIIIA^o), K the rate constant, Y the value at infinite time, and x represents the time in minutes. Moreover, One-way ANOVA using GraphPad Prism 9.2.0 was performed to determine whether there is significant difference in the fluorescence intensities among different concentrations and different ions tested. A probability value set at $P<0.05$ is automatically considered significant.

Calculation of ionic strength

Ionic strength, abbreviated, μ, is defined as the total concentration of all ions in a solution. Equation is given by $\mu = \frac{1}{2}\sum_{i=1}^{N} C_i \times Z_i^2$ where C_i represents the molar concentration of cationic/anionic species and Z_i, the charge of cationic/ anionic species (95).

RESULTS

In this study, nonproteolytic activation of FXIII A_2 to FXIII-A^o was first achieved by incubating the FXIII A_2 with different monovalent ions (LiCl, NaCl, KCl, or CsCl) in the presence of 4mM $CaCl_2$ at 37^{o}C for 60 min. FXIII-A^o transglutaminase activity was then measured in terms of the normalized increase in gel-based fluorescence intensities occurring as fluorescent monodansylcadaverine (Lysine mimic) was crosslinked to fibrinogen αC (233-425) as a glutamine donor (Fig. 10).

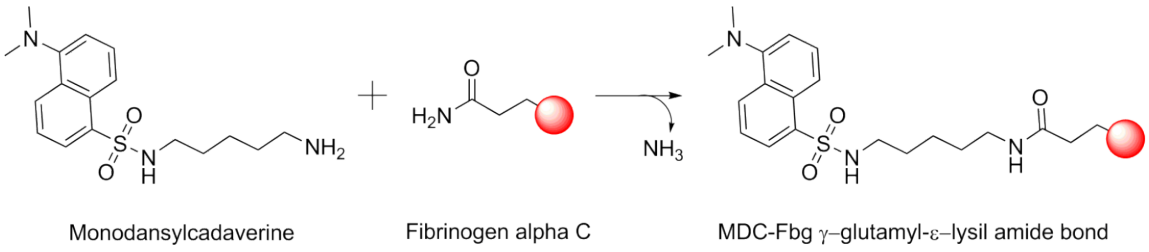

Figure 10 Mechanism of isopeptide bond formation between reactive "Gln" of Fbg αC (233-425) and "Lys" substrate MDC.

The salts tested in the present study were monovalent inorganic chloride-based salts (LiCl, NaCl, KCl, and CsCl), monovalent and divalent sulfate-based salt (Li_2SO_4 a and $MgSO_4$), monovalent organic chloride-based salts (TMAC and ChCl), divalent chloride-based salts ($CaCl_2$ and $MgCl_2$). Different periodic properties of these ions are proposed to influence FXIII activity. The table below shows the ionic radii (in pm) and ionic strengths (μ, in M) of the cations tested.

Table 2. Summary of periodic properties (Ionic radii and ionic strengths) of selected monovalent and divalent salts.

<table>
<tr><td></td><td colspan="8">Monovalent and Divalent ions</td></tr>
<tr><td>Periodic properties</td><td>Li^+</td><td>Na^+</td><td>K^+</td><td>Cs^+</td><td>Mg^{2+}</td><td>Ca^{2+}</td><td>TMA^+</td><td>Ch^+</td></tr>
<tr><td>Cationic radius (pm)</td><td>167</td><td>190</td><td>243</td><td>298</td><td>72</td><td>194</td><td>322</td><td>280</td></tr>
<tr><td rowspan="4">Ionic strength, μ, (M)</td><td rowspan="2">0.35[a1]</td><td>0.15[b1]</td><td>0.15[c1]</td><td rowspan="4">0.35[d]</td><td>1.05[e1]</td><td rowspan="4">1.05[f]</td><td rowspan="4">0.35[g]</td><td rowspan="4">0.35[h]</td></tr>
<tr><td>0.35[b2]</td><td>0.35[c2]</td><td rowspan="2">1.4[e2]</td></tr>
<tr><td rowspan="2">1.05[a2]</td><td>0.42[b3]</td><td></td></tr>
<tr><td>0.50[b4]</td><td>0.50[c3]</td></tr>
</table>

a1 = 350 mM LiCl, a2 = 350 mM Li_2SO_4, b1 = 150 mM NaCl, b2= 350 mM NaCl, b3 = 415 mM NaCl, b4 = 500 mM NaCl, c1 = 150 mM KCl, c2= 350 mM KCl, c3 = 500 mM KCl, d = 350 mM CsCl, e1= 350 mM $MgCl_2$, e2 = 350 mM $MgSO_4$, f = 100 mM $CaCl_2$, g = 350 mM TMAC, h = 350 mM ChCl.

MDC incorporation assay: FXIII activation using NaCl with 4 mM Ca

The NaCl concentrations used ranged from a physiological concentration of 150 mM NaCl to the supraphysiological concentrations of 350 mM, 425 mM, and 500 mM NaCl, all in the presence of 4 mM $CaCl_2$. The fluorescent bands, products of MDCxFbg αC crosslinking, were recorded under UV light. The Coomassie blue stained gels, recorded under white light, contain bands representing the amount of protein loaded in each of the lanes of the gel. As shown in Fig. 11A, as the NaCl concentrations increased, the fluorescent crosslinking bands also increased in intensity over time.

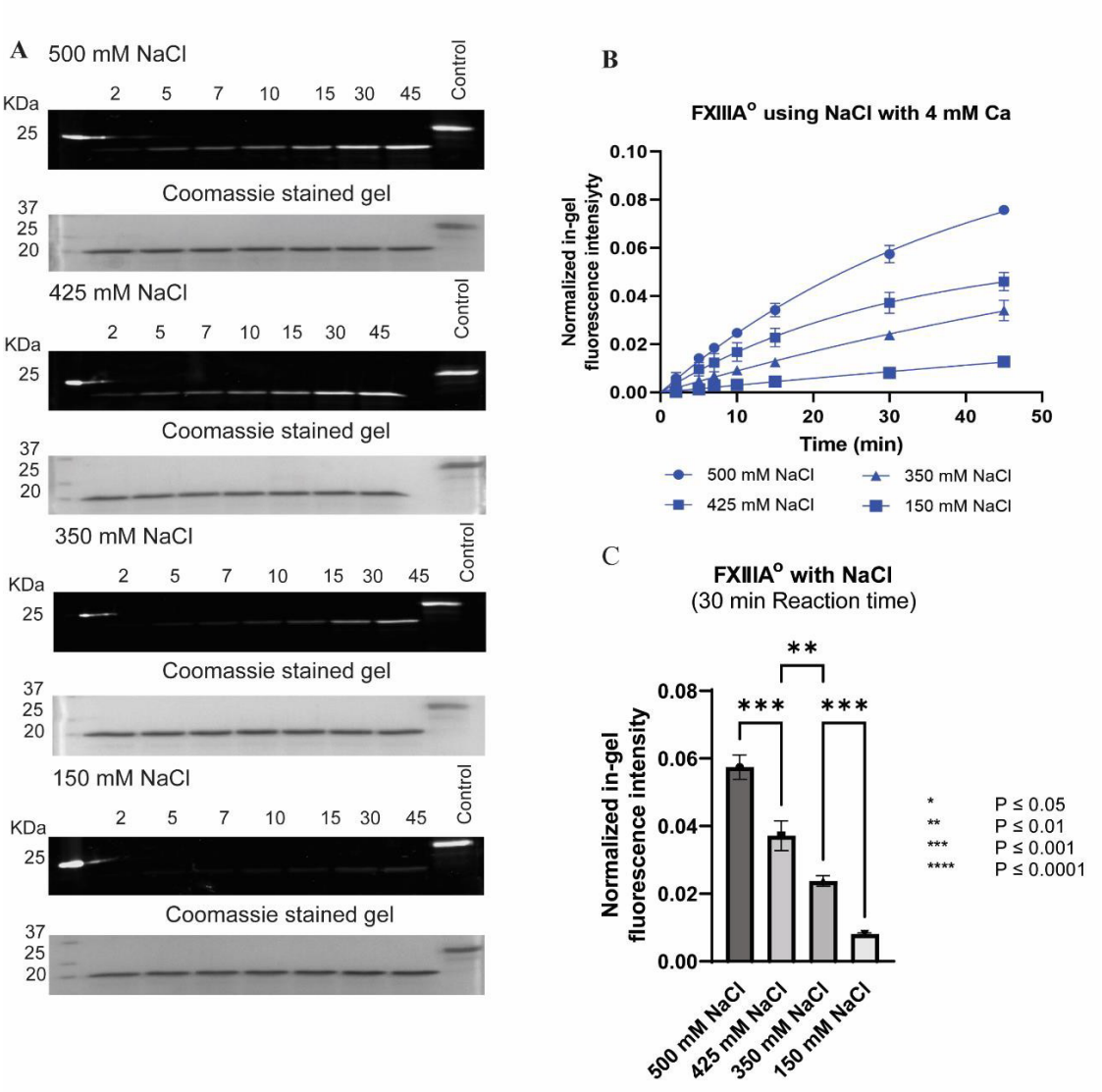

Figure 11. MDC assay results of FXIII A_2 with NaCl. A) Gel images of fluorescent MDCxFbgαC (top) and Coomassie blue stained gel (bottom) B) Plot of normalized in-gel fluorescence intensity C) Bar graph of normalized in-gel fluorescence intensity at 30 min

As graphically shown in Fig 11B, NaCl helps promote an increase in MDC incorporation into Fbg αC (233-425) over time in the presence of 4 mM $CaCl_2$. At the 30 min time point, there is a significant difference in the crosslinked FLR intensity for all the NaCl concentrations relative to 500 mM NaCl. The 500 mM NaCl reactivity is 1.5-fold higher at 30 min than 425 mM NaCl, 5-fold higher than 350 mM NaCl, and 10-fold higher

than 150 mM NaCl. In summary, the MDC incorporation into Fbg αC increases with increasing NaCl concentration which may provide a suitable additional electrostatic surface environment during nonproteolytic FXIII activation.

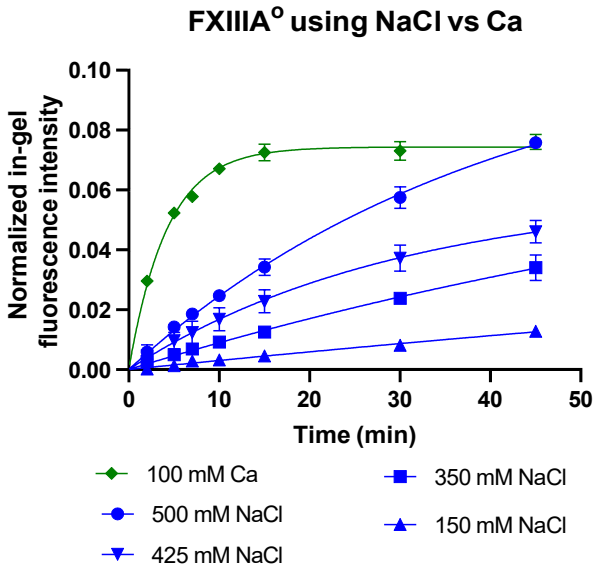

Figure 12. Plot of Normalized in-gel fluorescence intensity using FXIII-A° with NaCl vs FXIII-A° with $CaCl_2$

Fig. 12 shows how FXIII activated at the higher 100 mM $CaCl_2$ reaches a plateau for MDC incorporation at a much faster rate (K) than the NaCl series (all with 4 mM $CaCl_2$). A large increase in MDC incorporation rate into Fbg αC (233-425) is observed using 100 mM Ca^{2+} versus a combination of NaCl (150-500 mM) and 4 mM $CaCl_2$. The 500 mM NaCl condition achieved a similar final fluorescence response as that of 100 mM $CaCl_2$ but required longer time points. Furthermore, the rate constant (K) of NaCl increased from 150 mM to 425 mM but slowed down slightly at 500 mM. Faster plateau formation was observed at 425 mM NaCl. At 150 mM, the K is very low and plateau formation is also not observed by 45 min (See Table. S1 in the supplemental table).

MDC incorporation assay: FXIII activation using KCl

Three concentrations of KCl were tested (150 mM, 350 mM and 500 mM) with 4 mM Ca to evaluate the effect of these varying concentrations of monovalent ion on FXIII's transglutaminase activity. Fig. 13a shows the SDS PAGE gel images of the MDC assay and then Fig. 13b the plot of fluorescence intensity with increasing KCl concentrations as a function of time.

Similar to the fluorescence intensity trend of 150 mM to 500 mM NaCl, Fig. 13a shows that increasing KCl concentrations increases transglutaminase activity for FXIII-catalyzed crosslinking of MDC into Fbg αC (233-425). Furthermore, the plateau formation with 500 mM KCl clearly displays a much faster (K) rate to reach a crosslinking plateau than the 350 mM (0.015 min^{-1} vs 0.08 min^{-1}) whereas the 150 mM KCl does not show plateau formation at all. This effect is similar to the fluorescence intensity response exhibited by 150 mM NaCl. Increasing the KCl concentration from 350 to 500 increased the FLR intensity by about ~1.5-fold and ~3.0-fold when elevated from 150 mM to 500 mM KCl.

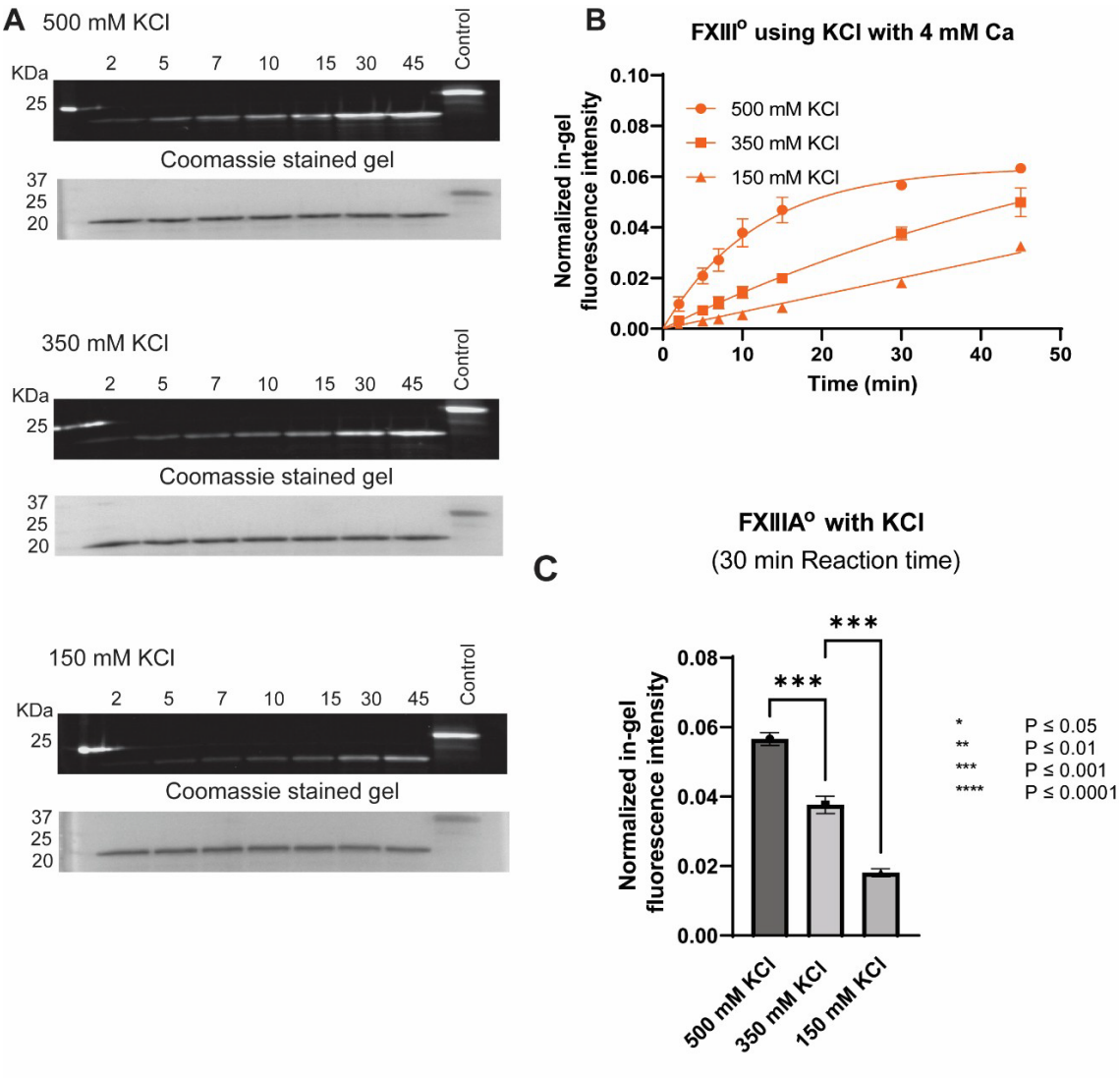

Figure 13. A. MDC assay results of FXIII A_2 with KCl. A) Gel images of fluorescent MDCxFbgαC (top) and Coomassie blue stained gel (bottom) using FXIII-$A^{o,KCl}$ B) Plot of normalized in-gel fluorescence intensity C) Bar graph of normalized in-gel fluorescence intensity at 30 min reaction time.

Comparing FXIII activation using KCl and NaCl

Both NaCl and KCl are physiologically present intra and extracellularly. Although NaCl effects have been well studied in coagulation systems (96,97), KCl is another potential ion of interest to study as it is also the most abundant cation intracellularly. Starting with the lowest concentration, 150 mM KCl and 150 mM NaCl show no plateau

formation even at longer reaction periods, but the final transglutaminase activity is higher for KCl than NaCl. For the 350 mM concentrations, KCl still promoted higher FXIII crosslinking activity than NaCl. At 500 mM concentration, KCl and NaCl both increased the formation of the MDC-Fbg product by the same amount at the 30 min reaction period, but KCl reached the fluorescence plateau earlier than 500 mM NaCl and obtained a much higher rate constant (K) at 500 mM and 350 mM concentrations. In this case, NaCl-promoted transglutaminase activity takes longer time to saturate, and consequently, will have a higher plateau value.

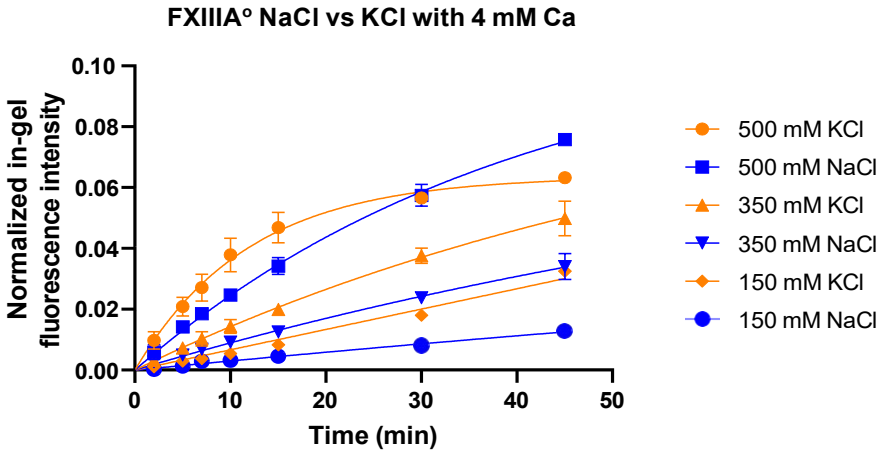

Figure 14. Plot of Normalized in-gel fluorescence intensity using FXIII-A° with KCl vs FXIII-A° with NaCl

FXIII activation using 350 mM monovalent cations (LiCl, NaCl, KCl, and CsCl)

Results from the transglutaminase studies done in the presence of Na^+ and K^+ led to interest into examining two other Group 1 cations, Li^+ and Cs^+. For this monovalent cation series, the ionic radii included: Li^+ (180 pm), Na^+ (227 pm), K^+ (280 pm), Cs^+ (343 pm). Among these Group 1 cations, only NaCl has been extensively studied in the past for FXIII transglutaminase activity (48,63). With these four-cation series, trends in MDC incorporation into Fbg αC were examined relative to cationic sizes (180 – 343 pm). In the

MDC assays, all the monovalent cations had the same concentration (350 mM). Figure 15 displays all the fluorescent bands generated in the crosslinking of MDC and Fbg αC WT in SDS PAGE gels. To correlate these gel results, a plot was created to show the different responses of these ions in terms of their normalized fluorescence intensities that reflect increases to FXIII-A^o activity.

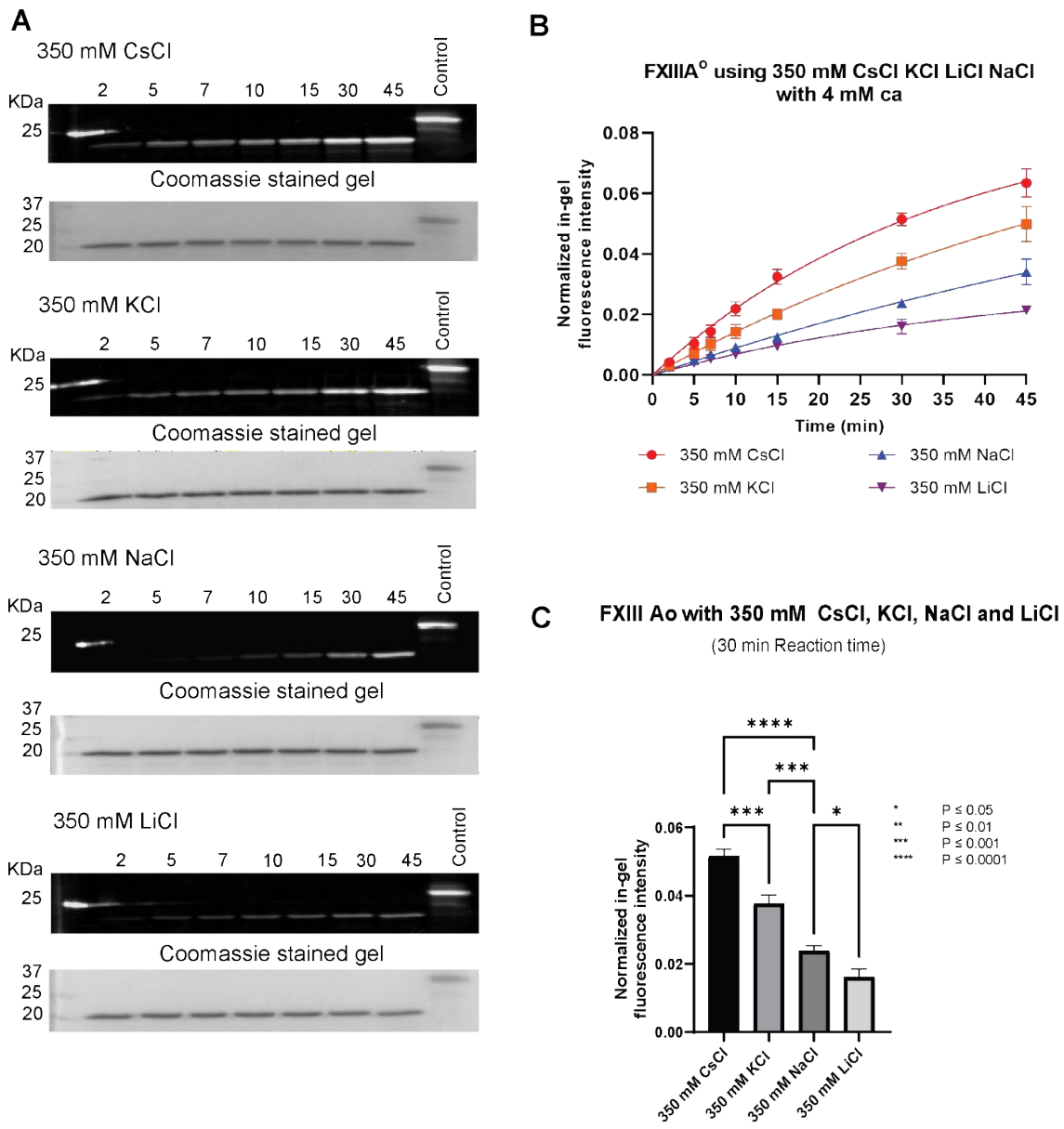

Figure 15. A. MDC assay results of FXIII A_2 with monovalent ions. A) Gel images of fluorescent MDCxFbgαC (top) and Coomassie blue stained gel (bottom) using FXIII-$A^{o,LiCl}$, FXIII-$A^{o,NaCl}$, FXIII-$A^{o,KCl}$ and FXIII-$A^{o,CsCl}$ B) Plot of normalized in-gel fluorescence intensity C) Bar graph of normalized in-gel fluorescence intensity at 30 min reaction time.

Comparing the transglutaminase activities of these monovalent ions after 30 min reaction period, the FLR intensity of CsCl surpassed KCl by about ~1.4-fold (0.052±0.002 vs 0.038±0.003). There is an even higher difference between CsCl vs NaCl, with an increase in fluorescence intensity of about ~2.0 fold (0.052±0.0025 vs 0.024±0.0001) with

P≤0.0001. The highest significant difference that was observed in terms of FXIII activity was between CsCl and LiCl by ~4.0 fold (0.052±0.0025 vs 0.038± 0.0015) at P≤0.001. Meanwhile, there was a ~2-fold increase in fluorescence intensity going down the group from Li^+ to Na^+. In summary, increasing ionic radii of the Group 1 cations, led to increases in the FXIII-A^o transglutaminase activity for crosslinking MDC into Fbg αC (233-425). For the rate constants generated by these ions, CsCl obtained the highest crosslinking rate value (0.029 min^{-1}) followed by LiCl (0.025 min^{-1}), KCl (0.015 min^{-1}), and NaCl (0.010 min^{-1}) (See Table. S1 in the supplemental table).

FXIII activation using 350 mM monovalent cations $LiCl_2$ vs Li_2SO_4

The effect of monovalent cationic salts containing Cl^- anions were already evaluated through the MDC incorporation assay. In this study, the effect of divalent SO_4^{-2} was assessed using Li_2SO_4. In physiological intracellular and extracellular environments, SO_4^{-2} is also present, making this divalent anion also valuable to evaluate the effect on FXIII-A transglutaminase activity. Based on the MDC-Fbg crosslinking by FXIII-A^o LiCl exhibited the lowest transglutaminase activity of the Cl^- containing monovalent ions. Surprisingly, Li_2SO_4, exceeded the crosslinking ability of FXIII-A^o + LiCl by about ~3.6 fold (0.057 min^{-1} vs 0.016 min^{-1}) after 30 min reaction time with p≤0.001 (See Fig. 16). Overall, Li_2SO_4 which has a higher ionic strength ($\mu = 1.05$) than LiCl ($\mu = 0.35$) exhibited a much higher transglutaminase activity than LiCl and even Na^+ and K^+. Interestingly, Li_2SO_4 promoted similar fluorescence transglutaminase activity as CsCl, which has the largest ionic size among the four monovalent ions tested. In summary, Li_2SO_4 promoted nonproteolytic FXIII activation at a level comparable to CsCl.

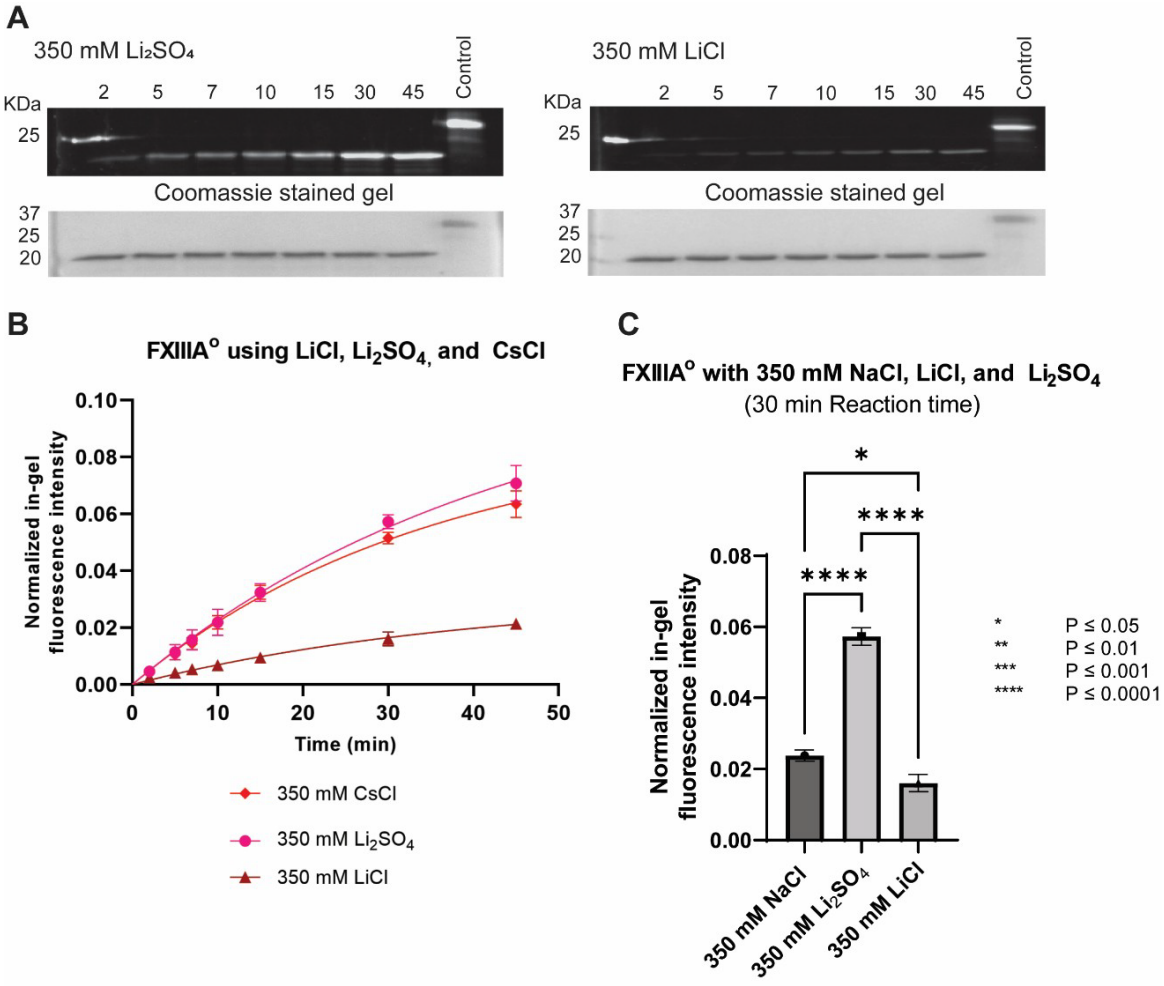

Figure 16. A. MDC assay results of FXIII A_2 with NaCl, LiCl, and Li_2SO_4. Gel images of fluorescent MDCxFbgαC (top) and Coomassie blue stained gel (bottom) using FXIII-$A^{o,LiCl}$, FXIII-$A^{o,Li2SO4}$ and FXIII-$A^{o,CsCl}$ B) Plot of normalized in-gel fluorescence intensity C) Bar graph of normalized in-gel fluorescence intensity at 30 min reaction time.

FXIII activation using organic monovalent salts ChCl and TMAC

Organic salts choline chloride (ChCl) and tetramethylammonium chloride (TMAC) were also compared in terms of their effects on transglutaminase activity of FXIII. Both compounds contain a positively charge nitrogen center covalently bonded with four carbons. The only difference in the structure of these two quaternary salts is that the

nitrogen center in TMAC contains 4 methyl groups but ChCl contains 3 methyl groups and one hydroxyl group.

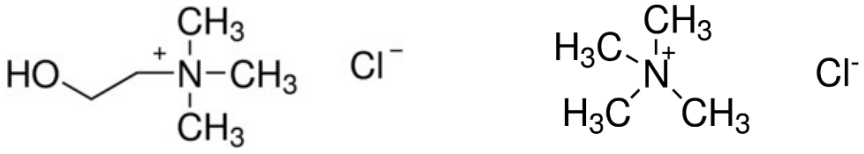

Tetramethylammonium chloride Choline chloride

Figure 17. Structures of organic salts Tetramethylammonium chloride (TMAC) and Choline Chloride (ChCl)

FXIII-A^{o} using 350 mM ChCl revealed a much lower rate of MDC incorporation into the Fbg αC fragment as compared to 350 mM NaCl by about ~3.0 fold after a 30 min reaction period (See Fig. 18b). These organic salt compounds can help probe whether FXIII contains a distinct Na^{+} binding site. Unlike the blood coagulation thrombin that has a strict requirement for Na^{+} binding (98), FXIII can still use the cationic and ionic strength properties of TMAC and ChCl to perform some crosslinking activity although at a slower rate than NaCl. The larger ionic size of Ch^{+} (329 pm) is not as well accommodated as the smaller TMA^{+} (280 pm).

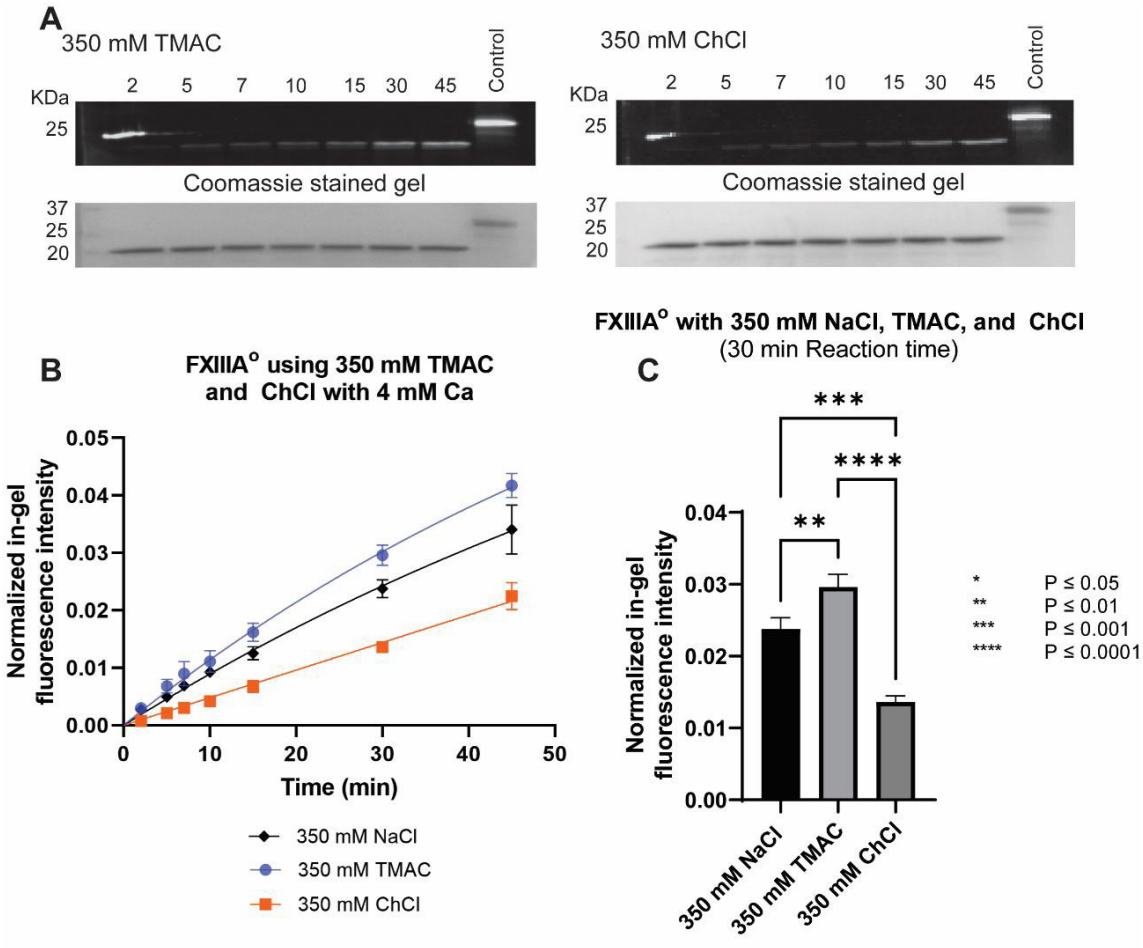

Figure 18. A. MDC assay results of FXIII A_2 with TMAC and ChCl. A) Gel images of fluorescent MDCxFbgαC (top) and Coomassie blue stained gel (bottom) using FXIII-$A^{o,NaCl}$, FXIII-$A^{o,TMAC}$ and FXIII-$A^{o,ChCl}$ B) Plot of normalized in-gel fluorescence intensity C) Bar graph of normalized in-gel fluorescence intensity at 30 min reaction time.

When comparing the result of ChCl with other monovalent ions tested, it appears that ChCl overlaps with LiCl which suggests that they have similar abilities to support FXIII activity (Fig. 19).

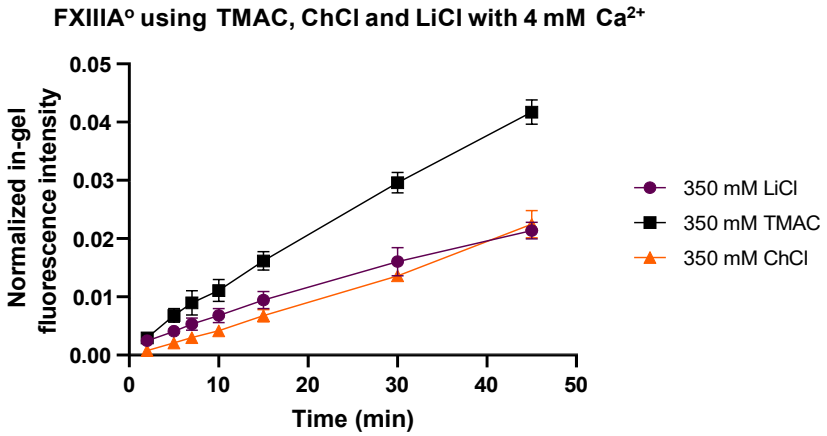

Figure 19. Plot of Normalized in-gel fluorescence intensity using FXIII-$A^{o,TMAC}$, FXIII-$A^{o,ChCl}$ and FXIII-$A^{o,LiCl}$

FXIII A activation using Divalent ions 350 mM $MgCl_2$ and $MgSO_4$

Studies with Group 1 monovalent ions demonstrated that these ions could increase FXIII activity in a manner directly proportional to the ionic sizes of these ions. Moreover, the fluorescence intensities with Li_2SO_4 exceeded that of LiCl making SO_4^{-2} also a good target to evaluate its effect on FXIII activation. Li^+ is the smallest ion (167 pm) in the Group 1 whereas in Group 2, physiological Mg^{2+} also has smaller ionic radius (72 pm). Since there was difference in the transglutaminase activity of FXIII when LiCl and $LiSO_4$ were tested, now $MgSO_4$ was also compared with $MgCl_2$.

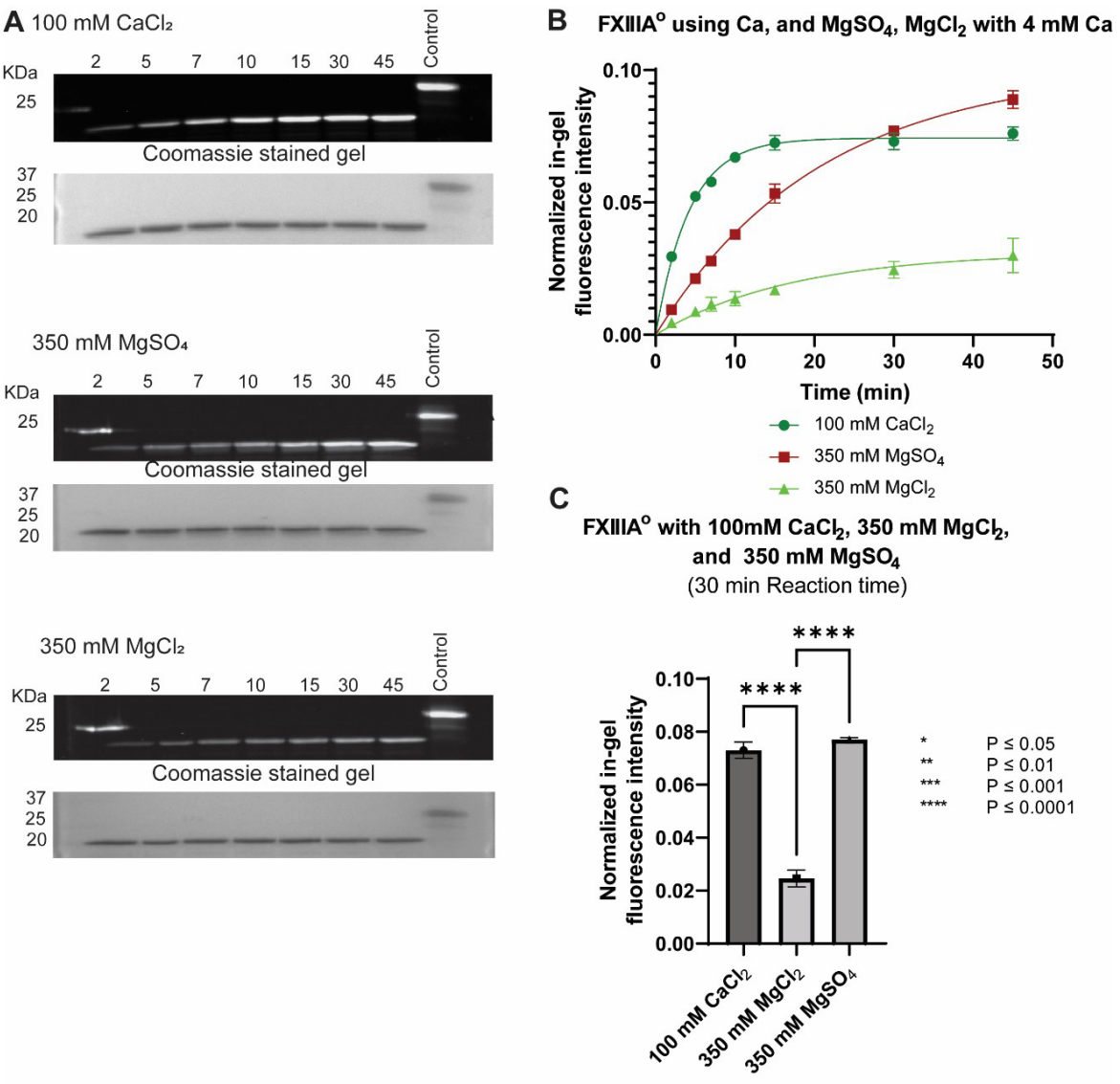

Figure 20. A. MDC assay results of FXIII A_2 with $CaCl_2$, $MgCl_2$, and $MgSO_4$. A) Gel images of fluorescent MDCxFbgαC (top) and Coomassie blue stained gel (bottom) using FXIII-$A^{o,\ CaCl2}$, FXIIIA$^{o,\ MgCl2}$ and FXIII-$A^{o,MgSO4}$ B) Plot of normalized in-gel fluorescence intensity C) Bar graph of normalized in-gel fluorescence intensity at 30 min reaction time.

$MgSO_4$ turned out to be a more-preferred divalent salt than $MgCl_2$ for nonproteolytic FXIII activity in the presence of 4 mM $CaCl_2$. The $MgSO_4$ increased the MDC incorporation amount by about 3-fold at the 30 min reaction time point relative to $MgCl_2$ (0.078±.00078 vs 0.026±0.0032) at P≤0.0001. Furthermore, $MgSO_4$ also exhibited the highest fluorescence intensity among all the ions tested (except 100 mM $CaCl_2$) for

MDC incorporation assays (See Fig. 20b). The $MgCl_2$ generated a higher rate constant (K) than $MgSO_4$ (0.048 vs 0.057). In addition, there was no significant difference in the fluorescence intensity at the 30 min reaction time between $CaCl_2$ and $MgSO_4$. Also, saturation forms faster for $MgCl_2$ (0.0261 to 0.040) than $MgSO_4$ (0.097 to 0.105). Moreover, in terms of rate constant (K), Ca^{2+} generated the highest value which is ~4.5 fold higher than $MgCl_2$ and $MgSO_4$ (See Table. S1 in the supplemental table). The ionic strength of $MgSO_4$ is 1.4 which is much higher than that of $MgCl_2$ which is only 1.05. The sulfate containing salts of Li^+ and Mg^{2+} revealed a relatively much higher transglutaminase activity than LiCl and $MgCl_2$.

Discussion

It is well established that cellular FXIII undergoes nonproteolytic activation transitioning from a zymogen dimer (FXIII A_2) to active monomer (FXIII-A^o) at high mM calcium concentration. Before activation, the cytoplasmic calcium level is only 0.0001 mM (79). This calcium level can become elevated to a supraphysiological concentration following release of Ca^{2+} by the endoplasmic reticulum (99) in bone marrow cells. The cytosolic environment not only contains Ca^{2+}, in fact, K^+ (150 mM) is the dominant ion followed by Mg^{2+} (17-20 mM). Several other ions (Cl^-, Na^+, SO_4^{2-}, etc.) also exist (see Table 1). In addition, some cations may be present in the human body due to medications such as Li^+ (100) for psychiatric medicine or Cs^+ for cancer treatment (101).

The research project described herein first examined the Group 1 cations Li^+, Na^+, K^+, and Cs^+. In most assays monitoring for FXIII transglutaminase activity, the Tris-Acetate buffer environment includes 150 mM NaCl which is the physiological concentration in plasma in the presence of Ca^{2+}. NaCl effects have previously been demonstrated to help increase FXIII activation/activity (48,63). Interestingly, K^+ levels are higher than Na^+ in the intracellular platelet environment due to the Na^+K^+ ATPase pump that maintains low Na^+ concentration inside the cell (102). The FXIII B_2 subunits in plasma help prevent premature activation of catalytic FXIII A_2 in the presence of Na^+ and K^+ (48).

Polgar et al. suggested that NaCl or KCl could be used as an ancillary ion to support enzymatic activity (48), but no assay data were presented for KCl. The paper also did not state which of these cations promoted higher transglutaminase activity. The FXIII catalyzed MDC-incorporation assays used in the present study employed 150 – 500 mM cationic salts in the presence of 4 mM $CaCl_2$. Based on an estimated K_D of 100μM, the 4

mM Ca^{2+} should occupy the main FXIII calcium binding site Cab1(63). For the NaCl and KCl studies, the higher the salt concentration the more FXIII transglutaminase activity was observed which also suggests more conversion to active monomeric forms ($FXIIIA^{o}$) has been achieved (60).

One of the major differences between Na^+ and K^+ is their ionic size. K^+ with a larger ionic radius (243 pm) supported higher transglutaminase activity than Na^+ (190 pm). Cationic ionic radius may affect the electrostatic protein surface of FXIII. Moreover, both Na^+ and K^+ showed increased MDC incorporation when ionic strengths (μ) of both ions increased from 0.15 M to .42 M. This increase in cationic concentration combined with constant low mM Ca^{2+} concentration suggested that Na^+ and K^+ supported Ca^{2+} in FXIII and substrates interactions. For two other monovalent Cl^--based salts (LiCl and CsCl), 350 mM LiCl (167 pm) exhibited the lowest MDC incorporation rate whereas the larger ionic 350 mM CsCl (298 pm) promoted the highest incorporation rate exceeding all the other monovalent ions tested. Overall, the order of promoting reactivity matched the changes in ionic radius with $Cs^+ > K^+ > Na^+ > Li^+$.

The cationic salts examined were all Cl^- based. The focus could therefore be on the cations since the anion Cl^- has very low or no interaction with protein surfaces (103). The organic salts ChCl and TMAC were also probed. These salts could support FXIII transglutaminase activity, but the rates of MDC incorporation into Fbg αC (233-425) were much slower than Na^+.

Current studies also explored the effects of the anion in the salt pairing. Li_2SO_4 generated a much higher transglutaminase activity by 3.6-fold than LiCl. Moreover, LiCl and Li_2SO_4 have different ionic strengths (at 350 mM), μ= 0.35 M and μ= 1.05 M,

respectively. The documented enhancements in crosslinking ability observed with Li_2SO_4 suggest an additional importance of ionic strength (μ) in promoting FXIII activity. Another study on the effect of anions focused on $MgCl_2$ vs $MgSO_4$. Magnesium ranks second in terms of cation concentration inside the cell and is fourth in the whole body (78). The results herein showed that $MgSO_4$ (μ=1.40 at 350 mM) generated a 3-fold higher FXIII transglutaminase activity than $MgCl_2$ (μ = 1.05 at 350 mM). Hence as observed with lithium-based salts, increasing ionic strength supported an increase in FXIII transglutaminase capability.

Importantly, 100 mM $CaCl_2$ promoted the greatest transglutaminase activity and achieved the fastest approach to a Fbg αC – MDC crosslinking reaction plateau. These effects can be correlated with more extensive calcium binding to FXIII at up to three different sites within the catalytic core domain (Cab1, Cab2, and Cab3). Previously published Molecular Dynamics simulations involving FXIII A_2 in 1 M NaCl reported that Na^+ alters the overall surface electrostatic distribution on FXIII (63). Such results suggest that FXIII does not have a distinct Na^+ binding site with a major impact on FXIII structure. The authors proposed instead that Na^+ creates disturbances in the pKa values of internal

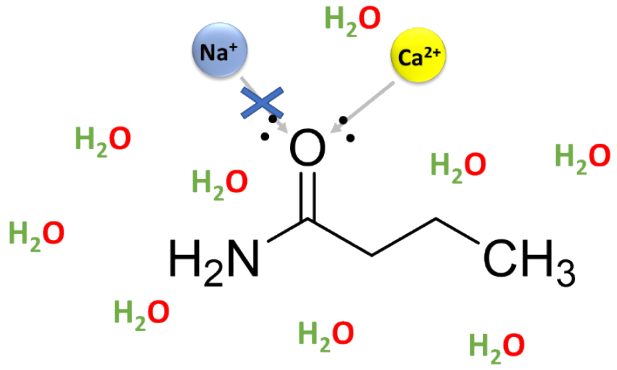

Figure 21. Metal binding to amide of protein backbone mimic (Butyramide). Calcium (Yellow), Sodium (Blue). Figure is adapted from Cremer Research group (J. Am. Chem. Soc. 2013, 135, 13, 5062–5067)

buried residues with a possible impact on domain-based interactions (63). Interestingly, the Cremer lab examined several Group 1(Alkali) and Group 2 (Alkaline) ions and found that only Ca^{2+} makes a strong interaction with the carbonyl of butyramide (Fig. 21) whereas other cations only bind very weakly (104). Similar effects are expected for the sequence of amino acids that make up FXIII A_2.

Another interesting insight to explain the role of Ca^{2+} or Na^{+} in FXIII comes from reviewing the results of amide proton to deuterium exchange studies coupled with mass spectrometry (HDX-MS). Woofter et al monitored for changes in FXIII amide proton solvent accessibility in the presence of Ca^{2+} and Na^{+} ions (105). Results in this study revealed that similar to the effect of Ca^{2+}, high mM Na^{+} helps promote exposure of FXIII amino stretches 220-230 (Q-substrate binding region), 240-270 (dimer interface), and 300-314 (FXIII active site) (105). The monovalent ion (Na^{+}) may thus be a valuable player in further supporting local and long-range conformational changes to FXIII that are otherwise dominated by Ca^{2+} binding.

Overall, for the monovalent ions, FXIII-A transglutaminase activity was found to be directly proportional to the increasing ionic radius of Group 1 cations containing Cl^{-}-based salts. In addition, increasing ionic strength in the presence of sulfate anions tended to exhibit additional benefit for FXIII activation and subsequent transglutaminase crosslinking ability. This study also highlighted the first report of the effect of LiCl, CsCl, $MgSO_4$, and Li_2SO_4 in FXIII activation. The order effect of the ions towards FXIII A_2 activation in the present study was $CaCl_2 > MgSO_4 > Li_2SO_4 \approx CsCl > KCl > MgCl_2 > NaCl$ > TMAC > LiCl > ChCl. This study provides valuable information on how specific cations and anionic species influence FXIII activation and function. Furthermore, the data could

help researchers optimize ionic conditions for examining proteolytic or nonproteolytic activation or activity of FXIII.

CHAPTER III

MONITORING INTRINSIC FLUORESCENCE OF HUMAN FXIII ACTIVATED FORMS UNDER DIFFERENT MONOVALENT AND DIVALENT SALTS

Introduction

Conformational monitoring studies of FXIII A_2 are of critical importance since this enzyme's activation is greatly dependent on a series of large protein domain rearrangements. Since FXIII A_2 contains aromatic amino acids, intrinsic fluorescence can be measured following excitation at 280 nm (106). Tryptophan (W or Trp) gives the highest quantum yield which is defined as the ratio of photons emitted, and photons absorbed (95,107). Among the three intrinsic fluorophores: Phenylalanine (F), Tyrosine (Y), and Tryptophan (W). FXIIIA contains 15 tryptophan residues (W57, W130, W164, W187, W225, W279, W292, W315, W370, W375, W379, W392, W664, W691, and W698- PDB ID: IF13) concentrated within the Cab2 and Cab3 regions located in the FXIII catalytic core domain (Fig. 22) (52,108).

Sixty percent of the FXIII Trp residues (W187, W225, W279, W292, W315, W370, W375, W379, W292) are located within the catalytic core region that is covered by β barrel 1 and 2. β barrel 1 itself contains 3 Trp residues (W664, W691, and W698) whereas no Trp residues are in β barrel 2. The β sandwich domain contains 3 Trp residues (W57, W130, and W164). Upon FXIII A_2 activation to FXIII-A^o, the catalytic core region where most of the tryptophan residues (9 Trp) are located becomes more exposed. Tryptophan

flourescence is sensitive to changes in the local environment such as the presence of ions. Fluorophores encountering less polar environment tend to increase λ_{max} and moves to shorter wavelengths whereas with high polar environment λ_{max} decreases. Neighboring protonated acidic groups quench Trp residues (109).

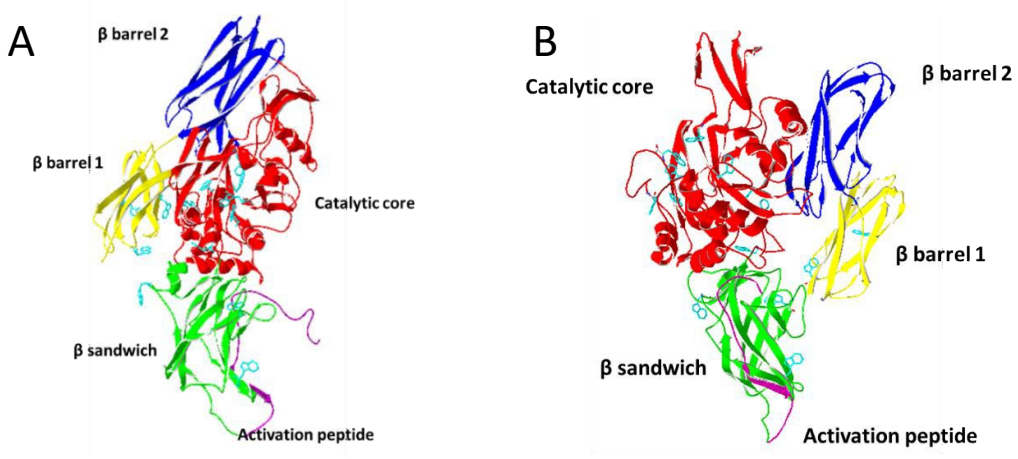

Figure 22. FXIII active and inactive structure containing tryptophan residues. FXIII showing all the 15 Tryptophan residues (sky blue) distributed on the catalytic core (9 Trp), β Barrel I (3 Trp), and β sandwich domain (3 Trp). A) FXIII A zymogen in inactive state (PDB IF13). B) FXIIIA^{o} bound with calcium + inhibitor in the trapped open conformation (PDB 4KTY).

In the crystal structure of FXIII (Fig. 22), the two β barrel domains which cover the catalytic core (where 60% of all the Trp residues are located) are largely moved away upon calcium binding as FXIII goes from an inactive to active state. The changes in the emission spectra of FXIII A_2 are an indication of a change in conformation.

In the case of FXIII A_2, fluorescent changes are proposed to monitor the movement of the β barrel domains to expose the Trp residues in the catalytic core. At high enough Ca^{2+} concentration, dissociation into monomers may also be occurring. Prior studies using AUC (analytical ultracentrifugation) and size exclusion chromatography methods have documented a shift from FXIII A_2 dimer into monomer at high calcium conditions (60).

In this study, selected monovalent and divalent salts were tested for their abilities to induce changes in the intrinsic fluorescence of FXIII A_2 which could help explain the transglutaminase results obtained from the MDC assay.

Materials and Method

Intrinsic tryptophan fluorescence study

The primary goal for the fluorescence studies was to obtain more information on the conformational changes FXIII undergoes upon activation. Previous published studies reported on FXIII fluorescence properties at room temperature in the presence of 100 mM $MgCl_2$ or 100 mM $CaCl_2$, both in borate buffer solution (61). The current study focused on the inorganic monovalent ions (LiCl, Li_2SO_4, NaCl, KCl, CsCl) and a set of divalent cations ($MgCl_2$ and $MgSO_4$). In addition, this study also monitored the effects of room temperature versus physiological temperature on the emission spectra.

Effect of monovalent and divalent cations with low calcium level

A Perkin Elmer LS 55 fluorimeter was used to evaluate the influence of different monovalent/divalent cations and incubation temperatures on the fluorescent intensity of FXIII A_2. Using the FLwinLab software, the sample was excited at 280 nm and scanned from 290 to 400 nm at a speed of 100 nm/min. For these experiments, the excitation and emission slits were adjusted to 3.5 nm.

The fluorescence emission spectrum of 500 nM FXIII A_2 in 20 mM Borate (pH 7.8) buffer served as a control sample. These FXIII concentrations and buffer environments were chosen so that conformational effects could be compared with earlier studies by Anokhin et al. 2017 (61). For the current research, a 500 μL total solution volume was prepared containing 500 nM FXIII A_2, 20 mM borate buffer (pH 7.8), and a monovalent and/or divalent cation (350 mM). Fluorescence measurements were then made in a 500 μL quartz cuvette. Emission spectra were collected at room temperatures after 10-, 20- and

30-minutes of incubation. Subsequently, a small volume of calcium stock solution was added to achieve a final concentration of 4 mM Ca^{2+}. This cation concentration would fill up Cab1, the main calcium binding site of FXIII. Fluorescence responses (at room temperature) were monitored again after 10-, 20-, and 30-mins. Immediately after these measurements, the mixture was incubated for 30 min at 37ºC, and the spectra were measured again following the same time intervals described above.

Effect of Calcium with and without 150 mM NaCl

FXIII emission spectra were collected at different calcium concentrations with and without NaCl in Borate buffer. The NaCl concentration was kept at a plasma physiological concentration of 150 mM (80,110). To perform this experiment, FXIII's fluorescence responses were examined for the following conditions: (1) 20 mM Borate buffer, 500 nM FXIII A_2 and 4 mM $CaCl_2$, (2) 20 mM Borate buffer, 500 nM FXIII A_2, and 150 mM NaCl, (3) 20 mM Borate buffer, 500 nM FXIII A_2, 4 mM $CaCl_2$, and 150 mM NaCl, (4) 20 mM Borate buffer, 500 nM FXIII A_2, 100 mM $CaCl_2$, (5) 20 mM Borate buffer, 500 nM FXIII A_2, 100 mM $CaCl_2$, and 150 mM NaCl. Furthermore, all these conditions were done at room temperature and at physiological temperature (37ºC).

Control experiment using free Tryptophan

A solution of free tryptophan was prepared by dissolving 100 mg of Tryptophan in 15 mL dI H_2O (633 mM Trp). Using 2 mL quartz cuvette, a mixture with a final concentration of 0.65 mM Trp and 350 mM salts ($CaCl_2$ and monovalent salts) was excited at 280 nm and scanned from 290 to 450 nm at a speed of 100 nm/min at room temperature. The effect of $CaCl_2$ and CsCl (8 mM, 16 mM, and 64 mM) to free Trp was also compared.

Results

FXIII A_2 in 20 mM Borate solution

The emission spectra results for FXIII A_2 in borate revealed no change in the maximum FLR intensity when the temperature was elevated from room temperature to 37ºC. The maximum intensity at room temperature was 26.9 whereas that at 37ºC was 26.5. Any subsequent changes observed would report on conformational properties influenced by particular cations, local environment polarity, and new influences from temperature.

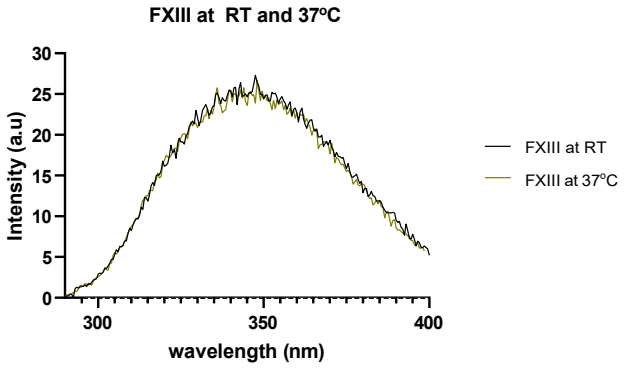

Figure 23. Emission spectra of FXIII A_2 in borate buffer at room temperature and 37ºC

FXIII A_2 with 150 mM NaCl vs 4 mM $CaCl_2$ and 100 mM $CaCl_2$

Plasma Na^+ concentration is around 142-150 mM (72) whereas the Ca^{2+} concentration typically used for *in vitro* studies is 2.5 mM Ca^{2+} . In this experiment, the effects of 4 mM Ca^{2+} vs 150 mM NaCl were probed. At 25ºC, the FLR intensity of FXIII in 150 mM NaCl exhibited a similar 24 % decrease in FLR as FXIII in 4 mM $CaCl_2$. When the temperature was elevated to 37ºC for 30 min, the maximal fluorescent intensity of FXIII+ 4 mM $CaCl_2$ decreased by 44% which is almost 2-fold greater than the effect of

150 mM NaCl which only exhibited a FLR decrease of 25.4% when the temperature was raised to 37°C. Moreover, increasing the calcium concentration up to 100 mM $CaCl_2$ resulted in an even greater decrease in maximum intensity of 66% (See Table. S2 in the supplemental table).

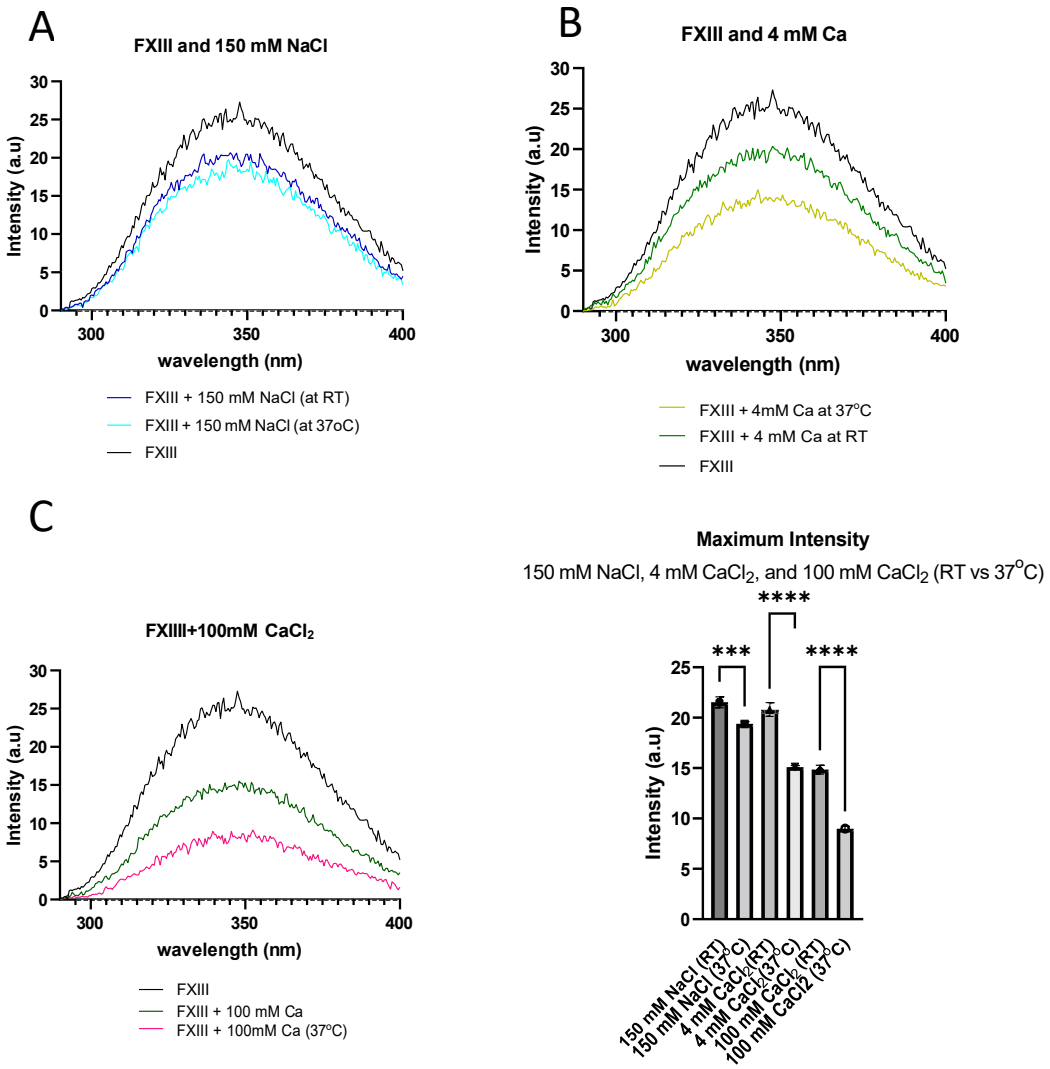

Figure 24. Emission spectra comparison of NaCl vs $CaCl_2$. A) FXIII +150 mM NaCl B) FXIII + 4 mM $CaCl_2$ C) FXIII +100 mM $CaCl_2$ all at RT and 37°C. D) Maximum intensity comparison of FXIII +150 mM NaCl vs FXIII + 4 mM $CaCl_2$ all at RT and 37°C. The asterisk represents the p values (* =P≤0.05, **=P≤0.01, *** P≤0.001, **** = P≤0.0001, ns, not significant = P≥0.05).

In previous studies by Anokhin et al 2020, 100 mM Ca alone induced full nonproteolytic activation of FXIII A_2 to FXIII-A^o as compared to 4 mM $CaCl_2$ which showed slow FXIII activation (60). As with the FLR result mentioned above, there was a larger decrease in FLR intensity for 100 mM $CaCl_2$ than the 4 mM $CaCl_2$.

Emission spectra of FXIII A_2 with Monovalent ions (LiCl, NaCl, KCl, and CsCl)

Calcium effects on FXIII A_2 conformational change have already been well studied (36,52), but reports on the effect of sodium are limited. By contrast, other cations such as LiCl, KCl, and CsCl have not yet been explored. Among the monovalent ions in Group 1 of the periodic table, MDC crosslinking studies demonstrated (chapter 2) that NaCl can act as an auxiliary ion for FXIII A_2 activation by 4 mM Ca^{2+}. From top to bottom of the Group 1 elements, Li^+ has the smallest atomic radius followed by Na^+, K^+ and Cs^+. A drop in maximal FLR intensity occurred when these monovalent cations were combined with 4 mM Ca at room temperature (LiCl-19%, NaCl-29%, KCl-30%, and CsCl-49%). When ion combinations (350 mM monovalent salt + 4 mM Ca) were incubated at 37°C, the decrease in maximal FLR became even larger: LiCl-34%, NaCl-43%, KCl-45%, and CsCl-49%. Furthermore, the Na^+ and the K^+ generated very close values at RT and 37°C. In summary, the 4 mM Ca^{2+} acts as the main driving force for conformational change and these effects increase with temperature. The monovalent ions tend to introduce additional, smaller supporting effects. Similar to MDC crosslinking assay, the decrease in maximum intensity increased in percentage as ionic size of the monovalent ions increased.

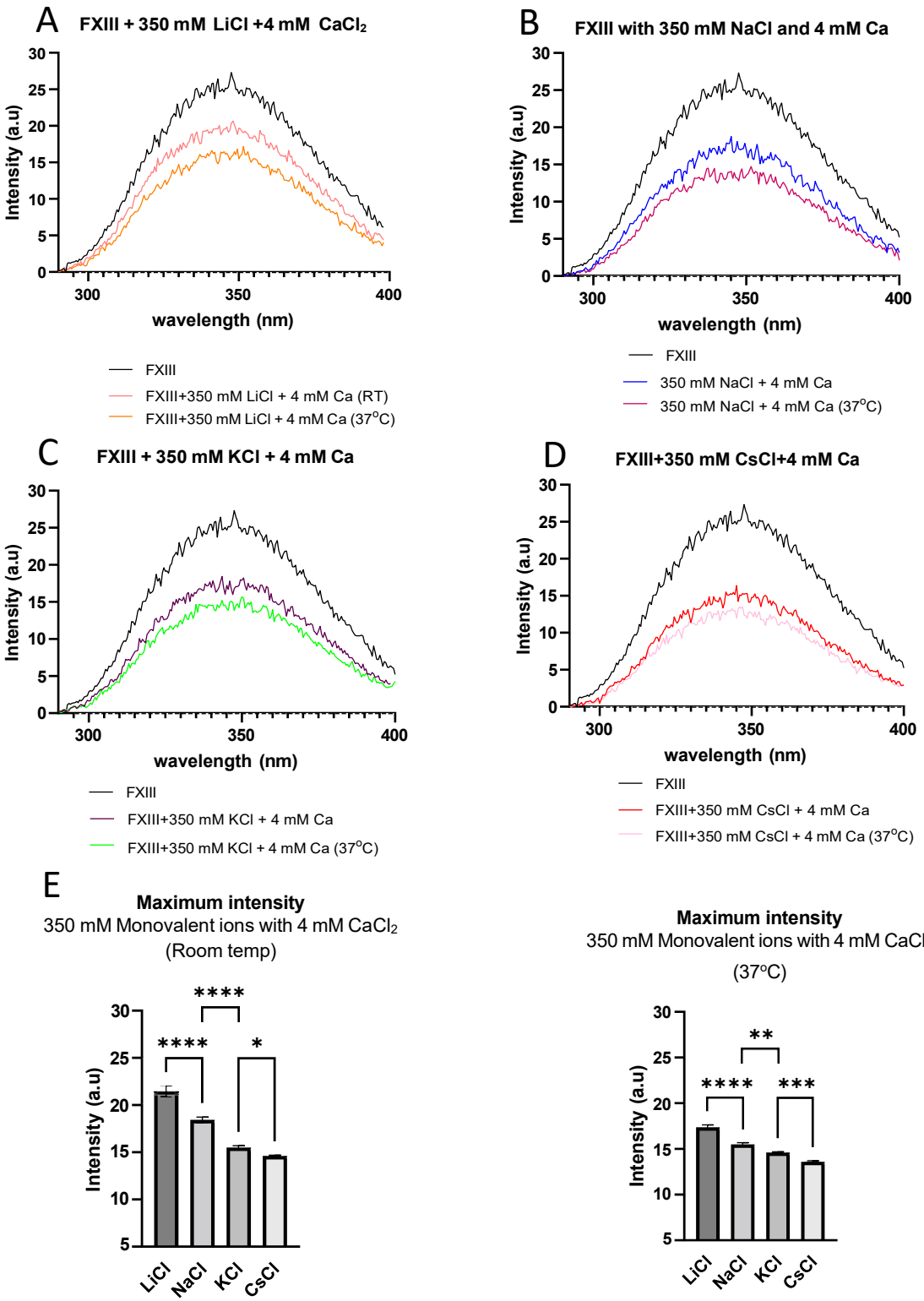

Figure 25. Emission spectra of FXIII A_2 with monovalent ions under RT and 37ºC A) Emission spectra of $FXIIIA_2$ + 350 mM LiCl, B) $FXIIIA_2$ + 350 mM NaCl, C) $FXIIIA_2$ + 350 mM KCl, D) $FXIIIA_2$ + 350 mM CsCl under RT and 37ºC. E) Maximum intensity of $FXIIIA_2$ + 350 mM LiCl, 350 mM NaCl, 350 mM KCl, 350 mM CsCl all with 4 mM CaCl2 under RT and F) 37oC. The asterisk represents the p values (* = p≤0.05, **=p≤0.01, *** p≤0.001, **** = p≤0.0001, ns, not significant = p≥0.05).

When working with Trp residues, there may be concerns that the Trp fluorescence is being quenched by Cs^+ (Komiyama et al 1979). Therefore, control experiments (Supp. Fig. S2) were performed comparing the effects of 350 mM CaCl2 and 350 mM monovalent ions (LiCl, NaCl, KCl, and CsCl) on free Trp. Of these cations, only CsCl showed a substantial decrease in maximal intensity which confirms that CsCl can be a Trp quencher. At varying concentrations of CsCl or $CaCl_2$ (8 mM, 16 mM, and 64 mM), no changes in maximal Trp fluorescence intensities were observed with $CaCl_2$ whereas a gradual increase in CsCl concentration led to a gradual increase in Trp quenching. By contrast, the effects of CsCl on intact FXIII were far more modest than those with $CaCl_2$. FXIII contains three Ca^{2+} binding sites that upon Ca^{2+} binding cause FXIII to expose its catalytic core where 60% of the 15 Trp residues are located.

350 mM Li_2SO_4 vs 350 mM LiCl

LiCl contributed the smallest decrease in the fluorescence effect among the Cl^- containing monovalent ions (Cl^- containing anions). This experiment aimed to determine the effect of the counter ion Cl^- vs SO_4^{-2}. At room temperature, 350 mM LiCl and 350 mM Li_2SO_4 combined with 4 mM $CaCl_2$ exhibited 19 and 24% drops in intensity, respectively. Finally, when these samples (350 mM LiCl or Li_2SO_4 with 4 mM $CaCl_2$) were incubated, the maximum intensity drop, 32-34%, did not show significant difference. These results suggest that the counter ions (Cl^- or SO_4^{-2}) of Li^+ play minimal roles, and cation Ca^{2+} is still the main contributor to FXIII conformational change. The effects of anions were more dominant in crosslinking studies involving the MDC assay most probably due to much higher ionic strength of Li_2SO_4 over LiCl (Chapter 2).

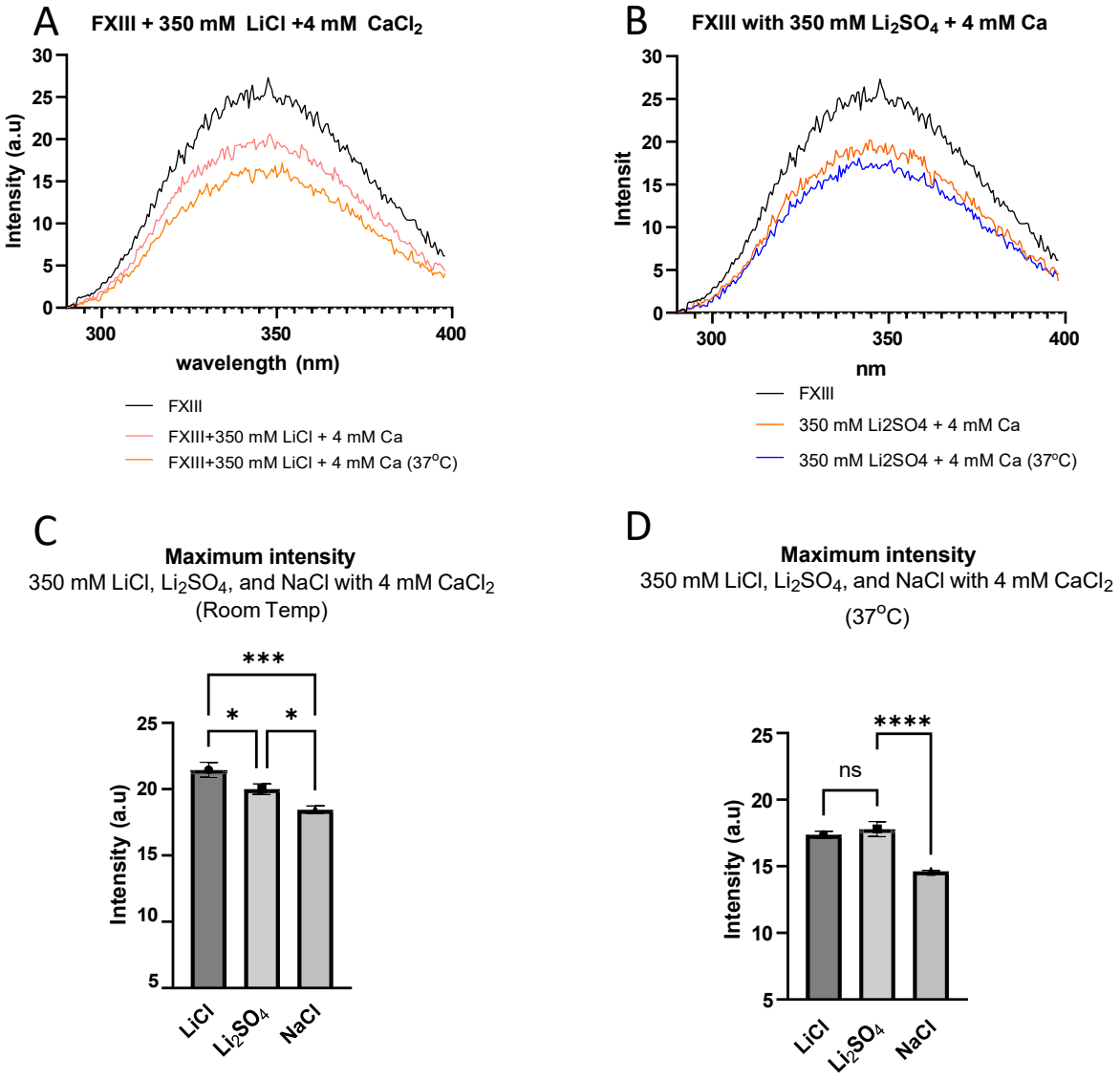

Figure 26 A) Emission spectra of LiCl vs Li_2SO_4 at RT and 37°C. Emission spectra of FXIII-A_2 + 350 mM LiCl B) FXIII-A_2 + 350 mM Li2SO4 under RT and 37oC. C and D) Maximum intensity of FXIII + 350 mM LiCl and FXIII-A_2 + 350 mM Li_2SO_4 under RT and 37°C. The asterisk represents the p values (* = p≤0.05, **=p≤0.01, *** p≤0.001, **** = p≤0.0001, ns, not significant = p≥0.05).

FXIII A_2 with 350 mM $MgCl_2$ vs 350 mM $MgSO_4$

$MgCl_2$ has also been previously studied as an auxiliary ion in FXIII activation. The concentration of this divalent cation magnesium intracellularly is between 17-20 mM (73,77,78) whereas extracellularly is only about 0.7-1.08 mM (111) making the intracellular Mg^{2+} level 20-fold higher than in plasma. There is only a very small difference on the emission spectra generated by $MgCl_2$ and Mg_2SO_4 when 4 mM $CaCl_2$ (at room temp) was combined with them, the drop in intensities recorded were 28% and 29%, respectively. Even when these samples were incubated at 37ºC for 30 min, only a slight difference in intensity were generated: 38% for $MgCl_2$ and 39% drop for Mg_2SO_4 (See Table. S2 in the supplemental table). Counter ions of Mg^{2+} (Cl^- or SO_4^{2-}) showed a similar trend like the LiCl vs Li_2SO_4 with only the cations playing a role in promoting conformational change.

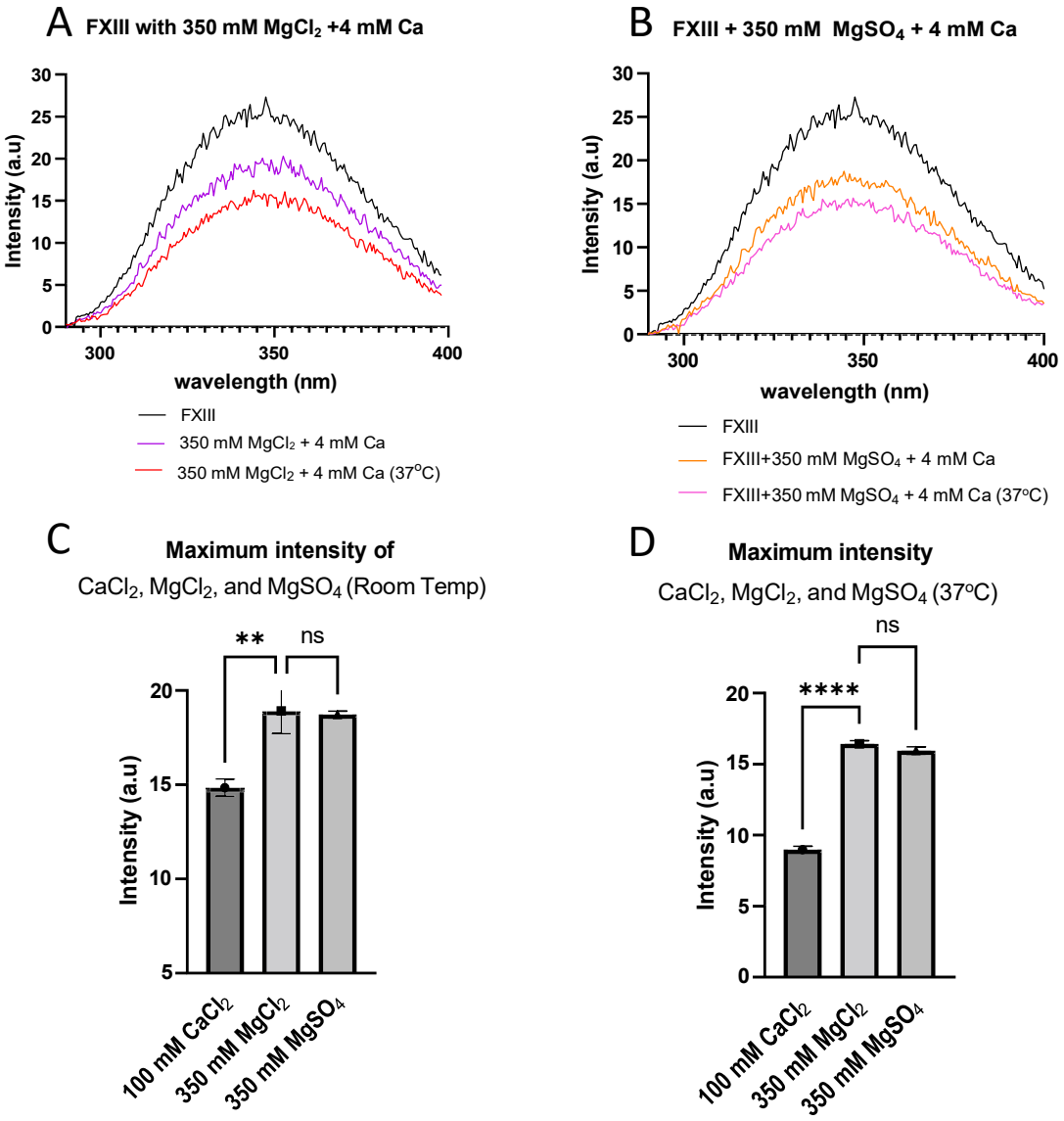

Figure 27. Emission spectra of (A) FXIII + 350 mM $MgCl_2$ and (B) FXIII + 350 mM $MgSO_4$ under RT and 37°C. Maximum intensity of (C) FXIII + 350 mM $MgCl_2$ vs (D) FXIII + 350 mM $MgSO_4$ under RT and 37°C. The asterisk represents the p values (* = $p \leq 0.05$, **=$p \leq 0.01$, *** $p \leq 0.001$, **** = $p \leq 0.0001$, ns, not significant = $p \geq 0.05$)

Discussion

Tryptophan is the dominant amino acid for protein fluorescence (112). When tryptophan residues within a protein experience an increase in the polarity of their surrounding environments, a decrease in the intensity of the emission spectrum is observed. Such changes can be correlated with alterations in the conformational properties of the protein (95). Previous studies demonstrated that FXIII A_2 in the presence of 100 mM $CaCl_2$ undergoes a significant decrease in fluorescent emission intensity. The same effect cannot be mimicked by the divalent cation Mg^{2+} (60). Both HDX-mass spectrometry (105) and X-ray crystallography (52) have previously documented that FXIII A_2 undergoes conformational changes in the presence of increasing concentrations of Ca^{2+}. Moreover, Ca^{2+} ions can interact with FXIII A_2 at up to three binding regions (Cab1, 2 and 3) (52).

The MDC crosslinking studies described in Chapter 2 that involved 4 mM Ca^{2+} revealed that as the atomic radii of supporting monovalent cations increased, the FXIII transglutaminase activity also increased with a ranking of ($Cs^+ > K^+ > Na^+ > Li^+$). The current project described in Chapter 3 focused on using fluorescence emissions spectra to monitor FXIII A_2 for conformational changes occuring in the presence of these different monovalent cations.

On their own, the monovalent cations showed a modest ability to quench maximal FLR intensity. More of the fluorescence decrease occurred in the presence of 4 mM $CaCl_2$, a concentration that would target the major FXIII calcium binding segment Cab1. In the presence of such low mM Ca^{2+}, 350 mM NaCl or KCl had greater benefits than 150 mM . The monovalent cations and their contributions to increasing ionic strength are proposed to support changes in the FXIII conformation beyond that provided by Ca^{2+}. The decreases

in fluorescence intensity occurred with a ranking of monovalent cations that matched the ionic radii ($Cs^+ > K^+ > Na^+ > Li^+$). Raising the temperatures from 25ºC to physiological 37ºC led to the largest conformational impact. For sulfate-based salts such as Li_2SO_4 and $MgSO_4$, both salts did not create large differences in the FLR intensities against their Cl^--based counterpart (LiCl and $MgCl_2$). This result suggests the decrease in FLR intensity is associated with the cations whereas counterions (Cl^- and SO_4^{2-}) did not have an effect which is contrary to the MDC assay results where SO_4^{2-}-based salts generated higher transglutaminase activity.

The greatest decreases in fluorescent emission spectral intensity occurred for FXIII A_2 in the presence of 100 mM Ca^{2+}, a concentration that would fill all three FXIII calcium binding sites. Furthermore, Ca^{2+} has a stronger affinity for the carbonyl group of peptide amides than other cations (102). Binding of divalent Ca^{2+} is still considered the primary driving force in causing significant conformational changes in FXIII both at low and high mM calcium concentrations. A modest further decrease in maximum fluorescent intensity could be promoted by including monovalent cations and working at a physiological temperature. Control experiments confirmed that CsCl can serve as a quencher of Trp fluorescence. However, the fluorescence effects are far less than those introduced by the binding of up to 3 $CaCl_2$ to intact FXIII. Binding of Ca^{2+} to generate FXIII A° exposes the FXIII catalytic core which contains a majority of the Trp residues.

Molecular Dynamics simulations done by the group of Singh et al 2019 reported that there is no drastic change in the overall structure of FXIII A_2 when the concentration of NaCl was raised from 150 mM to 1M (63). Increasing the NaCl concentration made the FXIII electrostatic surface potential more positive but no large conformational changes

were observed in this computational study (63). Using these results from the Biswas lab as a guide, the following model can be developed. Divalent Ca^{2+} ions bind to FXIII-A at distinct sites. The Ca^{2+} ions bind initially to Cab1 and later fill Cab2 and Cab3. X ray crystal structures have shown that FXIII A_2 in the presence of 40 mM $CaCl_2$ and an active site inhibitor undergoes a significant change in conformation that focuses on movemment of FXIII β-barrels 1 and 2 that contributes to FXIII catalytic core domain exposure. The Na+ ions (and other monovalent cations) must play additional supporting roles promoting an electrostatic surface environment that helps maintain the active FXIII conformation. The lower the Ca2+ concentration, the greater the contribution can be from monovalent cations.

In summary, the fluorescence studies suggested that only the cationic species could influence conformational properties detected by the FXIII Trp residues. The MDC crosslinking studies revealed that the cations and anions could influence interactions with its substrates and the resultant transglutaminase activity. With both experiment strategies, the larger the cationic radii of the supportingt salts the greater the impact on FXIII function and structure.

CHAPTER III

CHARACTERIZING HUMAN FXIII WILD TYPE vs G262V

Introduction

FXIII and Transglutaminase 2 (TG2) are among the transglutaminases that exhibit high structural similarity. These two enzymes share common structural domains including β barrel 1 and 2, the catalytic core, and the β sandwich domain (113). FXIII is unique in having an Activation Peptide (AP) segment that is cleaved by thrombin during the activation process. Moreover, Ca^{2+} binding to FXIII promotes conversion from a dimer to monomers. TG2 does not contain an AP segment, but its activation is regulated by a redox reaction involving Ca^{2+}, GTP, and thioredoxin (67). TG2 becomes inactive upon binding GTP. In the presence of appropriate calcium concentrations, the GTP is released and TG2 becomes activated. In contrast to the zymogen FXIII A_2 dimer, zymogen TG2 is a

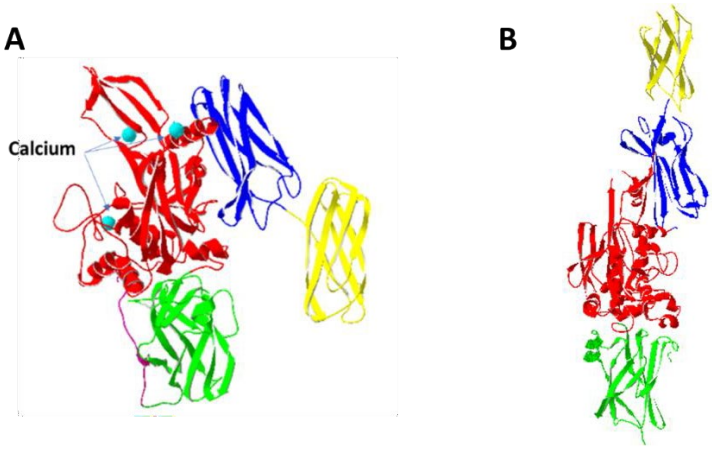

Figure 28. Conformational changes of FXIII and TG2 upon activation. A) Activated monomeric FXIII-A^o + bound inhibitor (PDB 4KYT B) TG2 activated + inhibitor trapped (fully extended) conformation – PDB 2Q3Z).

monomer (47). Both FXIII and TG2 expose their catalytic core domains during activation by large movement of both the β barrels 1 and 2 (Fig. 28).

Human TG2 was sequenced and cloned in the early 1990s, and this sequence was used in many published studies (114). When the TG2 was resequenced in 2014 (115), a cloning error was discovered at the 224 position. The TG2 G224 should instead be a Val224, (114,116). The natural variant exhibited an enhanced calcium binding affinity thereby increasing transglutaminase activity. The sequences of FXIII (254-271) and TG2 (220-233) are highly conserved. An interesting exception is FXIII G262 located at the same position as TG2 V224. This FXIII A structural position is situated within a helix near the calcium binding Cab3 region, and TG2 has a highly conserved corresponding Cab3 region (Fig. 29A). The primary goal of the study was to examine if FXIII G262V would exhibit the same improvement in transglutaminase activity as TG2 G224V.

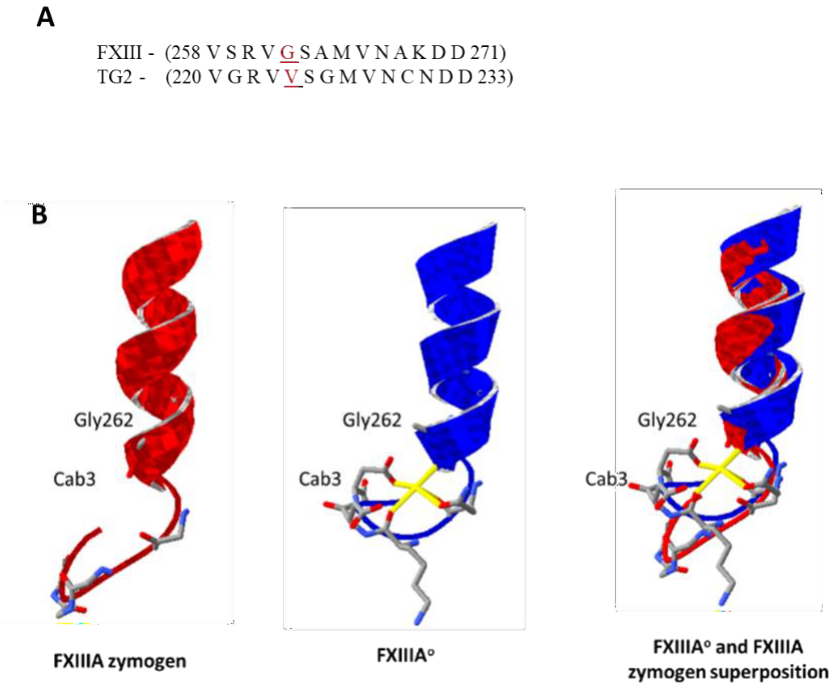

Figure 29. A) Sequence alignment of FXIII and TG2 showing G262 of FXIII

Materials

Mutagenesis of FXIII A_2 Glycine 262 to Val262 (G262V) was performed using the QuikChange II Site-Directed Mutagenesis kit (Agilent Tech, Santa Clara, CA) on glutathione S-transferase (GST) tagged FXIII DNA serving as the template DNA. The forward and reversed primers for the site-directed mutagenesis were synthesized by IDT (Coralville, IA, USA). The FXIII A G262V Forward primer sequence was 5'- GTC AGC CGT GTG GTG TCT GCA ATG GTG -3' whereas the reversed primer was 5'- CAC CAT TGC AGA CAC CAC ACG GCT GAC -3' (Length: 27 bp, % GC: 59.26 % and melting temp: 65.3 °C).

Bacteriological grade Tryptone, sodium dodecyl sulfate (SDS), KH_2PO_4 and $(NH_4)_2SO_4$ were purchased from VWR (OH, USA), Bacto™ yeast extract (MD, USA), EDTA from Fisher Bioreagents (NJ, USA), glycerol from MP Biomedicals (Ohio, USA), glucose, lactose and ampicillin from Sigma (MO, USA). Deoxyribose nucleotide triphosphate (DNTP), Phusion® High-Fidelity (PFQ) DNA polymerase by IDT (Coralville, IA, USA). Gluthatione, RNAse, TritonX, leupeptin, aprotinin, benzamidine HCl and streptomycin sulfate were from Calbiochem (Darmstadt, Germany), and the lysozyme from Sigma (MO, USA).

Methods

Site directed mutagenesis

A pGEX-6P-1 (Protein expression vector, GST-Precission™ protease), vector system, provided by the Ariens and Philippou Labs of the University of Leeds, was used as the vector for setting up the FXIII expression system. The FXIIIA has been inserted downstream from the GST-tag sequence via the restriction sites *Bam*H1 at the 5' position and *Sal*1 at the 3'. The PGEX-6P-1 vector also provides resistance to ampicillin and other related antibiotics since it encodes β lactamase (Fig. 30). Following expression and purification, the GST is removed from the fusion protein by using the proteolytic enzyme HRV3C that hydrolyzes the recognition sequence (Leu Glu Val Leu Phe Gln | Gly Pro)(117).

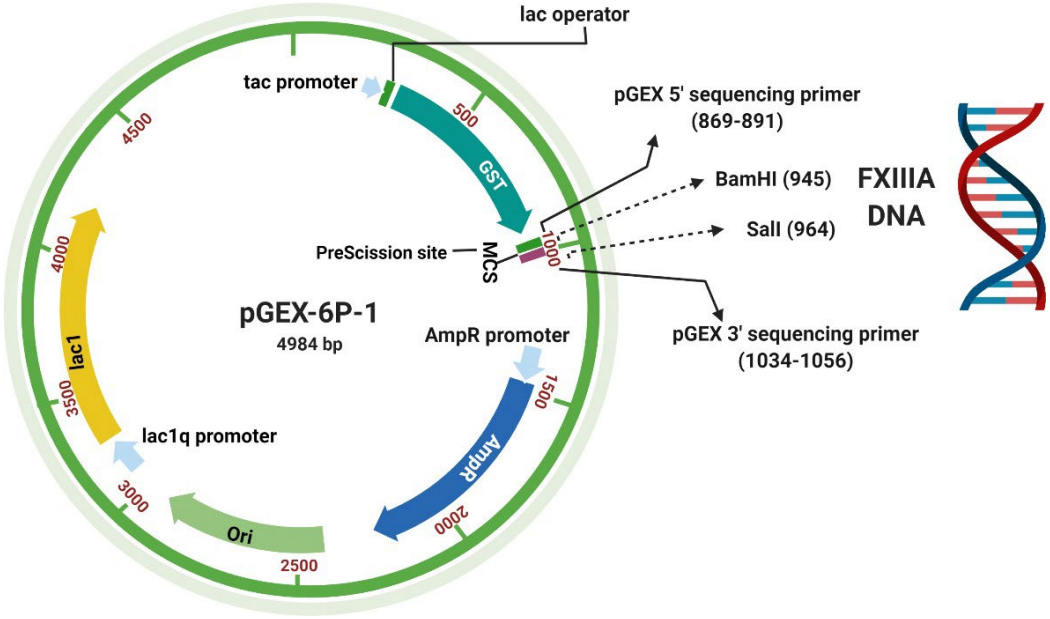

Figure 30. A pGEX-6P-1 plasmid DNA map for FXIII A DNA. Left arrows shows the 5' and 3' sequence primer and origin of replication is in green arrow (middle), AmpR gene encoding β lactamase (blue), lac1 gene encoding lac repressor (yellow), GST-encoding sequence (blue green). FXIIIA DNA is inserted downstream of the GST-sequence using Sal1 and BamH1 restriction sites (Created with BioRender).

Mutagenesis of FXIII A_2 G262V was performed using the QuikChange II Site-Directed Mutagenesis kit from Agilent Technologies, Santa Clara, CA. Following the manufacturer's protocol, the DNA template (20-50 ng) was mixed with the synthesized forward and reverse DNA primers (120-150 ng), reaction buffer, DNA polymerase, and dNTPs. This mixture was then run for 16 cycles in an Eppendorf 5332 PCR instrument. For each PCR cycle, the parameters were: 30 sec at 95 °C for denaturation, 1 min at 55°C, and 7 min at 68 °C for annealing. After completing the 16 cycles, the sample was chilled for 2 min in the PCR instrument and transferred on ice for 30 minutes and subsequently the restriction enzyme, Dpn1 was added. Since the DNA template was expressed in *E. coli*, the DNA becomes methylated. Methylated DNA when used as the template in PCR will produce non-methylated DNA. Upon introduction of restriction enzyme Dpn1, the original methylated DNA will be digested and only the non-methylated DNA will be left. The tube was then placed back in the PCR instrument for incubation at 37 ºC for 1 h. The remaining non-methylated DNA product was then transformed into *E. coli* XL-1 blue super competent cells.

Transformation and Expression

Transformation was performed by placing the DNA product in a 42 ºC water bath for 45s. During transformation, supercompetent cells (*E. coli* XL-1) are capable of up taking exogenous DNA (PCR product) which can eventually be used for downstream application. After the 45s incubation, the sample was placed on ice for about 2 min. Next, 500 µL of preheated (42ºC) Super Optimal Broth with Catabolite expression (SOC) medium were added, mixed, and then incubated for 1 h at 37ºC, 195 rpm. Using a ZYP 0.8G plates, 100 µL, 75 µL, and 50 µL of the transformed cells were streaked on the gel

media. After incubation at 37ºC for 16 hrs, a single colony was then selected and cultured using a newly prepared LB broth containing 100 µg/mL ampicillin. The transformed *E. coli* XL-1 was incubated in ZYP 0.8G non-inducing media overnight at 37ºC. Cultured cells were then harvested by centrifugation at 5000 rpm. The Qiagen Miniprep kit^{TM} was used for the plasmid DNA extraction, and the concentration was subsequently determined using a Nanodrop spectrophotometer (Health Science Campus), University of Louisville. The extracted DNA sample was then submitted for sequencing at the DNA Core facility of the University of Louisville. After getting confirmation of the DNA sequence, the plasmid vector was then subjected to transformation into *E. coli* BL21-Gold (DE3) competent cells where ampicillin serves as the selection marker. The autoinduction protocol was then utilized to perform the overexpression of FXIII A_2 G262V variant using the same method as described in Chapter 2 for Fbg αC (233-425).

Protein purification

The GST-tagged FXIII A_2 G262V lysate underwent purification using GST-affinity column chromatography on an AKTAprime chromatography system (GE Healthcare). HRV3C protease was then added to cleave the GST tag by in-column digestion to obtain the GST-free FXIII G262V. This purified FXIII G262V was then eluted with TBS buffer containing 150 mM NaCl, 50 mM Tris acetate (pH 7.4) and its concentration was determined spectrophotometrically (Agilent technologies, Cary 60 UV VIS) at 280 (Cary WinUV version 5.0.0.999 program) nm using an extinction coefficient of 41480 M^{-1} cm^{-1} for FXIII G262V. Finally, the FXIII G262V fractions were run via SDS PAGE (4% stacking gel and 8% resolving gel) to check for purity.

Activation peptide cleavage of FXIII by rhIIa

Using activated recombinant human thrombin (rhIIa), the activation peptide (AP) of FXIII A_2 was cleaved off specifically at the R37-G38 peptide bond and released as a 4kDa AP (1-37) fragment. The progress of hydrolysis of the FXIII AP segment was monitored by SDS-PAGE. The purpose for this experiment was to determine if mutation of FXIII G262 to V262 would affect the rate of thrombin cleavage which is an important step in proteolytic FXIII activation.

Initially, 9 tubes were prepared where one tube was intended for the zero point (sample without rhIIa) and the 8 remaining other tubes contained 1 μL of 190 nM PPACK that served to inhibit thrombin when the FXIIIA sample was mixed with it. The activation mixture was prepared by mixing Tris acetate buffer, 2.2 μM FXIII A_2, and 30 nM human thrombin followed by incubation at 37ºC. Next, 20 μL was removed at each time point (1, 2, 5, 10, 15, 30, 45, and 60 min) and added to the tube containing PPACK followed by addition of 7 μL of 5X reducing buffer. The quenched samples were then boiled for 3 min prior to gel loading. For each of the quenched samples, 20 μL were loaded into the SDS PAGE gel wells (8% acrylamide of resolving gel and 4% acrylamide of stacking gel) and run at 180 V for about 45 min. Finally, the gel was viewed under white light using a BioRad GelDoc XR, and the saved image was used for quantification of how much FXIII zymogen was left per unit time.

MDC Assay: FXIII A_2 WT and FXIII A_2 G262V

Proteolytic activation

FXIII-A* was achieved by preparing the same total volume for activation (20μL) and reaction mixture (160 μL) as used for the above mentioned FXIII activation studies. The activation mixture was composed of 50 mM Tris acetate buffer saline, 2μM FXIII A_2, 4 mM $CaCl_2$, and 30 nM recombinant human thrombin (rhIIa). This mixture was then incubated at 37 ºC for 30 minutes. When the 30 min incubation period was reached, 1μL of 1.9 mM PPACK was then added and mixed with the activation mixture to inhibit the conversion of FXIII A_2 to FXIII-A^* via deactivation of rhIIa. When 8 μL FXIIIA* were added to the reaction mixture, the final concentrations of the components were 4 mM $CaCl_2$, 5μM Fbg αC, 1 mM MDC, and 100 nM FXIII. The same procedure was taken for quenching, loading, and viewing of gels as described in Chapter 2 (MDC assay). The series of quenching time points included 1, 2, 3, 5, 10, 15, and 30 min.

Non-proteolytic activation

The MDC assay for the FXIIIA WT and mutant contained the same components as described in Chapter 2 (MDC assay) except that the new time points (1, 2, 3, 5, 10, 15, and 30 min) were used to compare FXIII-A* and FXIII-A^o.

RESULTS

Monitoring the rate of Activation Peptide (AP) cleavage of FXIIIA WT vs FXIIIA G262V

Using thrombin (rhIIa), the activation peptide (AP) of the FXIII A_2 WT and FXIII G262V were cleaved at the Arg37-Gly38 peptide bond. Releasing these AP segments does not activate FXIII A_2 to FXIII-A* unless calcium is present to promote further conformational changes to allow active site exposure. The ability of FXIII A_2 to be proteolytically activated depends on how readily the AP R37-G38 peptide bond is cleaved by thrombin.

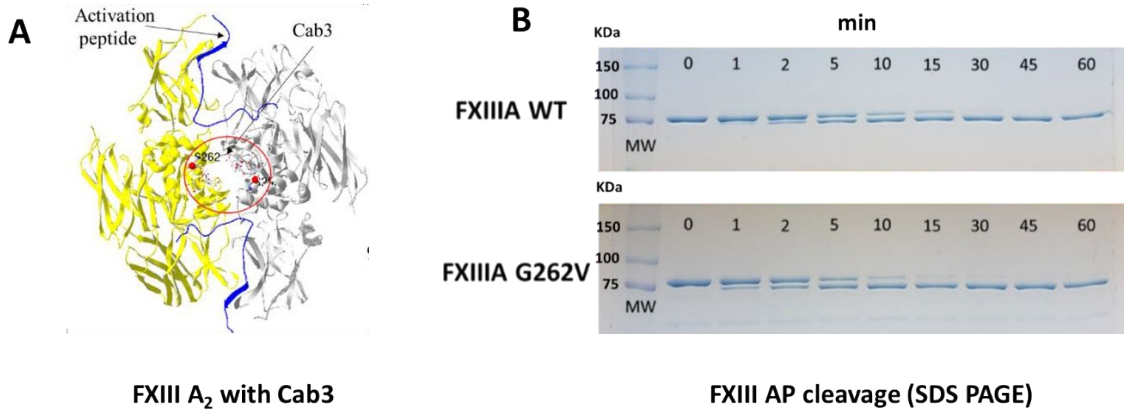

Figure 31. A) Crystal structure of FXIII-A showing the AP segments, G262 and the Cab3 residues B) SDS PAGE of FXIII AP-cleavage by thrombin as a function of time of FXIIIA WT and FXIII G262V.

The SDS PAGE results showed thrombin fully cleaved the AP segment for WT and mutant FXIII after 15–30-minute reaction times (Figure 31). The zero-time point corresponds to the quenched sample containing FXIII-A (~83kDa) before thrombin was added. The extent of AP cleavage could be monitored for the 1-60 min reaction period. A new band at ~79 kDa increased in intensity as a function of reaction time that corresponded to the loss of the FXIII (1-37) AP segment (4 kDa) following thrombin cleavage. The strong similarities in the two-cleavage time point series imply that the mutation of G 262 to V262

in FXIII does not affect the ability of thrombin to cleave the AP segment at FXIII R37-G38.

MDC incorporation assay of FXIII-A^o WT vs FXIII-A^o G262V

The MDC crosslinking assay revealed that FXIII-A^o WT catalyzes a faster rate of MDC incorporation into the Q-containing substrate Fbg αC than the FXIII-A^o G262V (Fig. 32). However, by 30 min, both FXIII forms approached a similar crosslinking plateau (Fig 33D). These results suggest the G262V does not enhance nonproteolytic activation of FXIII or transglutaminase activity. Instead, some hindrances in ability of FXIII G262V to crosslink MDC into Fbg αC has occurred. This result suggests that mutation of Gly262 to a larger hydrophobic Val262 creates a hindrance in the ability of FXIII-A^o to crosslink its lysine substrate MDC into Fbg αC (233-425).

MDC incorporation assay of FXIII-A* WT vs FXIII-A* G262V

Proteolytically activated FXIII (FXIII-A*) forms were also evaluated to determine the impact of the FXIII G262V variant (Fig. 33A and 33B). The concerted action of thrombin-catalyzed AP cleavage and the presence of calcium makes the proteolytic activation a more efficient mechanism than the nonproteolytic one. In the MDC incorporation assay, results showed that there was no significant difference in the MDC incorporation between the FXIII WT and its G262V variant (Fig. 33A and 33B). With FXIII-A*, 4 mM $CaCl_2$ can fill the main calcium binding site (Cab1) of FXIII and subsequently, the other binding sites Cab2 and Cab3 are available to achieve full calcium occupancy. However, kinetics data showed similar rates of plateau formation for FXIII WT

and FXIII G262V which signifies that the mutation has no impact on the transglutaminase activity of the FXIII-A* form (Fig 33D).

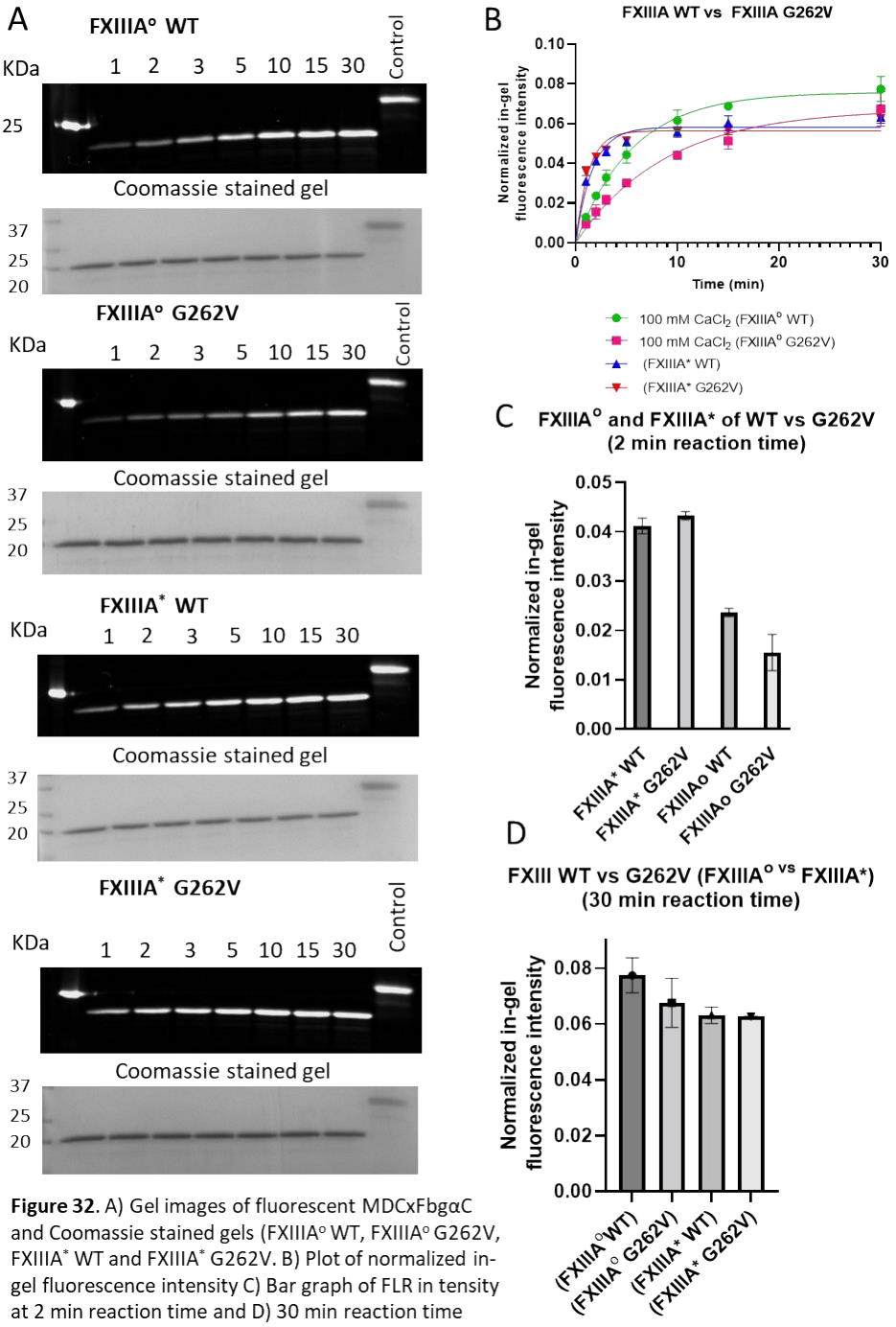

Figure 32. A) Gel images of fluorescent MDCxFbgαC and Coomassie stained gels (FXIIIA° WT, FXIIIA° G262V, FXIIIA* WT and FXIIIA* G262V. B) Plot of normalized in-gel fluorescence intensity C) Bar graph of FLR in tensity at 2 min reaction time and D) 30 min reaction time

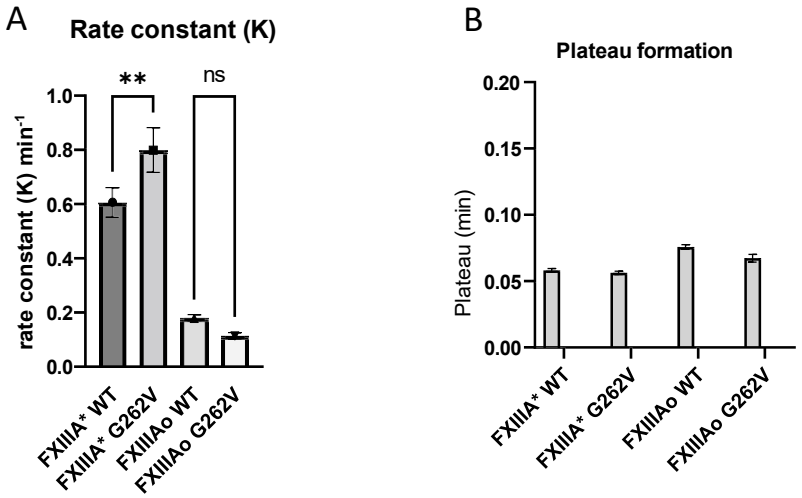

Figure 33. A) Rate constant B) Plateau formation of FXIII WT and mutant.

Discussion

The design of FXIII G262V was based on a TG2 mutation G224V which led to increased calcium binding and transglutaminase activity (116,118). The crystal structures of FXIII and TG2 indicate (Fig. 31) that FXIII Gly262 and the TG2 Gly224 both are located within an α helix that connects to a Ca^{2+} binding loop in the catalytic core domain (52,119). In the nonproteolytically activated FXIII-A^o crystal structure (PDB 4KTY), the Cab3 loop utilizes Ala264, Asn267, K269, Asp270, and Asp271 to bind calcium. In the TG2 loop (Fig. 34), Asp232 and Asp233 correspond to FXIII Asp270 and Asp271 which are part of the calcium binding site 3. With TG2, the Cab3 sequence serves as the main calcium binding site whereas with FXIII, Cab1 is actually the primary calcium binding site while Cab2 and Cab3 play additional roles.

The purified FXIII G262V variant was first evaluated for its response to thrombin cleavage of AP fragment. This N-terminal 37 amino acid segment Ala1-Gly37 (4 kDa) of FXIII is connected to the β sandwich. A review of FXIII A_2 structure reveals that the AP segment binds not only to its own catalytic core domain but also straddles across the dimer interface to interact with the other dimer partner (Fig. 35A). For the activation peptide cleavage assay times, both the FXIII-A WT and the mutant FXIII-A G262V could become completely free of the AP fragment by 30 min as seen by the expected 4 kDa decrease in molecular weight (Fig. 34B). This result suggests that the G262V mutation did not affect thrombin cleavage of the AP fragments. FXIII residues Phe8-Arg15 of AP make interactions with the other FXIII subunit. The Arg11 and Arg12 of the AP segment form salt bridge interactions with Asp343, one of the residues directly bound to Cab2, whereas the remaining residues in Phe8-Arg15 only form hydrogen bonds. The absence of Ca^{2+} in

the SDS PAGE based cleavage assay means that AP hydrolysis can be monitored, but no enzymatic activity can be induced.

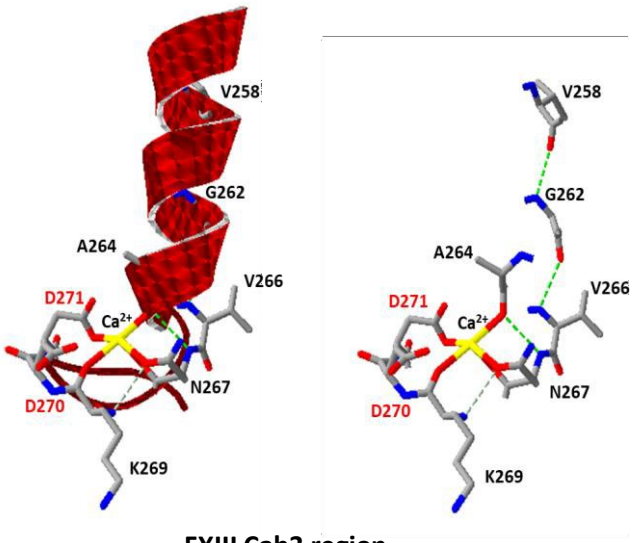

Figure 34. FXIII-A Calcium binding site 3 (PDB 4KTY) and TG2 major calcium binding region (FXIII Cab3 equivalent, PDB 2Q3Z)

Using proteolytically activated FXIII-A*, the MDC incorporation assays revealed, no significant difference between the transglutaminase activities of FXIII WT and FXIII G262V. Both WT and mutant FXIII-A* generated the same high rates of crosslinking with

the plateaus reached by 5 min. The FXIII-A* G262V mutation in the α helix could have caused changes in the noncovalent interactions of helical residues near Val262, but they did not impact the transglutaminase activity of proteolytically activated FXIII. This form of FXIII relies on Ca^{2+} binding to Cab1 to promote transglutaminase activity.

Under nonproteolytic activation conditions involving 100 mM $CaCl_2$, the FXIII-A^o G262V variant exhibited a slower rate of achieving transglutaminase activity than the FXIII-A^o WT. At 100 mM, this Ca^{2+} concentration is predicted to bind Cab1, Cab2, and Cab3. In the crystal structure of FXIII (4KTY), the FXIII-A G262 position does not have direct interaction with the Cab3 binding loop (Fig. 34). Instead G262 participates in a hydrogen bonding network that links G262, Val226, Leu275, and Ala268. Both Ala268 and Leu275 are within the Cab3 loop (Fig. 34). The G262V mutation introduces a more hydrophobic residue that may have promoted long-ranged instability in the Cab3 region. This structural review suggests the G262V mutant may have impacted calcium binding at Cab3 and influenced FXIII activity. In a previous study conducted by Souri et al 2014, another known Gly mutation (G273V) within the Cab3 region was detected in patients with severe congenital FXIII deficiency (120). The FXIII variant G273V has also been reported to promote instability and this Gly is positioned within the Cab3 binding loop. Directly altering the Ca^{2+} binding site may have had a greater effect than FXIII G262V impacting the neighboring α helix.

Furthermore, a study by Li et al 2020 revealed that Arg260 and Lys257 within the Cab3 region are considered essential residues for promoting FXIII core domain-core domain interactions along the FXIII A_2 dimer interface (121). Arg260 and Lys257 are both

within the α helix where the Gly262 is also positioned. The G262V variant may have further impacted interactions in the proximity of Arg260 and Ly257.

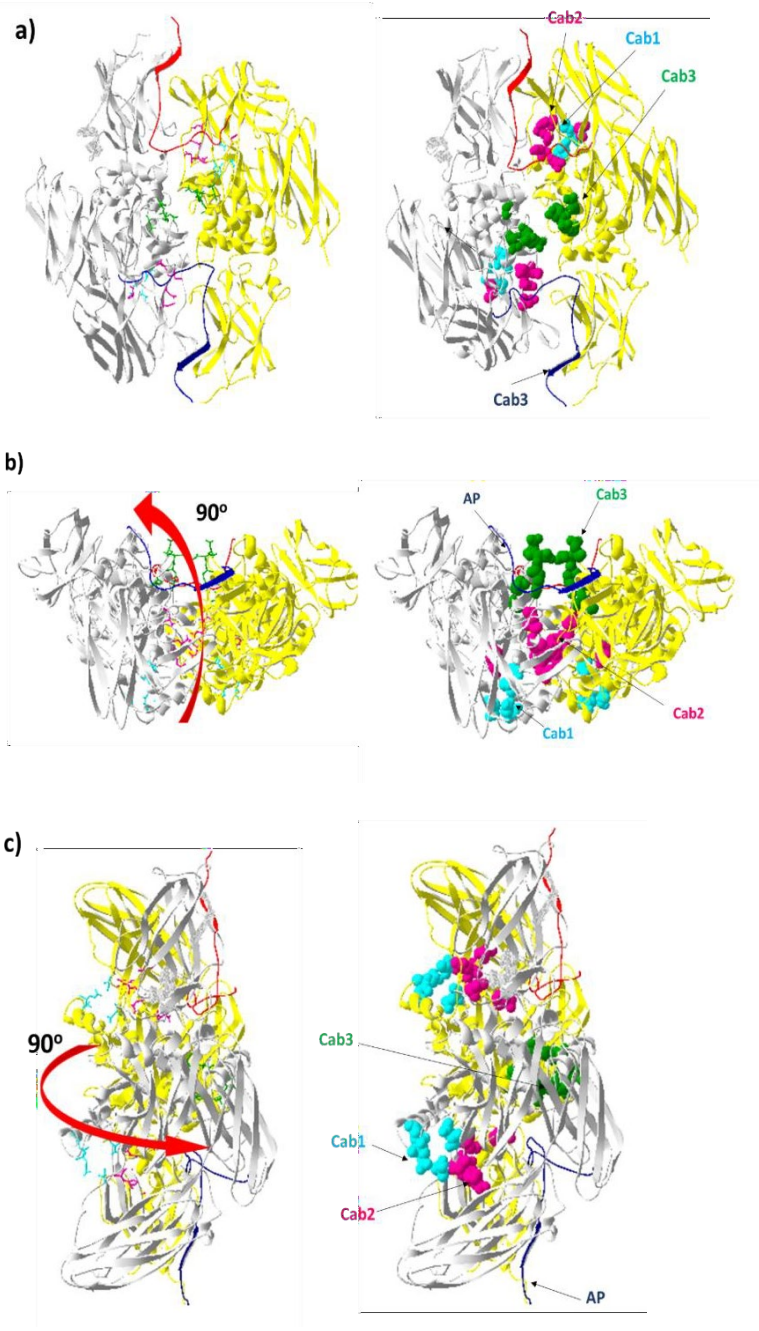

Figure 35. FXIII A_2 spatial views showing the residues in Cab1 (sky blue), Cab2 (pink) and Cab3 (green). The AP peptide (blue and red) are from two FXIII-A subunits. a) shows the FXIII A_2 front view, b) FXIII A_2 view flipped vertically backward at 90° c) FXIII A_2 view flipped counterclockwise at 90°.

Figure 35 shows the structure of zymogen FXIII A_2 in different spatial orientations. At the dimer interface, where most of the subunit interactions occur, the AP segment segments of both A subunits and the Cab3 residues are the most exposed for solvent or ionic interactions (Fig 35B and 35C). Cab2 residues are positioned in the middle and Cab 1 at the bottom. Fig. 35A also reveals that among the Cab sites, the two Cab3 positions are positioned in close proximity along the A_2 dimer interface. By contrast, individual Cab1-Cab1 and Cab2-Cab2 sets are each located at opposite positions along the dimer interface.

Since nonproteolytic activation benefits from high Ca^{2+} concentrations to promote filling of all Cab sites, the G262V variant has slightly affected binding at Cab3 which resulted in a decrease in FXIII activity. This impact on calcium binding could be overcome when the mutant was activated proteolytically. There was no significant difference in the transglutaminase activity between the FXIII WT and G262V mutant when tested following proteolytic activation. The low mM Ca^{2+} would primarily target Cab1. In the previous AUC studies performed by Anokhin et al (60), FXIII-A* WT was demonstrated to be more conformationally flexible than FXIII-A^o and served as a better transglutaminase for promoting MDC crosslinking to FbgαC.

The contrasting results of FXIII-A^o vs FXIII-A* suggest that upon thrombin cleavage, the instability caused by the G262V variant is overcome in proteolytic activation since the FXIII A_2 to FXIII-A* formation is an AP-cleavage driven activation and reliant on low mM calcium concentration levels. FXIII-A* G262V is predicted to be more driven by calcium binding to Cab1 than Cab3. Meanwhile, nonproteolytically activated FXIII A_2 to FXIII-A^o, is a calcium-driven activation and instability within Cab3 would impact FXIII activation and activity. The sequences surrounding FXIII G262V or TG2 G224V have

highly conserved residues, but the mode of activation of TG2 and FXIII are different. The main calcium binding site of FXIII is Cab1(63) whereas that of TG2 is Cab3 (122) although they are positioned in the same location in catalytic core domain. The sequences of the TG2 main calcium binding site have high similarity to the Cab3 region of FXIII. In future research studies, other residues within the Cab3 region that are involved in binding of Ca^{2+} and the lysine-containing substrate could be further investigated for effects on transglutaminase activity.

Summary and Conclusion

This MS Thesis project explored the effects of monovalent/divalent cations and their accompanying anions on the transglutaminase activity and conformational properties of Factor XIII. For the various studies, FXIII was activated non-proteolytically in the presence of elevated levels of Ca^{2+} (2 mM – 100 mM) or proteolytically by thrombin-catalyzed cleavage of the Activation Peptide in the presence of 4 mM Ca^{2+}.

Studies in Chapter 2 utilized fluorescent mondansylcadaverine SDS-PAGE crosslinking assays to examine the effects of ionic radius and ionic strength on promoting FXIII-A activity. FXIII A_2 was activated in the presence of 4 mM $CaCl_2$ and different concentrations of monovalent salts. Increasing concentrations of NaCl or KCl (150 mM – 500 mM) generated an increase in transglutaminase activity. Group 1 cations (Cl^--based salts) at 350 mM showed increased MDC incorporation as a function of ionic radius in the order $Cs^+ > K^+ > Na^+ > Li^+$. When sulfate-based salts were compared with chloride-based salts such as LiCl vs Li_2SO_4 or $MgCl_2$ vs $MgSO_4$, the higher ionic strength properties of the sulfates contributed to further increases in transglutaminase activity. Chapter 2 studies demonstrated that for monovalent ions, increasing ionic strengths or ionic radius promoted increased transglutaminase activity.

Studies in Chapter 3 focused on using intrinsic fluorescence to monitor for changes in FXIII conformation in the presence of divalent Ca^{2+} and the monovalent cation series. FXIII contains 15 Tryptophan residues that can become further exposed to solvent upon FXIII activation. In the presence the cations, decreases in fluorescence corresponding to increases in protein polarity could be detected. Binding of Ca^{2+} was found to be the main driver of the conformational changes detected to FXIII. The monovalent cations provided

additional supporting roles with their effects again tied with ionic radius ($Cs^+ > K^+ > Na^+ > Li^+$).

Studies in Chapter 4 involved determining whether the ability to nonproteolytically activate FXIII could be enhanced by introducing a G262V mutation from TG2 into the Cab3 calcium binding site. This mutation caused a hindrance in the ability of Ca^{2+} to bind at Cab3 resulting in a decrease in transglutaminase activity. The same mutation, however, did not alter proteolytic activation nor impact its transglutaminase activity. Mutation at the Cab3 region influenced nonproteolytic activation which is calcium driven, but this impact on Cab3 was overcome proteolytically which is considered a more thrombin-driven activation.

REFERENCES

1. Romijn, R. A., Bouma, B., Wuyster, W., Gros, P., Kroon, J., Sixma, J. J., and Huizinga, E. G. (2001) Identification of the collagen-binding site of the von Willebrand factor A3-domain. *J Biol Chem* **276**, 9985-9991
2. Moroi, M., and Jung, S. (1997) Platelet receptors for collagen. *Thrombosis and haemostasis* **78**, 439-444
3. Siljander, P., Farndale, R. W., Feijge, M. A., Comfurius, P., Kos, S., Bevers, E. M., and Heemskerk, J. W. (2001) Platelet adhesion enhances the glycoprotein VI–dependent procoagulant response: Involvement of p38 MAP kinase and calpain. *Arteriosclerosis, thrombosis, and vascular biology* **21**, 618-627
4. Paul, B. Z., Daniel, J. L., and Kunapuli, S. P. (1999) Platelet shape change is mediated by both calcium-dependent and-independent signaling pathways: role of p160 Rho-associated coiled-coil-containing protein kinase in platelet shape change. *Journal of Biological Chemistry* **274**, 28293-28300
5. Ghoshal, K., and Bhattacharyya, M. (2014) Overview of platelet physiology: its hemostatic and nonhemostatic role in disease pathogenesis. *The Scientific World Journal* **2014**
6. Golino, P., Ashton, J. H., Buja, L. M., Rosolowsky, M., Taylor, A. L., McNatt, J., Campbell, W. B., and Willerson, J. T. (1989) Local platelet activation causes vasoconstriction of large epicardial canine coronary arteries in vivo. Thromboxane A2 and serotonin are possible mediators. *Circulation* **79**, 154-166
7. Swieringa, F., Spronk, H. M. H., Heemskerk, J. W. M., and van der Meijden, P. E. J. (2018) Integrating platelet and coagulation activation in fibrin clot formation. *Research and Practice in Thrombosis and Haemostasis* **2**, 450-460
8. Gersh, K. C., Nagaswami, C., and Weisel, J. W. (2009) Fibrin network structure and clot mechanical properties are altered by incorporation of erythrocytes. *Thromb Haemost* **102**, 1169-1175
9. Sakata, Y., and Aoki, N. (1982) Significance of cross-linking of alpha 2-plasmin inhibitor to fibrin in inhibition of fibrinolysis and in hemostasis. *J Clin Invest* **69**, 536-542
10. Mosher, D. F. (1975) Cross-linking of cold-insoluble globulin by fibrin-stabilizing factor. *J Biol Chem* **250**, 6614-6621
11. ADAMS, R. L. C., and BIRD, R. J. (2009) Review article: Coagulation cascade and therapeutics update: Relevance to nephrology. Part 1: Overview of coagulation, thrombophilias and history of anticoagulants. *Nephrology* **14**, 462-470
12. Macfarlane, R. (1964) An enzyme cascade in the blood clotting mechanism, and its function as a biochemical amplifier. *Nature* **202**, 498-499
13. Mann, K. G., Brummel-Ziedins, K., Orfeo, T., and Butenas, S. (2006) Models of blood coagulation. *Blood Cells, Molecules, and Diseases* **36**, 108-117
14. Mackman, N., Tilley, R. E., and Key, N. S. (2007) Role of the Extrinsic Pathway of Blood Coagulation in Hemostasis and Thrombosis. *Arteriosclerosis, Thrombosis, and Vascular Biology* **27**, 1687-1693
15. Bittar, L., De Paula, E., Barnabé, A., Mazetto, B., Zapponi, K., Montalvao, S., Colella, M., Orsi, F., and Annichino-Bizzacchi, J. (2015) Plasma Factor VIII Levels as a Biomarker for Venous Thromboembolism. pp 1-19

16. Hoffman, M., and Monroe, D. M., 3rd. (2001) A cell-based model of hemostasis. *Thromb Haemost* **85**, 958-965
17. Osterud, B., and Rapaport, S. I. (1977) Activation of factor IX by the reaction product of tissue factor and factor VII: additional pathway for initiating blood coagulation. *Proceedings of the National Academy of Sciences* **74**, 5260-5264
18. Butenas, S., and Mann, K. (2002) Blood coagulation. *Biochemistry (Moscow)* **67**, 3-12
19. Walsh, P. (2003) Roles of factor XI, platelets and tissue factor-initiated blood coagulation. *Journal of Thrombosis and Haemostasis* **1**, 2081-2086
20. Zigler, M., Kamiya, T., Brantley, E. C., Villares, G. J., and Bar-Eli, M. (2011) PAR-1 and thrombin: the ties that bind the microenvironment to melanoma metastasis. *Cancer Res* **71**, 6561-6566
21. Ramakrishnan, V., DeGuzman, F., Bao, M., Hall, S. W., Leung, L. L., and Phillips, D. R. (2001) A thrombin receptor function for platelet glycoprotein Ib-IX unmasked by cleavage of glycoprotein V. *Proc Natl Acad Sci U S A* **98**, 1823-1828
22. Orfeo, T., Brufatto, N., Nesheim, M. E., Xu, H., Butenas, S., and Mann, K. G. (2004) The factor V activation paradox. *Journal of Biological Chemistry* **279**, 19580-19591
23. Mann, K. G., Brummel-Ziedins, K., Orfeo, T., and Butenas, S. (2006) Models of blood coagulation. *Blood Cells Mol Dis* **36**, 108-117
24. Weisel, J. W., and Litvinov, R. I. (2017) Fibrin Formation, Structure and Properties. *Subcell Biochem* **82**, 405-456
25. Weisel, J. W. (2005) Fibrinogen and fibrin. *Adv Protein Chem* **70**, 247-299
26. Medved, L., and Weisel, J. W. (2021) The Story of the Fibrin(ogen) αC-Domains: Evolution of Our View on Their Structure and Interactions. *Thromb Haemost*
27. Mouapi, K. N., Bell, J. D., Smith, K. A., Ariëns, R. A. S., Philippou, H., and Maurer, M. C. (2016) Ranking reactive glutamines in the fibrinogen αC region that are targeted by blood coagulant factor XIII. *Blood* **127**, 2241-2248
28. Budzynski, A. Z., Olexa, S. A., and Pandya, B. V. (1983) Fibrin polymerization sites in fibrinogen and fibrin fragments. *Ann N Y Acad Sci* **408**, 301-314
29. Lord, S. T. (2011) Molecular mechanisms affecting fibrin structure and stability. *Arterioscler Thromb Vasc Biol* **31**, 494-499
30. Okumura, N., Terasawa, F., Haneishi, A., Fujihara, N., Hirota-Kawadobora, M., Yamauchi, K., Ota, H., and Lord, S. T. (2007) B:b interactions are essential for polymerization of variant fibrinogens with impaired holes 'a'. *J Thromb Haemost* **5**, 2352-2359
31. Greenberg, C., Sane, D., and Lai, T. (2006) Factor XIII and fibrin stabilization. *Hemostasis and thrombosis*, 317-466
32. Grundmann, U., Amann, E., Zettlmeissl, G., and Küpper, H. A. (1986) Characterization of cDNA coding for human factor XIIIa. *Proceedings of the National Academy of Sciences* **83**, 8024-8028
33. Katona, E. E., Ajzner, E., Tóth, K., Kárpáti, L., and Muszbek, L. (2001) Enzyme-linked immunosorbent assay for the determination of blood coagulation factor XIII A-subunit in plasma and in cell lysates. *J Immunol Methods* **258**, 127-135
34. Adány, R., and Bárdos, H. (2003) Factor XIII subunit A as an intracellular transglutaminase. *Cell Mol Life Sci* **60**, 1049-1060
35. Cordell, P. A., Kile, B. T., Standeven, K. F., Josefsson, E. C., Pease, R. J., and Grant, P. J. (2010) Association of coagulation factor XIII-A with Golgi proteins within monocyte-macrophages: implications for subcellular trafficking and secretion. *Blood* **115**, 2674-2681
36. Muszbek, L., Bereczky, Z., Bagoly, Z., Komáromi, I., and Katona, É. (2011) Factor XIII: A Coagulation Factor With Multiple Plasmatic and Cellular Functions. *Physiological Reviews* **91**, 931-972

37. Shi, D. Y., and Wang, S. J. (2017) Advances of Coagulation Factor XIII. *Chin Med J (Engl)* **130**, 219-223
38. Inbal, A., and Dardik, R. (2006) Role of coagulation factor XIII (FXIII) in angiogenesis and tissue repair. *Pathophysiol Haemost Thromb* **35**, 162-165
39. Ichinose, A. (2012) Factor XIII is a key molecule at the intersection of coagulation and fibrinolysis as well as inflammation and infection control. *Int J Hematol* **95**, 362-370
40. HSIEH, L., and NUGENT, D. (2008) Factor XIII deficiency. *Haemophilia* **14**, 1190-1200
41. Lorand, L., and Graham, R. M. (2003) Transglutaminases: crosslinking enzymes with pleiotropic functions. *Nat Rev Mol Cell Biol* **4**, 140-156
42. Lorand, L., Jeong, J. M., Radek, J. T., and Wilson, J. (1993) Human plasma factor XIII: subunit interactions and activation of zymogen. *Methods Enzymol* **222**, 22-35
43. Karimi, M., Bereczky, Z., Cohan, N., and Muszbek, L. (2009) Factor XIII Deficiency. *Semin Thromb Hemost* **35**, 426-438
44. Kattula, S., Byrnes, J. R., Martin, S. M., Holle, L. A., Cooley, B. C., Flick, M. J., and Wolberg, A. S. (2018) Factor XIII in plasma, but not in platelets, mediates red blood cell retention in clots and venous thrombus size in mice. *Blood Adv* **2**, 25-35
45. Aleman, M. M., Byrnes, J. R., Wang, J. G., Tran, R., Lam, W. A., Di Paola, J., Mackman, N., Degen, J. L., Flick, M. J., and Wolberg, A. S. (2014) Factor XIII activity mediates red blood cell retention in venous thrombi. *J Clin Invest* **124**, 3590-3600
46. Gifford, J. L., Walsh, M. P., and Vogel, H. J. (2007) Structures and metal-ion-binding properties of the Ca2+-binding helix-loop-helix EF-hand motifs. *Biochem J* **405**, 199-221
47. Belkin, A. M. (2011) Extracellular TG2: emerging functions and regulation. *FEBS J* **278**, 4704-4716
48. Polgár, J., Hidasi, V., and Muszbek, L. (1990) Non-proteolytic activation of cellular protransglutaminase (placenta macrophage factor XIII). *Biochem J* **267**, 557-560
49. Souri, M., Kaetsu, H., and Ichinose, A. (2008) Sushi domains in the B subunit of factor XIII responsible for oligomer assembly. *Biochemistry* **47**, 8656-8664
50. Ambrus, A., Bányai, I., Weiss, M. S., Hilgenfeld, R., Keresztessy, Z., Muszbek, L., and Fésüs, L. (2001) Calcium binding of transglutaminases: a 43Ca NMR study combined with surface polarity analysis. *J Biomol Struct Dyn* **19**, 59-74
51. KOMÁROMI, I., BAGOLY, Z., and MUSZBEK, L. (2011) Factor XIII: novel structural and functional aspects. *Journal of Thrombosis and Haemostasis* **9**, 9-20
52. Stieler, M., Weber, J., Hils, M., Kolb, P., Heine, A., Büchold, C., Pasternack, R., and Klebe, G. (2013) Structure of Active Coagulation Factor XIII Triggered by Calcium Binding: Basis for the Design of Next-Generation Anticoagulants. *Angewandte Chemie International Edition* **52**, 11930-11934
53. Hethershaw, E. L., Adamson, P. J., Smith, K. A., Goldsberry, W. N., Pease, R. J., Radford, S. E., Grant, P. J., Ariëns, R. A. S., Maurer, M. C., and Philippou, H. (2018) The role of β-barrels 1 and 2 in the enzymatic activity of factor XIII A-subunit. *Journal of thrombosis and haemostasis : JTH* **16**, 1391-1401
54. Collet, J. P., Shuman, H., Ledger, R. E., Lee, S., and Weisel, J. W. (2005) The elasticity of an individual fibrin fiber in a clot. *Proc Natl Acad Sci U S A* **102**, 9133-9137
55. Ryan, E. A., Mockros, L. F., Weisel, J. W., and Lorand, L. (1999) Structural origins of fibrin clot rheology. *Biophys J* **77**, 2813-2826
56. Schroeder, V., and Kohler, H. P. (2016) Factor XIII: Structure and Function. *Semin Thromb Hemost* **42**, 422-428
57. Yee, V. C., Pedersen, L. C., Le Trong, I., Bishop, P. D., Stenkamp, R. E., and Teller, D. C. (1994) Three-dimensional structure of a transglutaminase: human blood coagulation factor XIII. *Proc Natl Acad Sci U S A* **91**, 7296-7300

58. Handrkova, H., Schroeder, V., and Kohler, H. P. (2015) The activation peptide of coagulation factor XIII is vital for its expression and stability. *J Thromb Haemost* **13**, 1449-1458
59. Protopopova, A. D., Ramirez, A., Klinov, D. V., Litvinov, R. I., and Weisel, J. W. (2019) Factor XIII topology: organization of B subunits and changes with activation studied with single-molecule atomic force microscopy. *J Thromb Haemost* **17**, 737-748
60. Anokhin, B. A., Dean, W. L., Smith, K. A., Flick, M. J., Ariëns, R. A. S., Philippou, H., and Maurer, M. C. (2020) Proteolytic and nonproteolytic activation mechanisms result in conformationally and functionally different forms of coagulation factor XIII A. *FEBS J* **287**, 452-464
61. Anokhin, B. A., Stribinskis, V., Dean, W. L., and Maurer, M. C. (2017) Activation of factor XIII is accompanied by a change in oligomerization state. *FEBS J* **284**, 3849-3861
62. Vasilyeva, A., Yurina, L., Shchegolikhin, A., Indeykina, M., Bugrova, A., Kononikhin, A., Nikolaev, E., and Rosenfeld, M. (2020) The Structure of Blood Coagulation Factor XIII Is Adapted to Oxidation. *Biomolecules* **10**
63. Singh, S., Dodt, J., Volkers, P., Hethershaw, E., Philippou, H., Ivaskevicius, V., Imhof, D., Oldenburg, J., and Biswas, A. (2019) Structure functional insights into calcium binding during the activation of coagulation factor XIII A. *Scientific Reports* **9**, 11324
64. Pedersen, L. C., Yee, V. C., Bishop, P. D., Le Trong, I., Teller, D. C., and Stenkamp, R. E. (1994) Transglutaminase factor XIII uses proteinase-like catalytic triad to crosslink macromolecules. *Protein Sci* **3**, 1131-1135
65. Schmitz, T., Bäuml, C. A., and Imhof, D. (2020) Inhibitors of blood coagulation factor XIII. *Anal Biochem* **605**, 113708
66. Case, A., and Stein, R. L. (2007) Kinetic Analysis of the Interaction of Tissue Transglutaminase with a Nonpeptidic Slow-Binding Inhibitor. *Biochemistry* **46**, 1106-1115
67. Melkonian, A. V., Loppinet, E., Martin, R., Porteus, M., and Khosla, C. (2021) An Unusual "OR" Gate for Allosteric Regulation of Mammalian Transglutaminase 2 in the Extracellular Matrix. *Journal of the American Chemical Society* **143**, 10537-10540
68. Achyuthan, K. E., and Greenberg, C. S. (1987) Identification of a guanosine triphosphate-binding site on guinea pig liver transglutaminase. Role of GTP and calcium ions in modulating activity. *J Biol Chem* **262**, 1901-1906
69. Lorand, L., and Konishi, K. (1964) ACTIVATION OF THE FIBRIN STABILIZING FACTOR OF PLASMA BY THROMBIN. *Arch Biochem Biophys* **105**, 58-67
70. Hornyak, T. J., and Shafer, J. A. (1991) Role of calcium ion in the generation of factor XIII activity. *Biochemistry* **30**, 6175-6182
71. Kimura, M., Lu, X., Skurnick, J., Awad, G., Bogden, J., Kemp, F., and Aviv, A. (2004) Potassium Chloride Supplementation Diminishes Platelet Reactivity in Humans. *Hypertension* **44**, 969-973
72. Zacchia, M., Abategiovanni, M. L., Stratigis, S., and Capasso, G. (2016) Potassium: From Physiology to Clinical Implications. *Kidney Diseases* **2**, 72-79
73. Romani, A., and Scarpa, A. (1992) Regulation of cell magnesium. *Arch Biochem Biophys* **298**, 1-12
74. Gow, I. F., Padfield, P. L., Reid, M., Stewart, S. E., Edwards, C. R., and Williams, B. C. (1987) High sodium intake increases platelet aggregation in normal females. *J Hypertens Suppl* **5**, S243-246
75. Strazzullo, P., and Leclercq, C. (2014) Sodium. *Adv Nutr* **5**, 188-190
76. Thier, S. O. (1986) Potassium physiology. *Am J Med* **80**, 3-7
77. Wolf, F. I., and Cittadini, A. (2003) Chemistry and biochemistry of magnesium. *Mol Aspects Med* **24**, 3-9

78. Wolf, F. I., Torsello, A., Fasanella, S., and Cittadini, A. (2003) Cell physiology of magnesium. *Mol Aspects Med* **24**, 11-26
79. Bagur, R., and Hajnóczky, G. (2017) Intracellular Ca(2+) Sensing: Its Role in Calcium Homeostasis and Signaling. *Mol Cell* **66**, 780-788
80. Melkikh, A. V., and Sutormina, M. I. (2008) Model of active transport of ions in cardiac cell. *Journal of Theoretical Biology* **252**, 247-254
81. Atchison, D. K., and Beierwaltes, W. H. (2013) The influence of extracellular and intracellular calcium on the secretion of renin. *Pflugers Arch* **465**, 59-69
82. Clapham, D. E. (2007) Calcium signaling. *Cell* **131**, 1047-1058
83. Sarma, B., and Sarma, B. (2016) Role of magnesium on the biomimetic deposition of calcium phosphate. *Journal of Physics Conference Series* **765**, 012025
84. Bidlack, W. R. (2000) Nutritional Biochemistry, 2nd ed. Tom Brody. San Diego, 1999. *Journal of the American College of Nutrition* **19**, 419-420
85. Hargreaves, L. N. M., and Hayes, P. C. (1978) The influence of lithium and calcium ions on the aggregation of human blood platelets. *Thrombosis Research* **13**, 79-83
86. Joffe, R. T., Kellner, C. H., Post, R. M., and Uhde, T. W. (1984) Lithium increases platelet count. *N Engl J Med* **311**, 674-675
87. Young, W. (2009) Review of Lithium Effects on Brain and Blood. *Cell Transplantation* **18**, 951-975
88. Orthner, C. L., and Kosow, D. P. (1980) Evidence that human α-thrombin is a monovalent cation-activated enzyme. *Archives of Biochemistry and Biophysics* **202**, 63-75
89. Underwood, M. C., Zhong, D., Mathur, A., Heyduk, T., and Bajaj, S. P. (2000) Thermodynamic Linkage between the S1 Site, the Na+Site, and the Ca2+ Site in the Protease Domain of Human Coagulation Factor Xa: STUDIES ON CATALYTIC EFFICIENCY AND INHIBITOR BINDING*. *Journal of Biological Chemistry* **275**, 36876-36884
90. Mok, E., Wee, E., Wang, Y., and Trau, M. (2016) Comprehensive evaluation of molecular enhancers of the isothermal exponential amplification reaction. *Scientific Reports* **6**, 37837
91. Coggan, M., and Board, P. (1984) A fluorescent spot test for coagulation factor XIII. *Analytical biochemistry* **137**, 402-404
92. Duval, C., Allan, P., Connell, S. D., Ridger, V. C., Philippou, H., and Ariëns, R. A. (2014) Roles of fibrin α- and γ-chain specific cross-linking by FXIIIa in fibrin structure and function. *Thromb Haemost* **111**, 842-850
93. Schwartz, M. L., Pizzo, S. V., Hill, R. L., and McKee, P. A. (1973) Human Factor XIII from plasma and platelets. Molecular weights, subunit structures, proteolytic activation, and cross-linking of fibrinogen and fibrin. *J Biol Chem* **248**, 1395-1407
94. Matsuka, Y. V., Medved, L. V., Migliorini, M. M., and Ingham, K. C. (1996) Factor XIIIa-catalyzed cross-linking of recombinant alpha C fragments of human fibrinogen. *Biochemistry* **35**, 5810-5816
95. (2010) *Principles and Techniques of Biochemistry and Molecular Biology*, 7 ed., Cambridge University Press, Cambridge
96. Orthner, C. L., and Kosow, D. P. (1980) Evidence that human alpha-thrombin is a monovalent cation-activated enzyme. *Arch Biochem Biophys* **202**, 63-75
97. Tolstopiatov, S. M. (1997) [The effect of sodium ions in vitro on the hemostatic balance of whole blood in patients with ischemic heart disease and hypercoagulation]. *Lik Sprava*, 56-59
98. Wells, C. M., and Di Cera, E. (1992) Thrombin is a sodium ion activated enzyme. *Biochemistry* **31**, 11721-11730

99. Papp, B., Launay, S., Gélébart, P., Arbabian, A., Enyedi, A., Brouland, J.-P., Carosella, E. D., and Adle-Biassette, H. (2020) Endoplasmic Reticulum Calcium Pumps and Tumor Cell Differentiation. *Int J Mol Sci* **21**, 3351
100. Tondo, L., Alda, M., Bauer, M., Bergink, V., Grof, P., Hajek, T., Lewitka, U., Licht, R. W., Manchia, M., Müller-Oerlinghausen, B., Nielsen, R. E., Selo, M., Simhandl, C., Baldessarini, R. J., and for the International Group for Studies of, L. (2019) Clinical use of lithium salts: guide for users and prescribers. *International Journal of Bipolar Disorders* **7**, 16
101. Daza, E. A., Misra, S. K., Schwartz-Duval, A. S., Ohoka, A., Miller, C., and Pan, D. (2016) Nano-Cesium for Anti-Cancer Properties: An Investigation into Cesium Induced Metabolic Interference. *ACS Applied Materials & Interfaces* **8**, 26600-26612
102. Clausen, M. J., and Poulsen, H. (2013) Sodium/Potassium homeostasis in the cell. *Met Ions Life Sci* **12**, 41-67
103. Vrbka, L., Jungwirth, P., Bauduin, P., Touraud, D., and Kunz, W. (2006) Specific Ion Effects at Protein Surfaces: A Molecular Dynamics Study of Bovine Pancreatic Trypsin Inhibitor and Horseradish Peroxidase in Selected Salt Solutions. *The Journal of Physical Chemistry B* **110**, 7036-7043
104. Okur, H. I., Kherb, J., and Cremer, P. S. (2013) Cations Bind Only Weakly to Amides in Aqueous Solutions. *Journal of the American Chemical Society* **135**, 5062-5067
105. Woofter, R. T., and Maurer, M. C. (2011) Role of calcium in the conformational dynamics of factor XIII activation examined by hydrogen-deuterium exchange coupled with MALDI-TOF MS. *Arch Biochem Biophys* **512**, 87-95
106. Teale, F., and Weber, G. (1957) Ultraviolet fluorescence of the aromatic amino acids. *Biochemical Journal* **65**, 476
107. Lakowicz, J. R. (2006) *Principles of fluorescence spectroscopy*, Springer
108. Weiss, M. S., Metzner, H. J., and Hilgenfeld, R. (1998) Two non-proline cis peptide bonds may be important for factor XIII function. *FEBS Lett* **423**, 291-296
109. White, S. (2011) Principles and techniques of biochemistry and molecular biology, seventh edition. *Biochemistry and Molecular Biology Education* **39**, 244-245
110. Nguyen, T. Y., Liew, C. G., and Liu, H. (2013) An In Vitro Mechanism Study on the Proliferation and Pluripotency of Human Embryonic Stems Cells in Response to Magnesium Degradation. *PLoS One* **8**, e76547
111. Lowenstein, F. W., and Stanton, M. F. (1986) Serum magnesium levels in the United States, 1971-1974. *Journal of the American College of Nutrition* **5**, 399-414
112. Ghisaidoobe, A. B. T., and Chung, S. J. (2014) Intrinsic tryptophan fluorescence in the detection and analysis of proteins: a focus on Förster resonance energy transfer techniques. *Int J Mol Sci* **15**, 22518-22538
113. Gupta, S., Biswas, A., Akhter, M. S., Krettler, C., Reinhart, C., Dodt, J., Reuter, A., Philippou, H., Ivaskevicius, V., and Oldenburg, J. (2016) Revisiting the mechanism of coagulation factor XIII activation and regulation from a structure/functional perspective. *Sci Rep* **6**, 30105
114. Gentile, V., Saydak, M., Chiocca, E. A., Akande, O., Birckbichler, P. J., Lee, K. N., Stein, J. P., and Davies, P. J. (1991) Isolation and characterization of cDNA clones to mouse macrophage and human endothelial cell tissue transglutaminases. *J Biol Chem* **266**, 478-483
115. Jang, T. H., Lee, D. S., Choi, K., Jeong, E. M., Kim, I. G., Kim, Y. W., Chun, J. N., Jeon, J. H., and Park, H. H. (2014) Crystal structure of transglutaminase 2 with GTP complex and amino acid sequence evidence of evolution of GTP binding site. *PLoS One* **9**, e107005
116. Kanchan, K., Ergülen, E., Király, R., Simon-Vecsei, Z., Fuxreiter, M., and Fésüs, L. (2013) Identification of a specific one amino acid change in recombinant human

transglutaminase 2 that regulates its activity and calcium sensitivity. *Biochem J* **455**, 261-272
117. Smith, K. A., Adamson, P. J., Pease, R. J., Brown, J. M., Balmforth, A. J., Cordell, P. A., Ariëns, R. A. S., Philippou, H., and Grant, P. J. (2011) Interactions between factor XIII and the αC region of fibrinogen. *Blood* **117**, 3460-3468
118. Ha, H. J., Kwon, S., Jeong, E. M., Kim, C. M., Lee, K. B., Kim, I.-G., and Park, H. H. (2018) Structure of natural variant transglutaminase 2 reveals molecular basis of gaining stability and higher activity. *PLoS One* **13**, e0204707-e0204707
119. Pinkas, D. M., Strop, P., Brunger, A. T., and Khosla, C. (2007) Transglutaminase 2 undergoes a large conformational change upon activation. *PLoS Biol* **5**, e327
120. Souri, M., Biswas, A., Misawa, M., Omura, H., and Ichinose, A. (2014) Severe congenital factor XIII deficiency caused by novel W187X and G273V mutations in the F13A gene; diagnosis and classification according to the ISTH/SSC guidelines. *Haemophilia* **20**, 255-262
121. Li, B., Kohler, H. P., and Schroeder, V. (2020) Identification of amino acid residues that are crucial for FXIII-A intersubunit interactions and stability. *Blood* **135**, 145-152
122. Király, R., Csosz, E., Kurtán, T., Antus, S., Szigeti, K., Simon-Vecsei, Z., Korponay-Szabó, I. R., Keresztessy, Z., and Fésüs, L. (2009) Functional significance of five noncanonical Ca2+-binding sites of human transglutaminase 2 characterized by site-directed mutagenesis. *FEBS J* **276**, 7083-7096

APPENDICES

Supplemental figures and tables

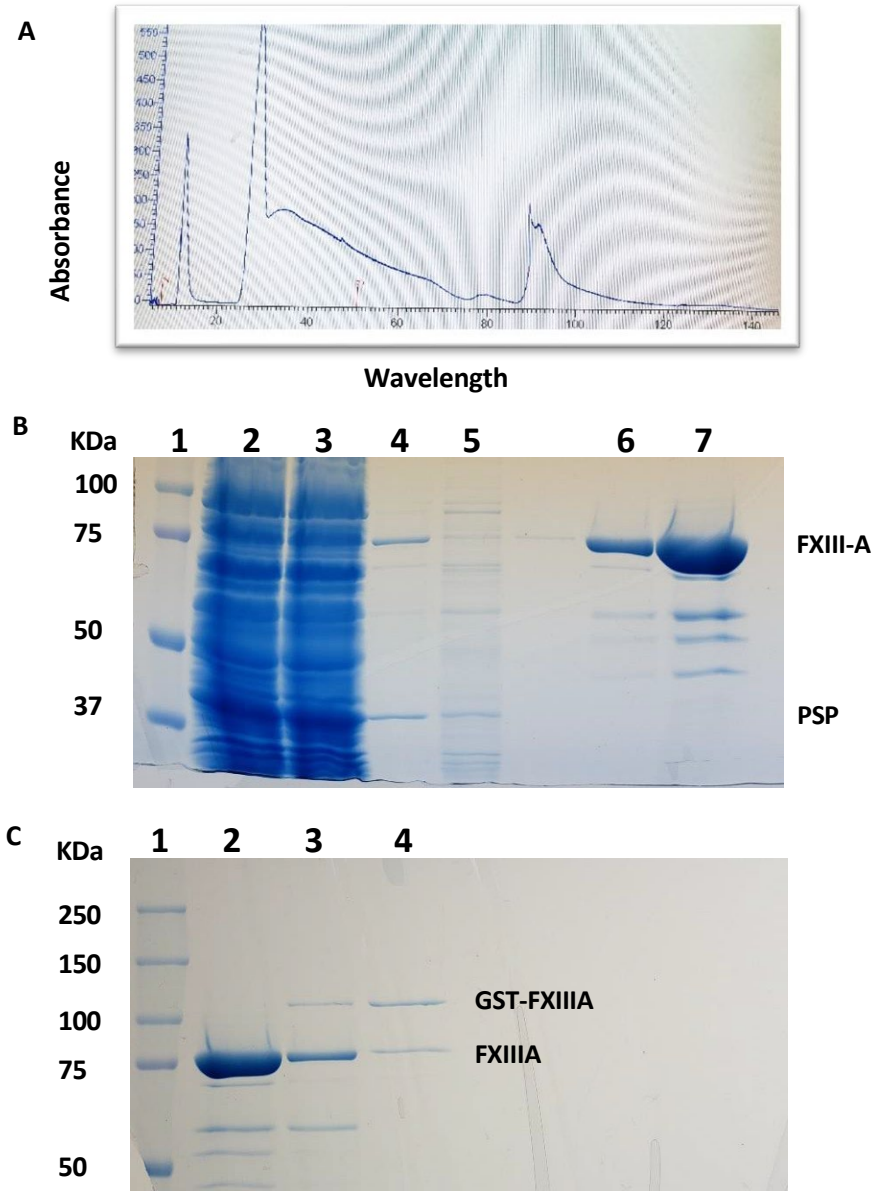

Supplemental Figure S1. Site directed mutagenesis purification results for FXIII-A G262V generation. A) Elution profile of FXIII-A mutant B) Lane 1 – Molecular weight marker, Lane 2 – Lysate, Lane 3 – load flow-through, Lane 4 – washed flow-through, Lane 5- washed flow-through, Lane 6- GST-PSP, Lane 7 – FXIII-A fraction A, C) Lane 2 – FXIII-A fraction B, Lane 3,4- Glutathione eluted fractions.

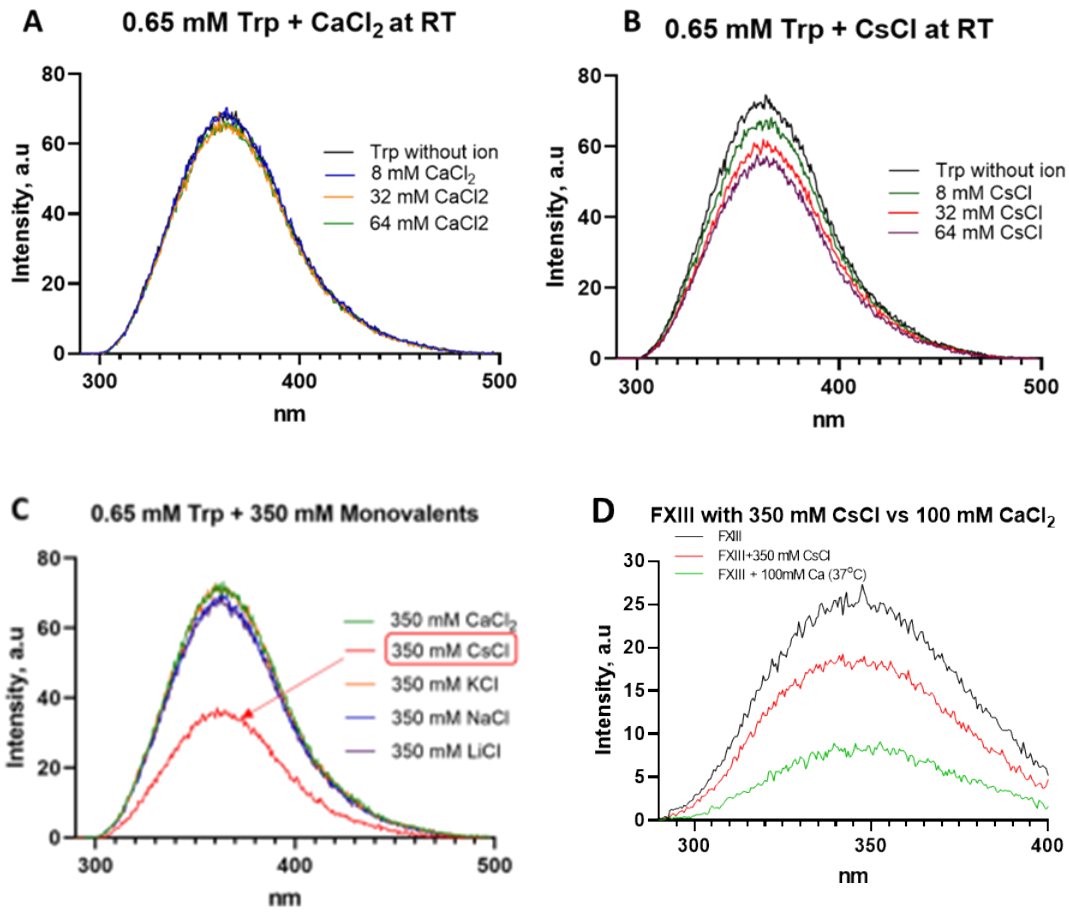

Supplemental Figure S2. Free Tryptophan fluorescence with cations. A) Emission spectra of free Trp in the presence of 8 mM, 16 mM and 64 mM $CaCl_2$ B) Emission spectra of free Trp in the presence of 8 mM, 16 mM and 64 mM CsCl C) Emission spectra of $CaCl_2$ vs monovalent salts D) Emission spectra of FXIII with CsCl vs $CaCl_2$.

Supporting Table S1. Curved fit and Bar Graph data (30 min reaction time) of MDC incorporation assay (Chapter 2 and 4)

	FLR intensity (30 min reaction time)	E_{max} (Plateau)	Initial reaction rate K (s^{-1})
NaCl			
150 mM	0.008±0.000	0.071	0.004
350 mM	0.024±0.002	0.090	0.010
415 mM	0.037±0.004	0.059	0.033
500 mM	0.057±0.004	0.112	0.025
KCl			
150 mM	0.018±0.001	Unstable	0.00
350 mM	0.038±0.003	0.101	0.015
500 mM	0.057±0.002	0.064	0.084
LiCl			
350 mM	0.016±0.002	0.031	0.025
Li_2SO_4			
350 mM	0.057±0.002	0.113	0.023
CsCl			
350 mM	0.052±0.002	0.088	0.029
TMAC			
350 mM	0.030±0.002	0.093	0.013
ChCl			
350 mM	0.014±0.001	Unstable	0.00
$MgCl_2$			
350 mM	0.025±0.003	0.101	0.048
$MgSO_4$			
350 mM	0.077±0.001	0.046	0.923
FXIIIA* WT	0.069±0.001	0.058	0.607
FXIIIA* G262V	0.051±0.004	0.056	0.799
FXIIIA^o WT	0.063±0.000	0.076	0.178
FXIIIA^o G262V	0.063±0.003	0.067	0.113

Data for normalized in-gel fluorescence intensities via MDC incorporation assay were plotted using One-phase association GraphPad prism 9.2.0 software. The equation used was $Y=Y_o + (Plateau-Y_o)x(1-exp(-Kx))$ where Y represents the normalized in-gel fluorescence intensity with β-CaseinXMDC as a positive control, Y_o is the sample at zero time point (quenched FXIII-A_2 before reaction), K as the rate constant in min^{-1}, Plateau or E_{max} (Y value at infinite time), and t as time in minutes.

Supporting Table S2. Percent change in terms Maximum fluorescence intensity of FXIII under different ionic and temperature conditions (Chapter 3)

$FXIIIA_2$ plus ions	**% drop against FXIII (RT)**	**% drop against FXIII (37°C)**	**$FXIIIA_2$ plus ions**	**% drop against FXIII (RT)**	**% drop against FXIII (37°C)**
350 mM LiCl + 4 mM $CaCl_2$	19	34	**4 mM $CaCl_2$**	20	44
150 mM NaCl	24	25	**100 mM $CaCl_2$**	44	66
350 mM NaCl + 4 mM $CaCl_2$	30	43	**350 mM $MgCl_2$+ 4 mM $CaCl_2$**	29	38
350 mM KCl + 4 mM $CaCl_2$	29	45	**350 mM $MgSO_4$+ 4 mM $CaCl_2$**	29	40
350 mM CsCl + 4 mM $CaCl_2$	42	49	**350 mM Li_2SO_4+ 4 mM $CaCl_2$**	24	33

Trp fluorescence data were analyzed using GraphPad 9.2.0 software to determine the maximum intensity (a.u). Percent decrease in terms maximum intensity using the emission spectra results were compared with the generated maximum intensity of FXIII-A_2 in borate solution at room temperature and 37°C, physiological temperature.

CURRICULUM VITAE

Richard Laporca Lumata
M.S in Chemistry with emphasis in Protein Chemistry
Email: richardlumata@gmail.com.
LinkedIn ID: https://www.linkedin.com/in/richard-lumata-33b09a92

EDUCATIONAL BACKGROUND

Master of Science in Chemistry (Successfully defended June 22, 2022)
Department of Chemistry, University of Louisville
Maurer Research Group – Protein Chemistry Lab
Thesis title: Effects of Monovalent and Divalent Ions on FXIII Activation and Crosslinking
Expected Graduation Date: August 2022

Graduate Student (2017-2018) – Online program, earned 12 out of 36 units- Master of Environment and Natural Resources Management, Faculty of Management and Development Studies at University of the Philippines -UPOULC-Diliman

Bachelor of Science in Chemistry (June 2002- March 2006)
College of Science and Mathematics
Western Mindanao State University, Philippines

WORK EXPERIENCES

A. University of Louisville, Department of Chemistry

1. Graduate Research – Maurer Protein Chemistry Lab

   Project 1- Effects of Ions in FXIII Activation via Monodansyl Cadaverine Incorporation to Fibrinogen αC (233-425)
   Project 2 – Monitoring Intrinsic Fluorescence of Human FXIII Activated Forms Under Different Monovalent and Divalent Salts
   Project 3 – Characterizing Human FXIII Wild Type vs G262V
   Project 4 - Influence of Monovalent and Divalent Ions in the Proteolytic activity of FXIII and Thrombin

   Skills gained: Protein expression and purification of blood coagulations factors, site directed mutagenesis, fluorescence studies, Kinetic and thermodynamic assays via Isothermal Titration Calorimetry, Gel electrophoresis assays, MALDI TOF MS.

Graduate Teaching Assistant

- Fall: 2019; Spring: 2020, 2021, 2022; Summer: 2022– CHEM 207/208 (Introductory to Chemical analyses I and II)

- Fall: 2020, 2021 – CHEM 545 (Advanced Biochemistry Lab)

SCIENTIFIC CONFERENCES (as Graduate student of UofL)

- ***Richard L Lumata,*** *Divya A. Kumaravelu, Anoushka Bhat, Rameesa D. Syed Mohammed, Muriel C. Maurer* - Factor XIII Activation and Substrate Crosslinking can be Influenced by Amino Acid Substitutions from Transglutaminase 2 - Gordon Research Conference– Hemostasis, 07/31/22 – 08/05/22. New Hampshire, USA

- *Divya A. Kumaravelu,* ***Richard L. Lumata****, Rameesa D. Syed Mohammed and Muriel C. Maurer "*Transglutaminase2-Inspired Factor XIII Mutants G262V and G262V, K269N Alter Non-Proteolytic Activation and Enzyme Activity" - Undergraduate Research Showcase Spring 2022 University of Louisville, Louisville, KY, USA

- *Muriel C. Maurer, Rameesa Darul Amne Syed Mohammed, Francis Dean O. Ablan, Nicholas M. McCann,* ***Richard L. Lumata*** - Factor XIII Crosslinking Activity is Proposed to be Influenced by its Mode of Zymogen Activation - International Fibrinogen Research Society: 2021 mini symposium (online – 06/15/21-06/16/21)

- ISTH 2021: XXIX Congress of the International Society of Thrombosis and Haemostasis (July 17-July 21, 2021)

MANUSCRIPTS IN PREPARATION (University of Louisville)

- Factor XIII Activation and Substrate Crosslinking can be Influenced by Amino Acid Substitutions from Transglutaminase 2 by ***Richard L Lumata***, Divya A. Kumaravelu, Anoushka Bhat, Rameesa D. Syed Mohammed, Muriel C. Maurer
- Effects of Monovalent and Divalent Ions on Factor XIII Activation and Crosslinking by ***Richard L Lumata*** and Muriel C. Maurer, *in preparation*.

B. Philippine Coconut Authority-Zamboanga Research Center

1. Sr. Science Research Specialist, Philippine Coconut Authority-Zamboanga Research Center, Non-Food products Development Division (January 2016- July 2019)
2. Contractual Research Assistant, Plant Genetic Resources Conservation and Utilization Division, October 2007- April 30, 2008, and July 2010- December 2015. Below are the projects served:

C. San Miguel Foods Inc.

3. Quality Control Analyst (B-MEG San Miguel Foods Inc.), San Miguel Corporation, May 1, 2008-April 30, 2009, Culianan, Zamboanga City

PUBLISHED

- Lumata, R.L (2017). Utilization of Coconut Ligno-cellulosic Waste Substrates for a Sustainable Spawns and Pure Cultures of Selected Edible Mushrooms. Book of Abstracts: International Conference on Sustainable Agriculture and Bioeconomy (AGBIO 2017). Bangkok, Thailand. pp170-171

- Lumata, R.L., Azcona, D.M (2006). *Averrhoa bilimbi* (kamias) Flower Extract as an Acid/Base Indicator. WMSU Research journal. Vol. 26 No. 1, ISSN 0115 6454
- R.L Lumata, L.J Peñamora, and A.L Lumata. (2018). Sustainable Spawns and Pure Cultures of Selected edible Mushrooms using Coconut (AROD, LAGT, MRD) Ligno-Cellulosic Media. Proceedings of the CSSP 48th Scientific Conference. The Philippine Journal of Crop Science, 43. Pp 37

RESEARCH AWARDS RECEIVED

1st Place, 2019 Regional Invention Contest, Department of Science and Technology, Philippines.

Coconut Male Flower (CMF) from hybridization wastes as Base component for pure culture and inoculum for various fungi cultures by ***Richard L. Lumata,*** L.J Peñamora, A.L Lumata

3rd Best Paper (National), 2018, Oral Presentation, 20th Annual Scientific Conference of the Mycological Society of the Philippines

Phase II Sustainable Pure Cultures and Spawns of Selected Edible Mushrooms from Coconut (LAGT, MRD and AROD) Ligno-cellulosic Waste Media (***Richard L. Lumata,*** L.J Peñamora, A.L Lumata)

2nd Place, 2018 Regional Symposium for Research and Development highlight (Oral presentation), Department of Science and Technology, Philippines

Physical and Mechanical test of Philippine Coir (L.G Baya, C.M Tagactac, ***R.L Lumata***, L.J Peñamora)

1st Place, 2018 Regional Symposium for Research and Development highlight (Oral presentation), Department of Science and Technology, Philippines

Development of Coir-coloring art filler and peat-based handicrafts (A.L Lumata, L.G Baya, C.M Tagactac, ***R.L Lumata***, L.J Peñamora)

2017 R&D Award (Qualifier) National Agriculture and Fisheries Modernization Act, Department of Agriculture, Philippines

Phase I Sustainable Pure Cultures and Spawns of Selected Edible Mushrooms from Coconut (LAGT, MRD and AROD) Ligno-cellulosic Waste Media (***R.L. Lumata***)

2016 R&D Award (Qualifier) National Agriculture and Fisheries Modernization Act, Department of Agriculture, Philippines

Application of Microsatellite Marker Technology in Establishing the Core Collection of Tall Coconut Accessions (R.L Rivera, S.M Rivera, E.E Emmanuel, ***R.L Lumata***)

University Best Research Paper Award (Undergraduate Thesis) Western Mindanao State University 2006
Averrhoa bilimbi (Kamias) flower Extract as Acid/Base Paper Indicator, (***R.L Lumata*** and D.M Azcona)

LABORATORY EQUIPMENT OPERATIONS:

(Department of Chemistry, University of Louisville)
GE Amersham AKTA FPLC, Nano Isothermal Titration Calorimetry (ITC), MALDI TOF Mass Spec, FTIR, Perkin Elmer LS 55 Spectrofluorimeter, UV/VIS.

(Previous work from 2008 to 2019)

Shimadzu MALDI-TOF Mass Spectrometer (at UPLB and Shimadzu Singapore), Shimadzu Prominence HPLC (RID Detector) and Ultrafast HPLC (PDA and UV VIS detectors), Sartorius BIOSTAT A Microbial System (Bioreactor at PCA), Thermoscientific UV-VIS Spectrophotometer with fiber optic probe, Foss Near Infrared Reflectance Spectrometer (NIR at SMFI), Kjeltech equipment (at SMFI), BIO-RAD Molecular Imager GelDoc XR+ imaging system (At PCA and UofL), BioScience RT PCR (At PCA), BIOMETRA-Analytikjena Gel Electrophoresis equipment, CBS Scientific Non-denaturing Vertical PAGE, SDS PAGE, Life Science Agarose Gel Electrophoresis, Instron Universal Testing Machine, PAGE Electrophoresis equipment (Cole Palmer and Life Technologies), Analytikjena thermal cycler, Geno grinder, MJ Research Thermal Cycler, Eppendorf Mastercycler nexus gradient PCR machine, Nanodrop spectrophotometer, Hoefer SQ3 Sequencer, Vertical PAGE Equipment